Comparison of Controllers for a Separate Meter-In Separate Meter-Out System

- 10th Semester Master Thesis -

- MCE4 - 1026 -

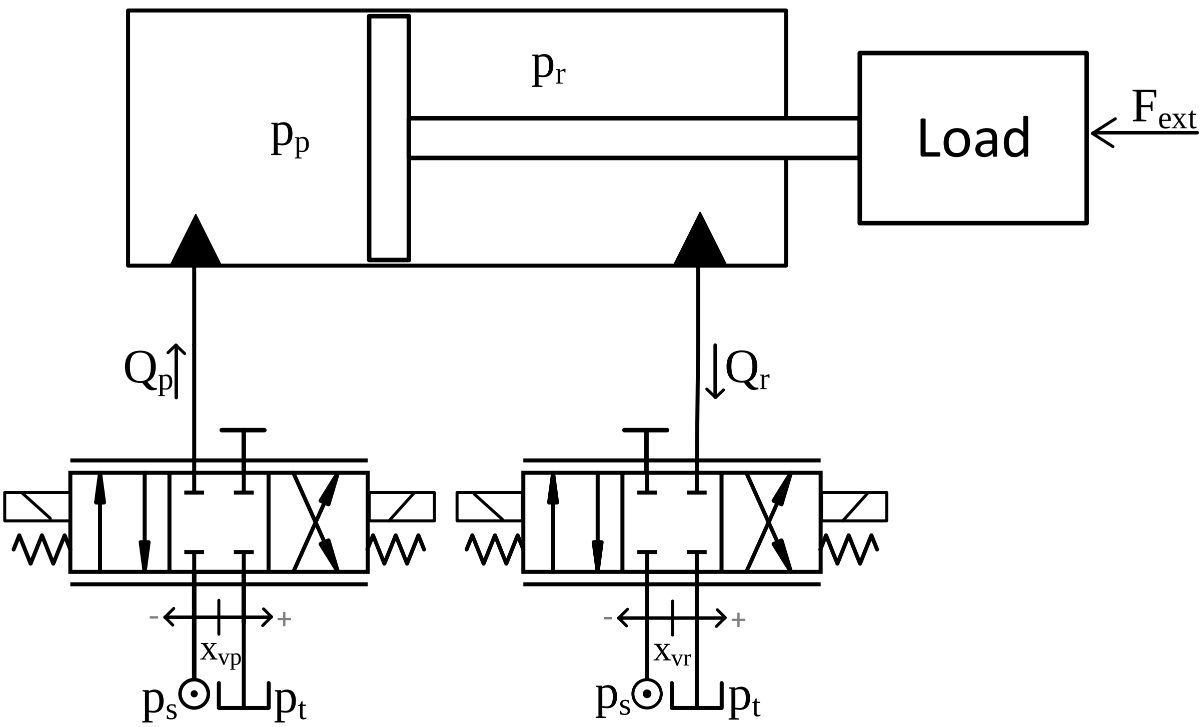

Aalborg University
The Department of Energy Technology
Pontoppidanstræde 111
DK-9220 Aalborg East

Board of Studies of Energy

Title: Comparison of Controllers for a Separate Meter-In and Separate Meter-out System
Semester: 10^{th}
Semester theme: Master's Thesis in Mechatronic Control Engineering
Project period: 03.02.20 to 29.05.2020
ECTS: 30
Supervisors: Henrik C. Pedersen
Project group: MCE4 - 1026

ABSTRACT:
The focus of this Master's Thesis is to compare different controllers in relation to performance and robustness for a given separate meter-in separate meter-out (SMISMO) hydraulic system with two proportional valves and a single degree-of-freedom inertia load. The thesis is focused on simulation study without experimental validation as no test bench was available. A non-linear model is developed, validated and linearised. Afterwards, the linear model is used in analysis to obtain an understanding of the system dynamics and input/output coupling, to determine how conservatively controllers should be tuned. The choice of MIMO controllers for implementation was selected towards variation of full-state feedback (FSF) and linear quadratic (LQ) controllers. As this is considered to be a good initial step into investigation whenever MIMO controllers are feasible. First, controllers are tested in the linear model and based on the results three are chosen for the further comparison in the non-linear model. The comparison is conducted in presence of white noise and a disturbance, besides that two positions of the cylinder are considered for the vertical and horizontal case. The main conclusion states that in horizontal position the linear quadratic integrator (LQI) controller performs better, and for the vertical position the linear quadratic Gaussian with integral action (LQG-I).

Oliver Gregory Inuk Slaughter Fleischer

Sergej Zubarev

Pages, total: 110(-8 blanks)
Pages, appendix: 31
Supplements: 0

By accepting the request from the fellow student who uploads the study group's project report in Digital Exam System, you confirm that all group members have participated in the project work, and thereby all members are collectively liable for the contents of the report. Furthermore, all group members confirm that the report does not include plagiarism.

Preface

This Master's Thesis is written by 10^{th} semester Master group MCE4-1026 studying Mechatronic Control Engineering at the Department of Energy Technology, Aalborg University. The final thesis is written in the period from the 3^{rd} of February to the 29^{th} of May 2020.

The preconditions for reading this report is an understanding of mechanical physics and control theory.

Reading Guide: All the quantity symbols, abbreviations and variables used in thesis are provided in the nomenclature. The references used throughout master's thesis are enclosed by square brackets indicating surname of the author and year it was produced. If a reference refers to an entire section, it is placed after the last period. Sections, equations, tables, and figures are referred to as: section/equation/table/figure, where the first number refers to the chapter.

All the figures and tables are provided with the corresponding caption underneath it. Relevant literature including books, scientific publications, manufacturer data-sheets are provided in the bibliography. Where the URL is written for Internet sources and ISBN for the books. Vectors are marked with the line above the variable and matrices are bold, throughout the report. The symbols with a dot above them are indicating the derivative with respect to time, and two dots are double derivatives.

Appendixes with supplementary information are provided in the end of the report after the bibliography.

The software that is used throughout the master thesis is listed below:

- MATLAB - for calculations
- Simulink - for simulations
- Overleaf - for writing report
- Microsoft Visio - for illustration and schematics

Deparment of Energy Technology - Aalborg University

Summary

The main objective of this Master's thesis is to analyse and compare different controllers for implementation in a separate meter-in separate meter-out (SMISMO) system. This involves conducting a literature review to attain which combination of control strategies and controllers has been implemented in prior research, as to avoid these. In cross reference with the literature review, the choice of control strategy takes base from the analysis conducted in [Berthing, 2019], where the chosen control strategy was to control for the velocity and pressure. From the findings of the literature review and considering a pressure/velocity control strategy, it is seen that linear-quadratic controllers have not been investigated thoroughly and it is decided to compare these in relation to each other. This leads to the problem statement:

"For a pressure/velocity control strategy, how does the chosen MIMO controllers compare in relation to performance when tracking a pre-defined reference set for the rod side pressure and piston velocity, when subjected to disturbance and noise."

A non-linear model is then derived with simplifying assumptions. The non-linear model is then linearised, creating the linear model with the purpose of using it for the system analysis and controller design. As this is a simulation study and no experimental data is available to thoroughly validate the non-linear model, steady state calculations are derived analytically and compared against results obtained in the non-linear model providing reasoning enough to assume the model is correctly implemented. Then the linear model is validated against the non-linear model, by initialising the linear and non-linear models in the same point and stepping the valve inputs by a few percentages to observe if the linearisation point captures the dynamics sufficiently in the operating range around the linearisation point.
A frequency analysis when moving the poles from one end of the cylinder to the opposite is conducted, to gain information regarding the dynamics of the system in regards to the frequency and damping of each pole in the system. Then the coupling analysis is conducted which includes the relative gain array (RGA) and singular value decomposition (SVD). The RGA is used when determining which linearisation point is chosen, as it is preferred to have it in a place where there are no severe couplings in the system. The severity of the couplings is also used in the considerations when tuning the controllers, as having a heavily coupled system may not allow for aggressive tuning.
From the findings of the problem analysis, full state feedback (FSF) and all linear-quadratic controllers are chosen for comparison. First the controllers are tested in the linear model, as this is viewed as a best case scenario where the controllers should perform near their best. Then from the results obtained from the linear model, three controllers are considered for further comparison in the non-linear model. In the testing of the controllers in the non-

linear model, they are excited by an external force and noise is added to the measurement as to emulate sensor noise. These tests are conducted for two different cases, one where the cylinder is horizontal and one where it is vertical. The results from the non-linear model show that for the horizontal case the linear-quadratic-integrator (LQI) controller performs the best, and for the vertical case the linear-quadratic-Gaussian integrator (LQG-I) controller performs best.

Contents

Nomenclature

Latin Symbol	Description	Unit
A_p, A_r	Cylinder piston and rod side areas	$[m^2]$
B_v	Damping coefficient	$[Ns/m]$
e_{ss}	Steady state error	[%]
$F_{friction}, F_c$	Total friction and Coulomb friction force	[N]
F_{ext}	External force load	[N]
g	Gravitation constant	$[m/s^2]$
k_v	Valve flow coefficients	[-]
L_{stroke}	Cylinder stroke length	[m]
m	Mass cylinder	[kg]
N	Nominal force	$[N]$
n	Poly tropic index	[-]
$\dot{p}_p, \dot{p}_r$	Cylinder pressure gradients	[Pa]
p_p, p_r	Cylinder piston and rod side pressure	[Pa]
p_t, p_s	Tank and supply pressure	[Pa]
p_0, p_n	Atmospheric and nominal pressure	[Pa]
Q_p, Q_r	Cylinder piston and rod side flows	$[m^3/s]$
Q_n	Nominal flows	$[m^3/s]$
t_s	Settling time	$[s]$
t_r	Rise time	$[s]$
V_{p0}, V_{r0}	Cylinder total dead volumes	$[m^3]$
V_{dead}, V_{hose}	Cylinder dead and hose volumes	$[m^3]$
$\ddot{x}_p$	Cylinder piston acceleration	$[m/s^2]$
$\dot{x}_p$	Cylinder piston velocity	[m/s]
x_p	Cylinder piston positions	[m]
$\overline{x}_{vp}, \overline{x}_{vr}$	Normalised valve slider positions	[-]
A, B, C, D	State space matrices	[-]
J	Cost function	[-]
$\mathbf{K}$	Gain matrix	[-]
$\mathbf{P}$	Solution of Riccati equation	[-]
$\mathbf{R}, \mathbf{Q}$	Weight matrices	[-]
q_1, q_2, q_3	Weighting parameters	[-]
x, u, y	State-, input-, and output vector	[-]
s	Laplace operator	[-]
r	Reference	[-]
y	Output	[-]

Greek symbols	Description	
α	Air in oil ratio	[-]
β, β_0	Bulk modulus and initial bulk modulus	[Pa]
β_p, β_r	Piston and rod side bulk modulus	[Pa]
ϵ_a	Ratio of air in oil	[-]
ζ	Damping coefficient	[-]
λ	RGA element	[-]
μ	Coefficient of friction	[-]
$\underline{\sigma}, \overline{\sigma}$	Minimum and maximum singular value	[-]
τ	Time constant	[s]
ω_n	Natural frequency	[rad/s]

Abbreviation	Description
AAU	Aalborg University
ELS	Electrical load sensing
FSF	Full state feedback
I/O	Input/Output
LQ	Linear quadratic
LQR	Linear quadratic regulator
LQI	Linear quadratic integrator
LQG	Linear quadratic Gaussian
LQGI	Linear quadratic Gaussian integrator
MIMO	Multiple input multiple output
PID	Proportional integral derivative
PI	Proportional integral
RGA	Relative gain array
RMSE	Root-mean-square error
SVD	Singular value decomposition
SISO	Single input single output
SMISMO	Separate meter-in separate meter-out

1 | Introduction

The focus of this project is to investigate and compare different controllers for a separate meter-in separate meter-out (SMISMO) system that makes use of proportional valves to control the flow, illustrated in figure 1.1. The investigation into which controllers are chosen for comparison is outlined in Chapter 2.

A SMISMO system makes use of typically either proportional or digital valves to separately control the meter-in and meter-out sides of an actuator (e.g. an asymmetrical cylinder). This opens up for different possibilities regarding control strategies compared to having a single proportional valve, as here the meter-in and meter-out sides are linked together due to the valve design. With two (or more) separate valves, it is possible to control a multitude of different states in combination with one another, such as: pressure, flow, acceleration, velocity, position, force.

A problem arises when the second valve is introduced to the system as it turns it into a MIMO control problem. This complicates the controller design process in several ways, mainly due to the couplings in the system where one of either inputs affect several outputs, but also implementing the best control strategy depending on the objective, be it: motion tracking, increasing energy efficiency, increased performance, ensuring stability in a system etc. Adding that model uncertainty is almost a guarantee therefore leaving the controller type to be chosen in such a way that it account for these issues.

This leaves the controller to be designed in such a way that it is able to control for situations when the system process is perturbed by any disturbances, subjected to a low signal-to-noise ratio or from any inaccuracies/uncertainties in the mathematical model. Considering these issues, the controller(s) should be of a robust nature, which prompts an investigation into which controllers seem feasible in implementation for the given purpose.

1.1 SMISMO System Description

The SMISMO topology is seen in Figure. 1.1. The system this simulation study uses as reference is located in the hydraulics laboratory at AAU.

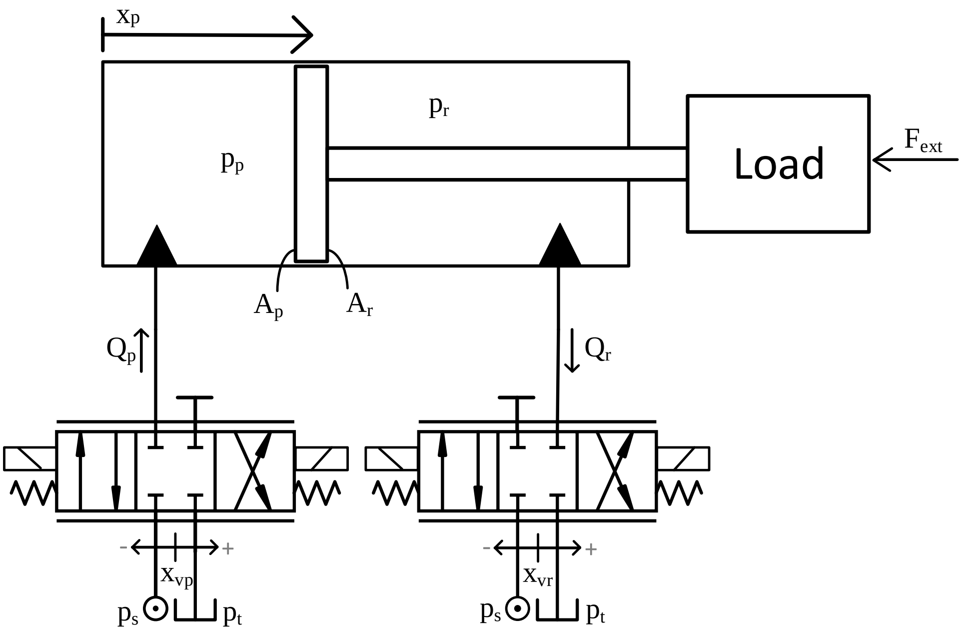

Figure 1.1: Separate Meter-In Separate Meter-Out Topology

In this simulation study the actuator is an asymmetrical cylinder with an inertia connected to the cylinder piston with 1 degree of freedom. The valves in use are 4/3 proportional valves from MOOG [MOOG, 2019]. The dimensions for the components modelled in the project can be seen below 1.1:

Cylinder	Ø0.140/Ø0.090/1.856 [m] $A_p = 0.0154$ [m^2] $A_r = 0.009$ [m^2]
Valves	MOOG D633 $Q_N = 40$ [l/min], $p_N = 35$ [bar]
Pressures	$p_s = 210$ [bar] $p_t = 3$ [bar]
Volumes	$V_{p,0} = $ 2.5335e-4 [l] $V_{r,0} = $ 8.5059e-4 [l]

Table 1.1: Component specifications

Not described are the hoses which are assumed lossless and stiff, as well as the pump which is assumed to supply flow with a constant supply pressure. These assumptions are discussed in later chapters.

2 | Problem Analysis

2.1 Literature Review

In the following chapter the different control strategies and types of controllers implemented in SMISMO systems in previous research is outlined. The SMISMO scheme might differ in some ways, but common should be that they employ the use of an asymmetrical cylinder, proportional valves in their setup as these are used in the setup illustrated in figure 1.1. The reason for doing this literature review is to avoid implementing the same combination of control strategy and controllers as previous researchers.

Literature

In the Ph.D thesis [Nielsen, 2005], decoupling efforts were employed for a pressure/velocity control strategy, where the control structures should control a bi-directional load. Here it was found that it was best to control the velocity on the chamber associated with the high-pressure side. The author designed two pseudo SISO controllers, for pressure and velocity respectively, that were validated in simulation only but still showing promising results.

In [Hansen et al., 2011] the authors considered, along with control, the switching of control strategies depending on the operating mode in a SMISMO-ELS setup. The different control strategies were a combination of the different chamber pressures and flows. Two different controllers were applied, for pressure control: gain scheduled PID feedback controller in addition with flow feed-forward, and for pump pressure control: A combined PI and flow feed-forward controller. Where the references for the pump pressure controller is dependent on the measurements of the chamber pressures and the actuator velocity reference, and the pressure controller reference for the experiments was set at 10[bar] for the non load carrying pressure. In this setup it was shown experimentally that the power demands for the engine connected to the pump could be lowered, whilst there was a drawback in controlling for the engine speed as it could impose limitations on the actuator performance.

In [Liu and Yao, 2004] the authors created a adaptive control algorithm for a SMISMO system with 5 proportional cartridge valves, with the primary purpose of doing motion control of a robot arm emulating the movement of a backhoe, with the secondary purpose of increasing energy efficiency. Pressure regulation is used to maintain a low pressure level in the back pressure chamber, as the secondary objective is to reduce the energy usage. The control strategy employed is to control for the velocity and the load pressure variable $P_L = P_p A_p - P_r A_r$. Where P_L is treated as a virtual input and implemented in the error dynamics in the adaptive control algorithm in order to drive the actual motion reference to the desired motion reference. The results showed increased energy efficiency whilst the robot arm was able to follow the motion reference.

In [Lu and Yao, 2014] the authors build on the work performed in [Liu and Yao, 2004], where the hardware configuration now includes an accumulator. Furthermore the adaptive control algorithm developed in previous research is expanded to include: motion tracking capabilities, flow and back pressure control in an attempt to further reduce energy consumption in a setup consisting of a 3 D.O.F robot arm. The authors synthesized control laws for the flows to control for the pressure and motion references by incorporating them into the error dynamics of the adaptive control algorithm. The algorithm showed increased energy efficiency and tracking capabilities compared to the authors previous research.

In [Pedersen et al., 2013] the authors designed several H^{∞} controllers that are evaluated against SISO control on a single axis robot arm. A pressure/velocity control strategy was employed where the controllers are tested for the control of velocity and both piston and rod side pressure (moving in the positive direction) where the non load carrying pressure reference is set to 20 [bar]. The controllers showed poor ability in tracking a reference set for the velocity and respective pressures. This was believed to be due to the controllers being tuned conservatively to account for a resonance peak seen in the SVD of the system, and the authors recommendation was to employ the use of active damping to account for this peak.

In [Jansson and Palmberg, 1990] a valvistor (hydraulic transistor - containing four proportional valves) are used to control for the pressure & flow in cases of lifting and lowering an inertia load, where the meter-in side is used to control for pressure and meter-out is used to control for flow. The chamber pressures are fed back to a computer that adjust the supply pressure via the pump (similar with ELS), no controllers are therefore implemented, as the pressure and flow are controlled through the pump and the switching of the valve openings. The authors showed that through the controlling of the separate valves via a MCU there were benefits in terms of increasing energy efficiency over traditional mechanical valves.

In [Jansson et al., 1992] the authors designed a non-linear control scheme decoupling the pressure and velocity with the addition of velocity feedback, using the force generated by the load to determine the pressure difference and controlling the pressures level by way of adjusting the meter-in and meter-out orifices. The system employs valvistors similar to that in [Jansson and Palmberg, 1990]. Using the non-linear control scheme the authors were able to decouple pressure and velocity and added that velocity feed-forward may be needed for the velocity to properly track the reference, as the pressure were able to follow the set reference of 1[MPa], the velocity showed discrepancies between the simulated and experimental values. This could according to the authors be attributed to a number of simplifications made where these are, neglecting friction in the model and considering the flow gain through the valve to be linear.

In [Kim Heybroek, 2008] the authors designed an open-circuit structure of four individually controlled propertional on/off valves. The authors distinguish which operating modes will enable the possibility of energy recuperation, which depends on the valve settings, where the control strategy relies on mode changing by actively controlling the valves and through these control for the velocity/flow and pressure.

2.2 Control Strategy

The benefit of SMISMO systems is the possibility of having two different control states which leads to many different possible combinations for control. The working principle is each valve can be used to control a state, e.g. the piston side valve can be used to control the flow/velocity whilst the rod side valve is used to control the rod side pressure in an example of velocity/pressure control. This section focuses on presenting the various combinations of control states and determine which of these appear most feasible. In a previous report by a student at AAU [Berthing, 2019], analysis of the different combinations was carried out for a SMISMO system similar to that of this report. In the report the author presents a figure that cross examines the different control states and determine which control states best fit together in terms of how feasible they are in terms of control, and also a discussion on the physical limitations of each combination. The meaning of the symbols in the figure are as following: horizontal line means it is an invalid control strategy, crooked line means its difficult to implement but possible and a cross means its a valid control strategy. The figure made with inspiration from said report is illustrated below:

x_{vp} \ x_{vr}	Q_p	Q_r	P_p	P_r	$\dot{x}_p$	x_p	Slave
Q_p	1. ⊖	2. ⊖	7. ⊘	7. ⊘	4. ⊖	4. ⊖	8. ⊘
Q_r	2. ⊖	1. ⊖	7. ⊘	7. ⊘	4. ⊖	4. ⊖	8. ⊘
P_p	7. ⊘	7. ⊘	1. ⊖	3. ⊖	9. ⊕	9. ⊕	6. ⊖
P_r	7. ⊘	7. ⊘	3. ⊖	1. ⊖	9. ⊕	9. ⊕	6. ⊖
$\dot{x}_p$	4. ⊖	4. ⊖	9. ⊕	9. ⊕	1. ⊖	5. ⊖	10. ⊕
x_p	4. ⊖	4. ⊖	9. ⊕	9. ⊕	5. ⊖	1. ⊖	10. ⊕
Slave	8. ⊘	8. ⊘	6. ⊖	6. ⊖	10. ⊕	10. ⊕	1. ⊖

Figure 2.1: Combination of control states [Berthing, 2019]

The figure serves as a reference for the control strategy analysis, which is compared to the analysis seen in [Berthing, 2019] to see if the same conclusion are made. The control state combinations are analysed by the number assigned to them.

1. Combinations designated with a **1.** are unattainable as the valves cannot control the same state. Furthermore, the purpose of SMISMO is it enables the possibility of controlling for an additional state, using both these to control for the same state invalidates the added control opportunities brought on by the additional valve. The same conclusion is reached by the author of [Berthing, 2019].

2. Controlling both flows with each input can prove difficult in the respect of attaining steady state. If say, the desired piston side flow is $10[\frac{l}{min}]$ but the desired rod side flow is $8[\frac{l}{min}]$ then through the steady state relation $\frac{Q_p}{A_p} \neq \frac{Q_r}{A_r}$ it shows that this is unattainable. In [Berthing, 2019] the author reaches a similar conclusion.

3. Controlling for both pressures simultaneously introduces similar problems as in point **2.**, where controlling for both pressures introduces problems in regards to attaining steady state. If the system is to achieve steady state then the following must hold that $\dot{p} = 0$, and if the desired piston side pressure is $100[bar]$ then due to coupling it would negate the possibility of controlling for the desired rod side pressure (e.g. $20[bar]$) as it is physically linked to the piston side pressure. If the two pressure are set at the desired values then, by way of calculating the force equilibrium it would be seen that steady state cannot be reached. In [Berthing, 2019] the author reaches a similar conclusion.

4. Controlling the velocity and flow simultaneously is not possible as they are proportional through the steady state relation $Q = \dot{x}_p A$. If the piston side flow is controlled at some arbitrary rate then it would yield a corresponding velocity meaning that the rod side valve would not be able to control for the velocity as intended. In [Berthing, 2019] the author reaches a similar conclusion.

5. Velocity and position control concurrent with each other is not possible as they are connected through integrals. If the desired velocity is set at some arbitrary value, then the other input would not be able to control for the desired position as they are dependent on one another, similar to that in point **4.**. In [Berthing, 2019] the author reaches a similar conclusion.

6. Introducing the slave function where the inputs are dependent on each other through some relation (i.e $x_{vr} = k_{relation} x_{vp}$). The valves control the flows into the cylinder and in turn some corresponding pressure drop occurs depending on the restriction imposed by the valve opening. Furthermore, the pressure gradient is positive or negative depending on the sign of the sum of flows ($\Sigma Q_p - \frac{\Sigma Q_r}{\alpha}$). So, the pressure levels would have to be controlled through the adjusting the flows. This could be difficult in terms of controlling for the pressure in the individual chambers, as the pressure levels are proportional to the valve openings which in turn are dependent on each other. In [Berthing, 2019] the author reaches a similar conclusion.

7. Controlling for both pressure and flow is a viable option, however as pointed out in [Berthing, 2019], flow meters are often only reliable within a certain flow range as they depend on the flow having a fully developed flow profile which can prove troublesome if the velocity of the fluid is lower than the range the flow meter can handle. Furthermore, flow meters with mechanical parts such as paddle wheels may be prone to wear over time [Nyberg, 2014].

8. Controlling for a slave function and the flow introduces similar problems as with the control strategy discussed in point **6.**. Where the flow on one side will be limited by the relation of the valve openings. It is therefore not preferred to use slave functions to control for either flow or pressure.

9. & **10.** The author of [Berthing, 2019], concludes that velocity & slave function control and pressure & velocity control are the most optimal control strategies. The inherent problem with using slave function to control the valve problem is that the respective flows and pressures on the secondary side is restricted by what is set as the valve opening on the primary side (using the relation in **6.** the primary side being the piston side). Due to this limitation control strategies using slave functions are disregarded.

The other valid control strategy is pressure & velocity control, where the benefit of this is that the pressure in either chamber can be controlled individually together with the control of the piston velocity. The most apparent benefit of controlling for the pressure is it ensures that the pressure level can be kept at a high enough level to ensure oil stiffness, and avoid cavitation. As this control strategy appear most feasible it is decided to use this when analysing the system

Conclusion on Choice of Controller

In previous literature, efforts on implementing control in SMISMO systems have largely been focused on decoupling efforts with SISO control and ELS schemes. Following the research revised in the literature review and based on the analysis of the different control strategies, there is an interest in designing controllers that has not been investigated for this control strategy, namely full state feedback controllers such as: pole placement/Full-state feedback (FSF), Full-state feedback integral (FSF-I), Linear-Quadratic-Regulator (LQR), Linear-Quadratic-Integrator(LQI) and Linear-Quadratic-Gaussian (LQG) controllers. Similar for these controllers is that they enable the possibility of re-locating the closed loop poles of the system, wherein a pole placement controller is manually tuned based on the desired closed loop poles and the Linear-Quadratic controllers makes use of an optimisation algorithm based on a cost function that is derived from the Ricatti equation.

It is recognised that LQG is a special case of H_2 control as noted in page 389 of [Sigurd Skogestad, 2005] and that H^∞ has already been implemented in previous literature to a SMISMO system as seen in [Pedersen et al., 2013]. However in the referenced article the authors recognize that the controllers were conservatively tuned and there were unknown discrepancies between the simulated and experimental values for both chamber pressures which the controllers were unable to adjust for due to the tuning. Therefore, it may be prudent to investigate whether more aggressive tuning is possible, thereby potentially reducing any error present at a faster rate which may lead to improved reference tracking. LQ-controllers are considered as they can be viewed as general MIMO controllers that provide a good first step into investigating whether MIMO control is at all feasible for the given setup.

3 | Problem Statement

The problem statement follows the research revised in the literature review, the analysis of control strategies and with the interest of designing MIMO controllers that have yet to be developed for a SMISMO scheme, the problem statement is formulated as follows:

"For a pressure/velocity control strategy, how does the chosen MIMO controllers compare in relation to performance when tracking a pre-defined reference set for the rod side pressure and piston velocity, when subjected to disturbance and noise."

In order to investigate the set problem, the following methodology is outlined which considers the main tasks of the project.

Methodology

1. Deriving the mathematical model describing the dynamics of the SMISMO scheme described in chapter 1.
    - The purpose of deriving the non-linear model, is to obtain the linearised model which is going to be used in the system analysis when describing the I/O couplings.
    - The linear model is needed when designing controllers which are later tested on the non-linear model in order to reflect for not accounted dynamics in the linear model.
2. Perform a system analysis taking its starting point in the analysis from [Berthing, 2019]. That report conducts an analysis of a similar SMISMO system as seen in this report.
    - Analysing the poles of the system to obtain an understanding on the change in system dynamics as a function of the piston position.
    - To perform coupling analysis with the purpose of determining the severity of the couplings, as they correspond to how the controllers are tuned. Besides that, the findings in the analysis relate to the choice of linearisation point used in the linear model.
3. Design and adjustment of MIMO controllers according to considerations which are based on results obtained from the system analysis.
    - The controllers are designed based on tuning parameters for LQ-control and pole locations for FSF, which relates to the desired system response.

4 Non-Linear Model of the Hydraulic System

In this chapter the mathematical model of the hydraulic system is outlined. This includes the governing equations of the hydraulic and mechanical system. The main purposes of presenting the governing equations of the system is to gain an understanding of the dynamics of the system, whether it is possible to simplify the model by making valid assumptions regarding the system and to obtain a linear model. The assumptions and simplifications considered before the modelling are presented below.

Assumptions

The model equations are derived based on these following assumptions.

1. The valve dynamics are assumed significantly faster than the system dynamics and are therefore disregarded.
2. Cylinder and hose leakage is neglected.
3. Hoses are stiff and lossless.
4. The density and temperature of the oil is assumed constant.
5. External force load is considered as an input to the system and looked as a disturbance.
6. The volumes are assumed constant around their linearisation point.
7. The pump is supplying flow with a constant pressure of 210[bar].

The assumptions are based on what has been done in prior research on similar systems, along with engineering intuition.

Firstly, as the dynamics of the proportional valves are significantly faster than the actuator dynamics, thus they will not affect the system and their impact is assumed negligible [Baratta and Rodellar, 1997] [MOOG, 2019]. This is further elaborated in Appendix C.

The cylinder and hose leakage is neglected as it is assumed that in a physical system that the fittings connecting the hoses to the hydraulic system are completely attached and allows no fluid through. This assumption was applied for a SMISMO system in [Yingjie Liu et al., 2009].

The hoses are assumed stiff and lossless. In a physical system an increase in pressure in the hoses could cause them to expand and reduce the stiffness of the oil, and if the hoses are of a short length the loss across them is assumed negligible.

The hydraulic oil density and temperature is assumed constant. In a physical system this may not be a valid assumption as with continued operation of the system the oil would heat up which would affect the density. This means the temperature would have to be measured at all times, to attain whether this assumption would hold.

The external force load is considered for the negative direction of the movement (i.e a pushing force) and is used as a disturbance input, because it is assumed to be of an unknown amplitude that is acting on the cylinder. This allows to test the model under different external force loads as it is not being the part of the system.

4.1 Proportional Valve Modelling

The proportional valves modelled are from MOOG with a nominal flow rate of $40[\frac{L}{s}]$ and a nominal pressure drop of $35[bar]$. The datasheet for which can be found in [MOOG, 2019]. It should be noted that the valves used on the meter-in and meter-out side are identical.

The flows through the valves are given by the following equations.

$$x_{v,n} \geq 0 \begin{cases} Q_p(x_{vp}) = x_{vp} \cdot k_v \cdot \sqrt{p_s - p_p} \cdot sign(p_s - p_p) \\ Q_r(x_{vp}) = x_{vr} \cdot k_v \cdot \sqrt{p_r - p_t} \cdot sign(p_r - p_t) \end{cases} \tag{4.1}$$

$$x_{v,n} < 0 \begin{cases} Q_p(x_{vp}) = x_{vp} \cdot k_v \cdot \sqrt{p_p - p_t} \cdot sign(p_p - p_t) \\ Q_r(x_{vr}) = x_{vr} \cdot k_v \cdot \sqrt{p_s - p_r} \cdot sign(p_s - p_r) \end{cases} \tag{4.2}$$

where:

k_v $= \frac{Q_n}{\sqrt{\Delta p_n}}$
p_s = Pump pressure [Pa]
p_t = Tank pressure [Pa]
p_p = Piston side pressure [Pa]
p_r = Rod side pressure [Pa]
Δp_n = Nominal pressure drop across valve [Pa]
Q_n = Nominal flow through the valve $[\frac{m^3}{s}]$
$x_{v,n}$ = Normalized valve displacement [-]

4.2 Actuator Expressions

Here, a summary of the forces acting on the actuator is given and the expressions for each are put in relation to one another to obtain the total expression in terms of Newton's 2nd law of motion. Also, the continuity equation will be applied when addressing the pressure changes within each chamber of the actuator.

4.2.1 Actuator Forces

The forces considered are seen in figures 4.1 and 4.2.

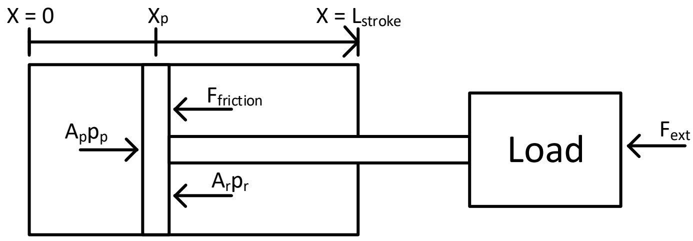

Figure 4.1: Horizontal Actuator

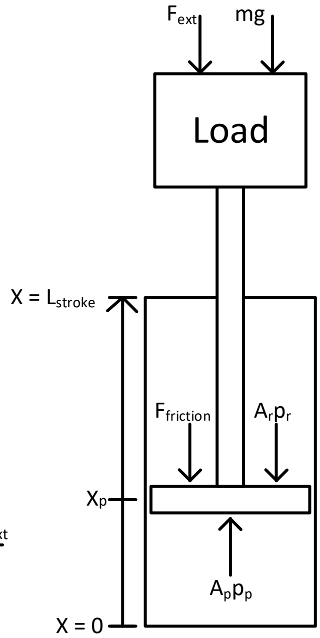

Figure 4.2: Vertical Actuator

From the figures the expressions for the total force exerted on the actuator is given for the horizontal case as:

$$m\ddot{x}_p = (A_p p_p - A_r p_r) - F_{friction} - F_{ext} \tag{4.3}$$

and for the vertical as:

$$m\ddot{x}_p = (A_p p_p - A_r p_r) - F_{friction} - F_{ext} - mg \tag{4.4}$$

where:

m	= Mass of piston and load [kg]
x_p	= Piston position [m]
$\ddot{x}_p$	= Piston acceleration [$\frac{m}{s^2}$]
A_p	= Piston side area [m^2]
A_r	= Rod side area [m^2]
p_p	= Piston side pressure [Pa]
p_r	= Rod side pressure [Pa]
$F_{friction}$	= Friction force [N]
F_{ext}	= Force exerted onto the load [N]
g	= Gravitational acceleration constant [$\frac{m}{s^2}$]

4.2.2 Pressure Gradients

The continuity equations 4.5 and 4.6 are utilised to account for the pressure changes in the piston and rod side of the chamber respectively. For the actuator the expressions are given as:

$$\dot{p}_p = \frac{\beta}{V_p} \cdot (Q_p - A_p \dot{x}_p) \tag{4.5}$$

$$\dot{p}_r = \frac{\beta}{V_r} \cdot (A_r \dot{x}_p - Q_r) \tag{4.6}$$

With:

$$V_p = \underbrace{(V_{dead,p} + V_{hose,p})}_{V_{p0}} + A_p x_p \tag{4.7}$$

$$V_r = \underbrace{(V_{dead,r} + V_{hose,r})}_{V_{r0}} + (x_{p,max} - x_p) A_r \tag{4.8}$$

Where:

β = Bulk modulus of hydraulic oil [Pa]
Q_p = Net flow through piston side orifice [$\frac{m^3}{s}$]
Q_r = Net flow through rod side orifice [$\frac{m^3}{s}$]
V_{dead} = Dead volume in cylinder [m^3]
V_{hose} = Volume of hoses connected to the cylinder [m^3]
V_{r0} = Total rod side dead volume [m^3]
V_{p0} = Total piston side dead volume [m^3]

4.2.3 Bulk Modulus

kThe bulk modulus refers to the compressibility of the hydraulic fluid within the system. The bulk modulus is computed with different levels of air content in the fluid mixture as it could have a significant impact on the dynamic performance of the system. Therefore the bulk modulus is modelled so as to see the effect it bears on the force exerted on the inertia load in the working pressure region. The expression for the bulk modulus is given as:

$$\beta_e = \frac{1}{\frac{1}{\beta_0} + \frac{\epsilon_{air}}{1.4(p_{atm}+p_{p,r})}} \quad , \quad \epsilon_{air} = \frac{1}{\frac{1-\epsilon_a}{\epsilon_a}\left(\frac{p_{atm}}{p_{atm}+p_{p,r}}\right)^{-\frac{1}{1.4}} + 1} \tag{4.9}$$

Where:

ϵ_a = Ratio of air in oil [-]
$p_{p,r}$ = Piston & rod side pressure respectively [Pa]
β_0 = Initial bulk modulus [Pa]

Using Eq. 4.9, the bulk modulus is computed as a function of pressure with different levels of air content in the fluid mixture and is illustrated in:

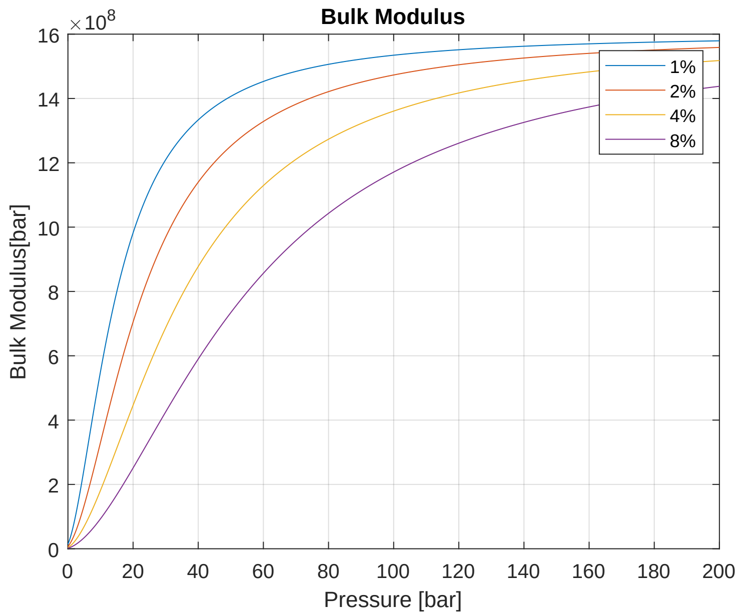

Figure 4.3: Bulk modulus as a function of pressure with different levels of air content

Here it can be seen that the bulk modulus is heavily affected by the amount of air content. In regards to determining the air content level to use in the model, the choice falls on $\epsilon = 1\%$ based on [Jing Wang, 2008], where the authors create a pressure-sealed reservoir connected to a pump that creates vacuum in the reservoir which lowers the air content in the oil to 1%. Similar efforts of degassing to reduce the air content were applied in [Hossein Gholizadeh, 2014], showing the possibility of achieving an undissolved air content of 1%. Furthermore, the level of dissolved air in the fluid is dependent on the pressure and assuming that the system operates mostly in the higher pressure region ($50[bar] <$), where the air content is $\approx 1\%$ it is deemed that $\epsilon = 1\%$ is a valid assumption when considering the project is a simulation study. However, should it turn out that this assumption does not hold and during operation the working and backside pressures are not operating in this region, analysis with changing bulk modulii may be carried out to observe whether the control is able to handle the effect thereof.

4.3 Friction Model

Friction occurs around any mechanical interfaces or when the moving parts move through some fluid. In the case of the actuator this involves the sliding between the rod and cylinder, as well as when the piston moves through the hydraulic fluid. In this simulation study a simplified friction model is employed, considering the coulomb and viscous friction. Each can separately be defined by the following expressions:

4.3.1 Coulomb Friction

For the Coulomb friction, the expression is given as:

$$F = F_c \cdot sign(\dot{x}_p) \tag{4.10}$$

With:

$$F_c = \mu N \tag{4.11}$$

Where:

μ = Coefficient of friction [-]
N = Normal force [N]

4.3.2 Viscous Friction

Viscous friction occurs as a body moves through a fluid. The expression for the viscous friction is given as:

$$F = B_v \cdot \dot{x}_p \tag{4.12}$$

Where:

B_v = Viscous friction coefficient
$\dot{x}_p$ = Piston velocity

4.4 Nonlinear Model Validation

In the validation of nonlinear model no experimental data is present, therefore an experiment has to be conducted to ensure that the model displays an expected behaviour. In this experiment piston is placed in fully extended position, and piston side valve is given a 10% opening to provide some flow into the chamber. In this case as velocity is equal to zero, and bulk modulus, volume is constant according to continuity equation 4.4 the relation between pressure gradient, flow should resemble linear behaviour.

$$\dot{p}_p = \frac{\beta}{V_p} \cdot (Q_p - A_p \dot{x}_p) \tag{4.13}$$

The pressure gradient and flow for the piston side are shown in figure 4.4.

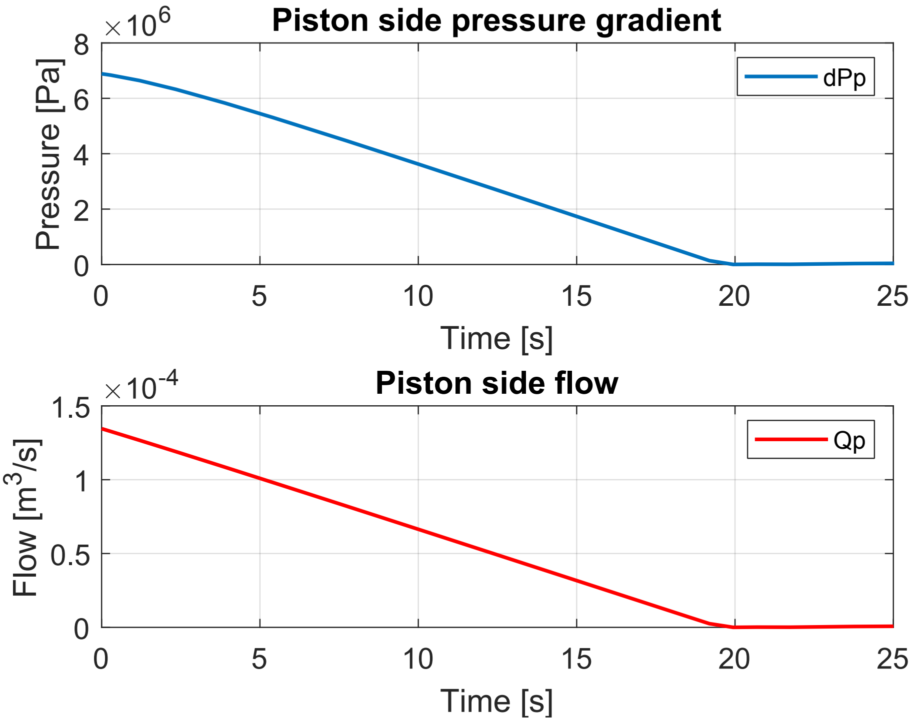

Figure 4.4: Comparison of pressure gradient and flow.

From the figure 4.4 it is seen that non-linear model shows the expected behaviour.

4.4.1 Steady State Analysis

The steady state analysis is used as part of the validation, where the steady state values are calculated analytically using the governing equations. Then compared against the steady state value observed in the model obtained through Simulink™. If the equations constituting the model are correctly applied in Simulink™, then the steady state values should match. The reasoning behind using only the steady state values is simply that determining the correct values during transient behavior is difficult.

The steady state calculations are based on these following equations:

$$Q_r = k_v x_{vr} \sqrt{|p_r - p_t|} sign(p_r - p_t) \tag{4.14}$$

$$Q_p = k_v x_{vp} \sqrt{|p_s - p_p|} sign(p_s - p_p) \tag{4.15}$$

$$\dot{x}_p = \frac{Q_p}{A_p} = \frac{Q_r}{A_r} \tag{4.16}$$

$$0 = p_p A_p - p_r A_r - B_v \dot{x}_p - F_c sign(\dot{x}_p) - F_{ext} \tag{4.17}$$

Where, equation 4.16 is the steady state relation between velocity and flow. Initially, there are 5 unknown variables: p_p, p_r, Q_p, Q_r, $\dot{x}_p$, granted that the flows and velocity are directly correlated with the surface areas. To enable the calculating of each of the steady state values, the number of unknowns should be reduced. This is performed in the following steps; equation 4.14 and equation 4.15 are substituted into equation 4.16 which yields:

$$\frac{k_v x_{vr} \sqrt{|p_r - p_t|}}{A_r} = \frac{k_v x_{vp} \sqrt{|p_s - p_p|}}{A_p} \tag{4.18}$$

This expression can be reduced if the valve openings are assumed fully open (i.e. $x_{vp} = 1$, $x_{vr} = 1$), removing k_v on both sides of the expression and for convenience keep the areas and pressures on opposite sides of the expression yields:

$$\frac{A_r}{A_p} = \frac{\sqrt{|p_r - p_t|}}{\sqrt{|p_s - p_p|}} \tag{4.19}$$

From here it is possible to calculate the steady state pressures for each chamber, using equation 4.19 and equation 4.17 leaves two equations with two unknowns. Computing these gives these values for the chamber pressures:

$$p_p = 36.75[bar] \quad p_r = 62.64[bar]$$

Having obtained these values they are used in equation 4.14 and equation 4.15 and from here the flows and velocity can be computed yielding:

$$Q_p = 1.48 \times 10^{-3}[\frac{m^3}{s}] \quad Q_r = 0.87 \times 10^{-3}[\frac{m^3}{s}] \quad \dot{x}_p = 0.096[\frac{m}{s}]$$

These values are compared against the values obtained through Simulink™. The flows and pressures obtained are seen in the figures below and the steady state values of the model and by analytical calculations are noted in table 4.1.

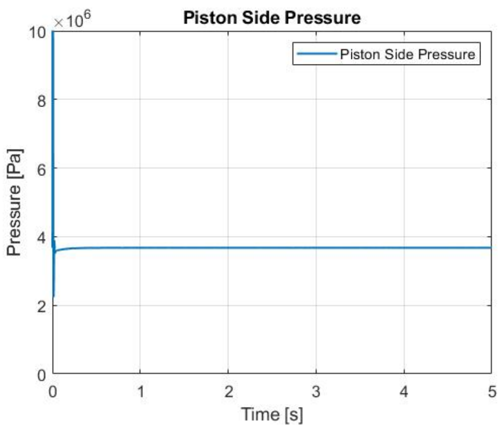

Figure 4.5: Steady State Piston side Pressure

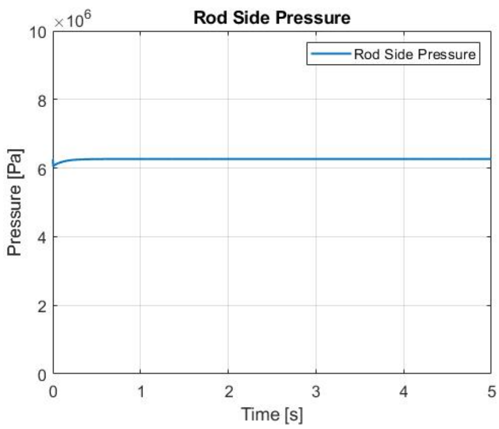

Figure 4.6: Steady State Rod side Pressure

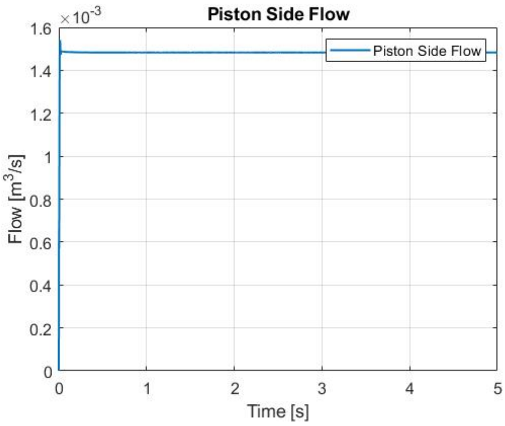

Figure 4.7: Steady State Piston side Flow

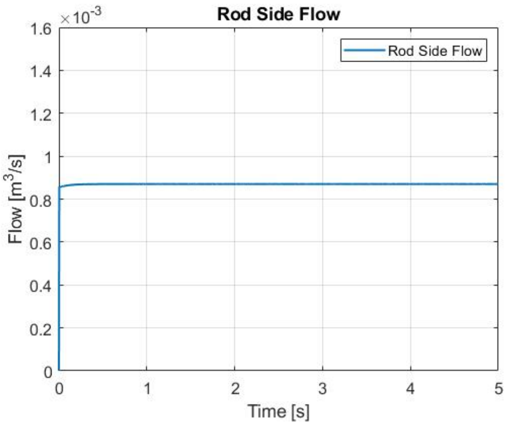

Figure 4.8: Steady State Rod side Flow

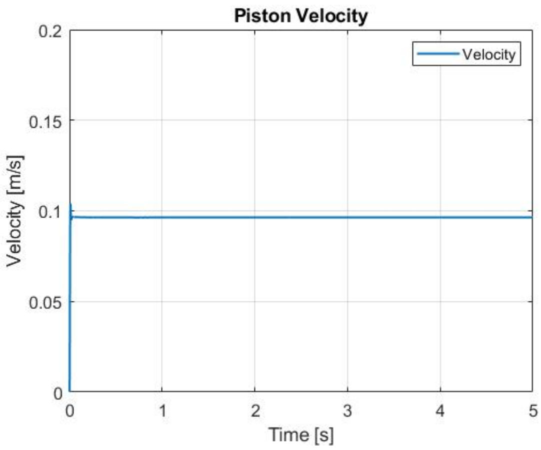

Figure 4.9: Steady State Piston Velocity

Comparison	p_p [bar]	p_r [bar]	$Q_p[\frac{m^3}{s}]$	$Q_r[\frac{m^3}{s}]$	$\dot{x}_p[\frac{m}{s}]$
Non-Linear	36.75	62.64	$1.48\ \times 10^{-3}$	$0.87\ \times 10^{-3}$	0.096
Analytical	36.75	62.64	$1.48\ \times 10^{-3}$	$0.87\ \times 10^{-3}$	0.096

Table 4.1: Parameters with steady state values

The steady state values between the analytical calculations and the non-linear model fit perfectly, which verifies that the equations are correctly implemented in Simulink™, as any discrepancy in the steady state values would indicate error in the model.

5 | Linear Model

In this chapter the linear model will be derived based on the governing equations of the non-linear model. Firstly, the derivation of the linear model will be discussed, then putting the model on state space form. Next, the considerations regarding the validation of the model as the project will only focus on simulations, and therefore not have experimental data to validate the results of the linear model. Lastly, a discussion about the choice of linearisation points and how to determine whether it represents the dynamics and steady state values sufficiently.

5.1 Linearisation

Linearisation is performed using first order Taylor expansion with respect to the variables, for each of the governing equations. It should be noted that both valves can operate with a negative or positive opening, where the pressures change in relation to the flow direction. Here it is decided to only derive the equations for the positive valve openings. Initially, the orifice equation for each valve is substituted into the equation describing the pressure gradients in both chambers yielding:

$$\Delta\dot{p}_p = \frac{\beta_p}{V_{p,0} + A_p x_p}(k_v \cdot x_{vp} \cdot \sqrt{|p_s - p_p|} \cdot sign(p_s - p_p) - A_p\dot{x}_p) \tag{5.1}$$

$$\Delta\dot{p}_r = \frac{\beta_r}{V_{r,0} + A_r(L_{stroke} - x_p)}(A_r\dot{x}_p - k_v \cdot x_{vr} \cdot \sqrt{|p_r - p_t|} \cdot sign(p_r - p_t)) \tag{5.2}$$

Then, in order to linearise the equations assumptions are made with the purpose of reducing the order of the model. This includes keeping the volumes and bulk modulus for each chamber constant. Keeping the volumes constant means it is no longer dependent on the piston position and therefore reduces the order of the model. After applying the assumptions in relation to the equations, the first order Taylor expansion is derived for each state and summed together yielding:

$$\Delta \dot{p}_p = \left.\frac{\partial \dot{p}_p}{\partial x_{vp}}\right|_0 \Delta x_{vp} + \left.\frac{\partial \dot{p}_p}{\partial p_p}\right|_0 \Delta p_p + \left.\frac{\partial \dot{p}_p}{\partial \dot{x}_{vp}}\right|_0 \Delta \dot{x}_{vp} \tag{5.3}$$

$$\Delta \dot{p}_r = \left.\frac{\partial \dot{p}_r}{\partial x_{vr}}\right|_0 \Delta x_{vr} + \left.\frac{\partial \dot{p}_r}{\partial p_r}\right|_0 \Delta p_r + \left.\frac{\partial \dot{p}_r}{\partial \dot{x}_p}\right|_0 \Delta \dot{x}_p \tag{5.4}$$

The linearisation constants used in the equation are as follows for the piston side:

$$\left.\frac{\partial \dot{p}_p}{\partial x_{vp}}\right|_0 = \frac{\beta}{V_{p0}}(k_v\sqrt{|p_s - p_p|}) = k_{xvp} \tag{5.5}$$

$$\left.\frac{\partial \dot{p}_p}{\partial p_s}\right|_0 = \frac{\beta}{V_{p0}}\left(\frac{k_v x_{vp}}{2\sqrt{|p_s - p_p|}}\right) = k_{psp} \tag{5.6}$$

$$\left.\frac{\partial \dot{p}_p}{\partial p_p}\right|_0 = \frac{\beta}{V_{p0}}\left(\frac{-k_v x_{vp}}{2\sqrt{|p_s - p_p|}}\right) = k_{ppp} \tag{5.7}$$

$$\left.\frac{\partial \dot{p}_p}{\partial \dot{x}_p}\right|_0 = \frac{-A_r\beta}{V_{r0}} = k_{\dot{x}_p p} \tag{5.8}$$

And for the rod side:

$$\left.\frac{\partial \dot{p}_r}{\partial x_{vr}}\right|_0 = \frac{\beta}{V_{r0}}(-k_v\sqrt{|p_r - p_t|}) = k_{xvr} \tag{5.9}$$

$$\left.\frac{\partial \dot{p}_r}{\partial p_t}\right|_0 = \frac{\beta}{V_{r0}}\left(\frac{-k_v x_{vr}}{2\sqrt{|p_r - p_t|}}\right) = k_{ptr} \tag{5.10}$$

$$\left.\frac{\partial \dot{p}_r}{\partial p_r}\right|_0 = \frac{\beta}{V_{r0}}\left(\frac{k_v x_{vr}}{2\sqrt{|p_r - p_t|}}\right) = k_{prr} \tag{5.11}$$

$$\left.\frac{\partial \dot{p}_r}{\partial \dot{x}_p}\right|_0 = \frac{A_p\beta}{V_{r0}} = k_{\dot{x}_p r} \tag{5.12}$$

The last equation to be linearised is Newton's 2nd law and is expressed as:

$$m\Delta \ddot{x}_p = \Delta p_p A_p - \Delta p_r A_r - \Delta \dot{x}_p B_v \tag{5.13}$$

Having defined the linear equations that outline the linear model, the model is placed in state space form.

5.2 System State Space Model

The system's state space representation can be defined by:

$$\dot{\bar{x}}_{sys} = \mathbf{A}_{sys}\bar{x}_{sys} + \mathbf{B}_{sys}\bar{u}_{sys} \tag{5.14}$$

$$\bar{y}_{sys} = \mathbf{C}_{sys}\bar{x}_{sys} + \mathbf{D}_{sys}\bar{u}_{sys} \tag{5.15}$$

Here noting that $D_{sys} = 0$, and bold indicates matrices and bar indicates vectors. The state space representation involves the state vector $x_{sys} = \begin{bmatrix}\dot{x}_p & p_p & p_r\end{bmatrix}^T$ and input vector $u_{sys} = \begin{bmatrix}x_{vp} & x_{vr}\end{bmatrix}^T$ together with the system and input matrix which is expressed as:

$$\mathbf{A}_{sys} = \begin{bmatrix} -\frac{B_v}{M} & \frac{A_p}{M} & -\frac{A_r}{M} \\ k_{\dot{x}_p p} & k_{ppp} & 0 \\ k_{\dot{x}_p r} & 0 & k_{prr} \end{bmatrix} \quad , \quad \mathbf{B}_{sys} = \begin{bmatrix} 0 & 0 \\ k_{xvp} & 0 \\ 0 & k_{xvr} \end{bmatrix} \tag{5.16}$$

The output matrix determines which states are used as output of the model, and is defined as:

$$\mathbf{C}_{sys} = \begin{bmatrix} 1 & 0 & 0 \\ 0 & 1 & 0 \\ 0 & 0 & 1 \end{bmatrix} \tag{5.17}$$

In the case where all the states are considered output.

5.3 Validation of Linear Model

In this section the method of validating the linear model is presented. This is based on comparison with the non-linear model, and determining how well the linear model represents the behaviour of the non-linear model. The comparison is utilised for cylinder in horizontal position when no gravitational force is present, and in the linearisation points, where the piston is placed in the middle position, valve openings are $x_{vp} = 0.5$, $x_{vr} = 0.25$, which results in steady state pressures and velocity that are used as a linearisation point. The validation of the model is conducted under given operating parameters which are presented in table 5.1. The non-linear model is given different control inputs for the hydraulic valves as seen in figure 5.1 to show what happens with the system moving away from the linearisation point. The validation of the model when valves are given negative input signals are presented in Appendix A.

Parameters used in linear model validation

Parameters	F_{ext} $[kN]$	m $[kg]$	x_{vp} $[\%]$	x_{vr} $[\%]$	$B_v[\frac{Ns}{m}]$	F_c $[N]$	$x_p[m]$
Values	100	12 $\times 10^3$	0.5-0.55	0.25	45 $\times 10^3$	200	0.928

Table 5.1: Parameters used in linear model validation

Valve openings for the hydraulic valves are presented in figure 5.1

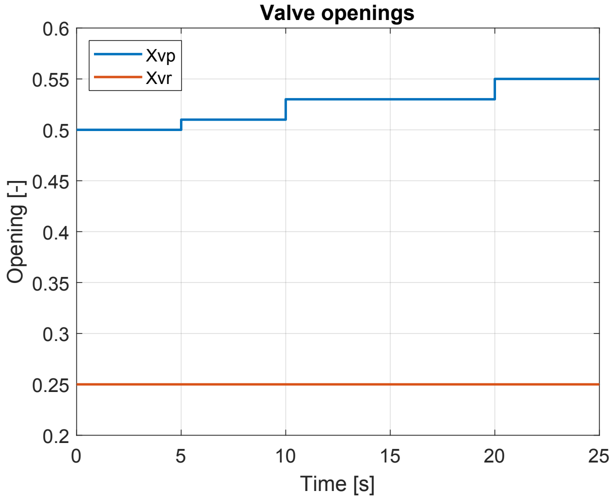

Figure 5.1: Valve openings

The comparison of position and velocity is shown in figures 5.2, 5.3.

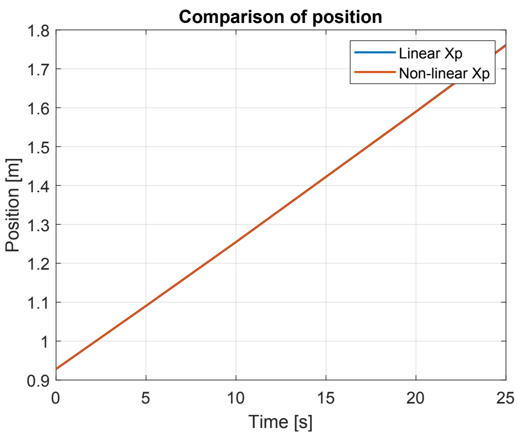

Figure 5.2: Comparison of Position

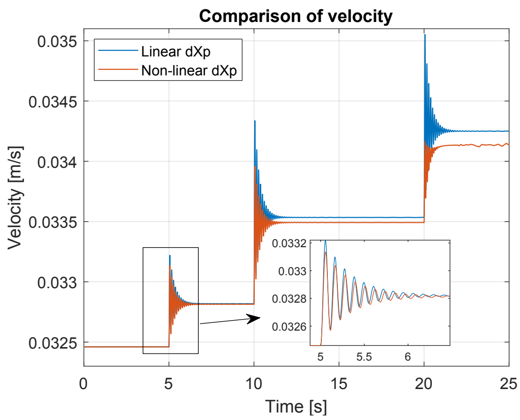

Figure 5.3: Comparison of Velocity

From the figure 5.2 can be noted that linear model follow non-linear precisely. The change in slope that appears with step is practically invisible, due to very small change in the velocity figure 5.3. At the first valve step, the non-linear model has an overshoot and reaches steady state after the linear model, which in and of itself does not constitute an error and both models appear to reach the same steady state value as expected as the system still operates near the linearised valve opening values. At the second valve step, a slight difference in steady state values occur but when considering that the application of the linear model is to design controllers, and considering the deviation is in the decimal range it is assumed that the linear model is still valid at this operating point. At the last valve step there is a more visible deviation, which is still at the decimal range and as such the linear model, at least regarding the velocity, fits the non-linear model sufficiently. The oscillations that are present in the velocity when the model is stepped have small magnitude maximum of ≈ 0.002 which are insignificant and would barely affect the system, since it is damped, due to larger volume of the cylinder.

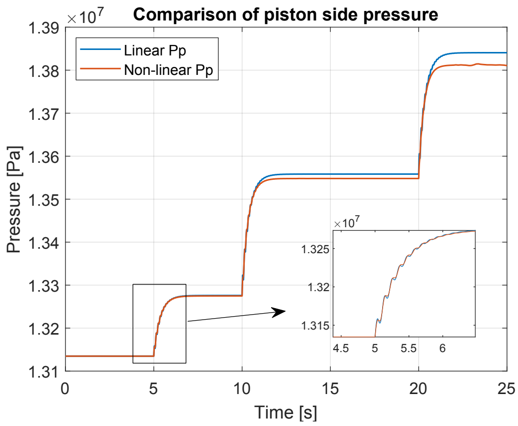

Figure 5.4: Comparison of Piston side Pressure

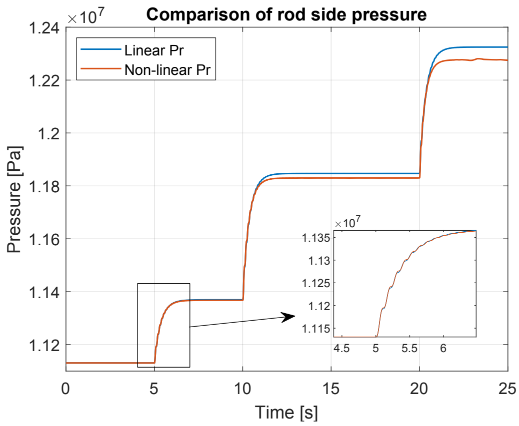

Figure 5.5: Comparison of Rod side Pressure

In Fig. 5.4 and 5.5, the pressure in each chamber is plotted for both the linear and non-linear models. The oscillations on the piston side and on the rod are present but have considerably small amplitude. In both figures the dynamic behaviour is seen for both models, where the linear accurately represent the transient of non-linear model. The models reach the same steady state values for the initial valve step and then increases in deviation as is expected when operating further away from the linearisation point. After the final valve step the deviation between the piston side pressures is $\approx 0.4[bar]$ and for the Rod side pressure the deviation is $\approx 0.4[bar]$. Considering then, the deviation between the initial piston side valve opening, which is the linearised valve opening, and the final valve opening is at 5% and the small discrepancies seen in the results for both the velocity and pressure, it is assumed that the linear model can be used when designing controllers.

6 | System Analysis

In this chapter the system analysis is conducted on the system presented in Chapter 1 and illustrated in Figure 6.1. The overall purposes of the system analysis is to gain an understanding of which control states would be best suited for control. In section 6.1 the natural frequency and damping is analysed depending on the piston position. In section 6.2 the coupling analysis is conducted to observe how coupled the system is and which state seems most prudent for control.

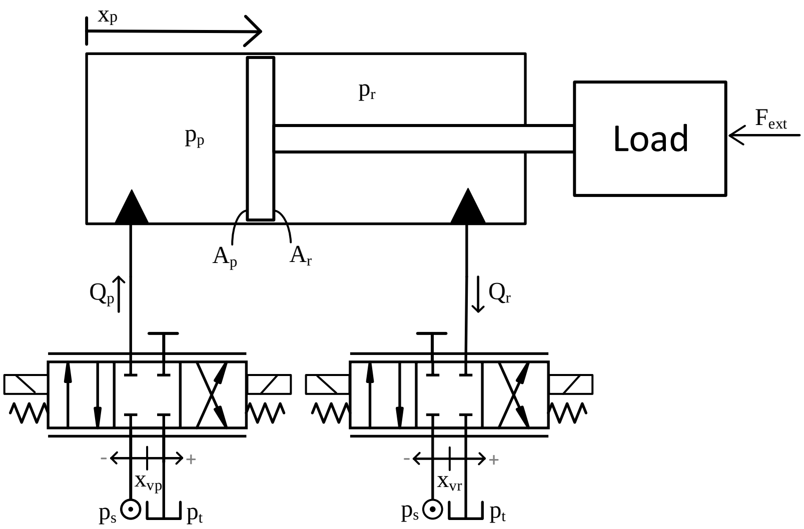

Figure 6.1: Separate Meter-In Separate Meter-Out System

This system analysis takes its starting point based on the previous work performed in [Berthing, 2019]. There, the different operating conditions are outlined in which cavitation and overpressure may occur for this type of system. Furthermore, an analysis of the control strategies that are possible and are best suited for control is conducted in the same report which serves as the starting point for this analysis, as mentioned previously.

6.1 Analysis of Damping Ratio and Natural Frequency

In this section poles of the system are analysed, and described in order to get a better understanding of the system dynamics. The analysis is conducted under different operating conditions to investigate how change of parameters such as velocity, and external force load are affecting the natural frequency, damping in the system. The analysis of investigated hydraulic system is considered for two main positions, and moving directions: horizontal, vertical, and positive, negative respectively. To guide the reader through this section the observations are presented in the following order. First, the horizontal position of the cylinder is presented together with corresponding table of parameters used to create a figure, following with an explanation of the made observations. Thereafter, presenting figure with cylinder placed in vertical position, and argumentation on seen changes. Secondly, the force load is increased, and new figures are given in respective order. Furthermore, the supplementary information is provided in Appendix A.2 to illustrate the change of damping ratio and natural frequency for the negative velocity.

Horizontal position

Parameters	p_p [bar]	p_r [bar]	F_{ext} [kN]	x_{vp} [%]	x_{vr} [%]	$\dot{x}_p[\frac{m}{s}]$	m [kg]
Values	77.7	20	100	0.356	0.583	0.03	12 $\times 10^3$

Table 6.1: Parameters used in analysis

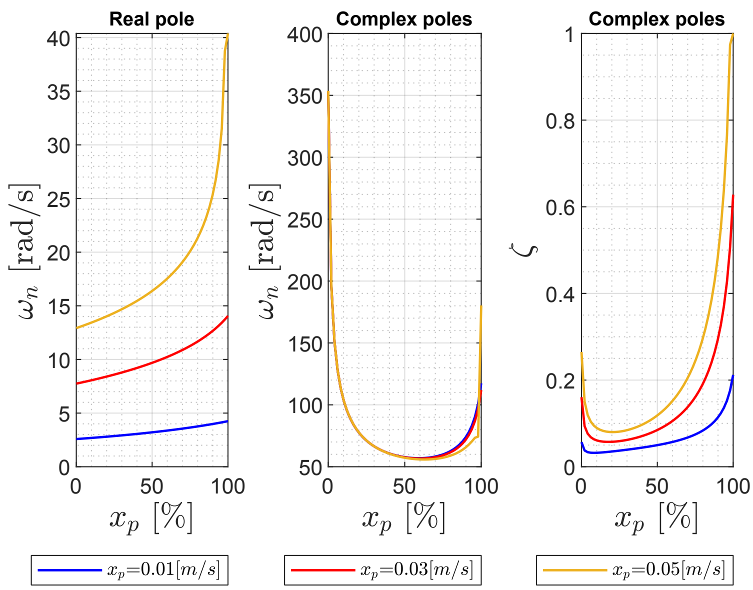

Figure 6.2: Damping ratio and natural frequency of poles for whole piston stroke with $F_{ext} = 100kN$, $p_r = 20bar$ in horizontal position

The frequency of poles is plotted as a function of the piston position in percentage illustrated in the figure 6.2. It is seen that curves of complex poles resemble the shape of a bathtub curve. Where in the first part it is observed that when piston is at the beginning the natural frequencies are considerably high, which results in faster frequency response. This is due to low volume of hydraulic fluid present in the cylinder's piston side chamber, which results in faster dynamics of pressure this can be seen in figure 6.6 with step response. The second part of the curve is when piston is in the middle position, which contributes in approximately constant rate of natural frequency and again by virtue of relatively close volumes in both chambers. Finally, the third part is when piston is approaching the end position resulting in increase of natural frequency.

Vertical position

Parameters	p_p [bar]	p_r [bar]	F_{ext} [kN]	x_{vp} [%]	x_{vr} [%]	$\dot{x}_p[\frac{m}{s}]$	m [kg]
Values	154.7	20	100	0.55	0.583	0.03	12 $\times 10^3$

Table 6.2: Parameters used in analysis for $\dot{x}_p = 0.03[\frac{m}{s}]$

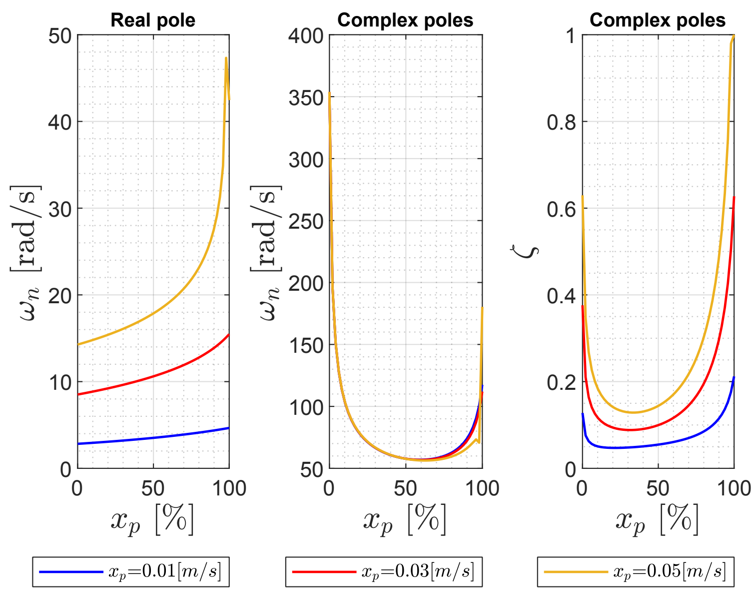

Figure 6.3: Damping ratio and natural frequency of poles for whole piston stroke with $F_{ext} = 100kN$, $p_r = 20bar$ in vertical position

From the figure 6.3 it is noted that response in horizontal position, and vertical is very similar, some deviations are seen in damping of the complex poles, they are slightly higher for the cylinder in vertical position. The explanation for this is due to gravitational force the pressure in piston side chamber, p_p, is higher then in horizontal position, which requires a larger valve opening, and more flow into the chamber corresponding to an increase in the volume and damping. The comparison of both positions is for purpose of understanding how severe the change of damping, and natural frequency in the system, due to contribution of gravitational force under the same external force load. Besides that, the parameters are affected quite significantly, the piston side pressure and valve opening increased approximately by half of the initial value.

Horizontal position with increased force load

Parameters	p_p [bar]	p_r [bar]	F_{ext} [kN]	x_{vp} [%]	x_{vr} [%]	$\dot{x}_p[\frac{m}{s}]$	m [kg]
Values	188.1	20	270	0.876	0.583	0.03	12 $\times 10^3$

Table 6.3: Parameters used in analysis

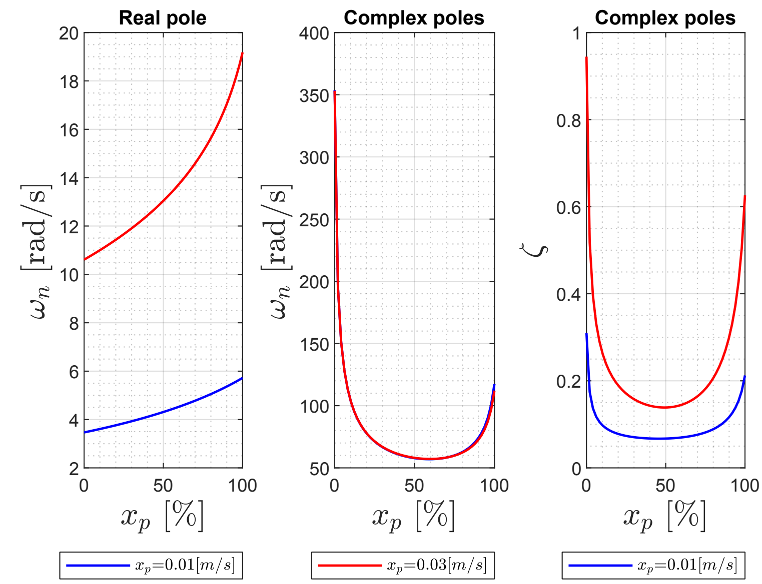

Figure 6.4: Damping ratio and natural frequency of poles for whole piston stroke with $F_{ext} = 270kN$, $p_r = 20bar$ in horizontal position

The objective of greatly increasing the force load is to comprehend the affect it has on the system dynamics. The figure 6.4 is illustrating consequence of increased external force load, it is indicating that higher force loads slightly affecting both the natural frequency and damping ratio. However, it is difficult to conclude what parameter have more influence on system dynamics since they are interlinked together. The change of external force load affects other parameters, and comparison can not be concluded under the same operating conditions. Overall contribution results in the increase in damping, and can be explained by that higher force load results in larger piston side valve opening, which increases flow in order to keep constant velocity of the piston, furthermore affecting pressure and stiffness of the fluid in the system. The velocity of $\dot{x}_p = 0.05$ is absent in the figure, because it is not achievable under high load operation since the valve is under dimensioned, and can not provide sufficient amount of flow to the chamber.

Vertical position with increased force load

Parameters	p_p [bar]	p_r [bar]	F_{ext} [kN]	x_{vp} [%]	x_{vr} [%]	$\dot{x}_p[\frac{m}{s}]$	m [kg]
Values	187.1	20	150	0.566	0.512	0.03	12 $\times 10^3$

Table 6.4: Parameters used in analysis

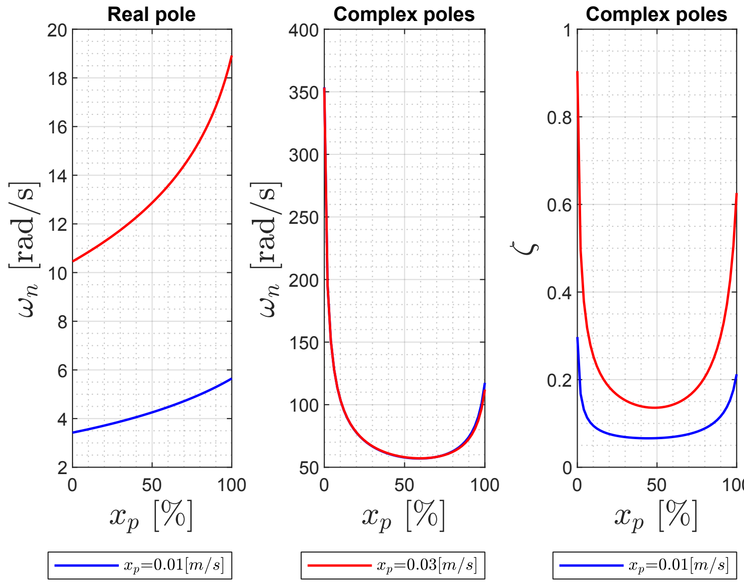

Figure 6.5: Damping ratio and natural frequency of poles for whole piston stroke with $F_{ext} = 150kN$, $p_r = 20bar$ in vertical position

The increase of force load for vertical position is presented in figure 6.5. It is observed that force load affects the system similarly to horizontal case, and there are practically no deviations from the figure 6.4, both cases are examined close to their extremes.

Step Response of the System

In order to verify results of the damping and natural frequency described above, the step is given to the piston side valve to illustrate the actual response of the system. The steps from simulation are made for different piston positions the parameters used to create figures are presented in the table 6.5 below.

Step for horizontal position

Parameters	p_p [bar]	p_r [bar]	F_{ext} [kN]	x_{vp} [%]	x_{vr} [%]	$\dot{x}_p[\frac{m}{s}]$	m [kg]
Values	77.7	20	100	0.356	0.583	0.03	12 $\times 10^3$

Table 6.5: Parameters used in analysis

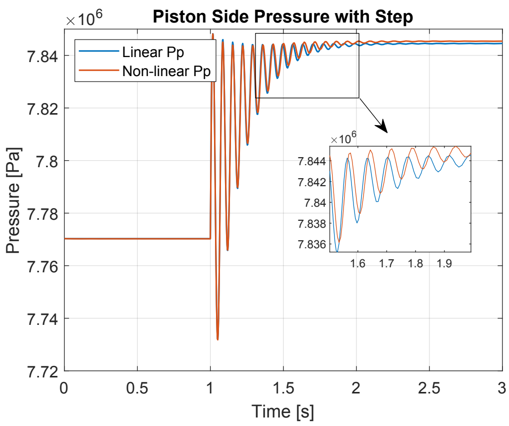

Figure 6.6: Step with $x_p = 0.185m$

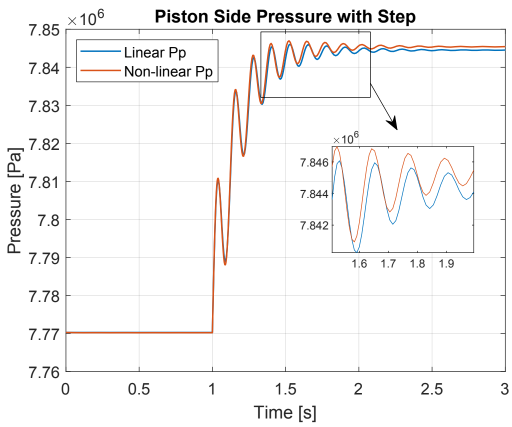

Figure 6.7: Step with $x_p = 0.928m$

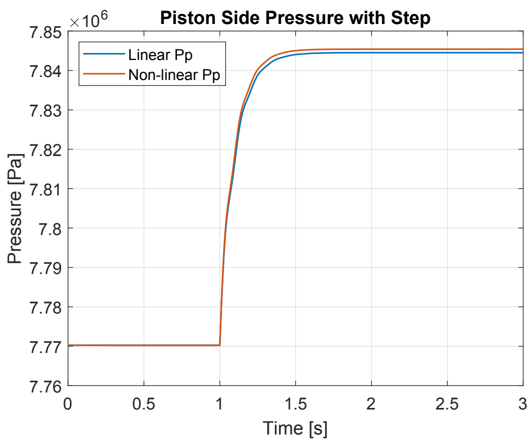

Figure 6.8: Step with $x_p = 1.67m$

From the first figure 6.6 it is seen that response resembles the second order system with oscillations of $\omega_n = 103.9[\frac{rad}{s}]$, which corresponds both with figure 6.2, and A.20.

The second figure 6.7 has less oscillations, indicating decrease of natural frequency and increase of damping ratio as volume is increasing, which again correlates with the results of both figures 6.2, A.22 where conjugate poles move closer to the origin, and have natural frequency of $\omega_n = 57.06[\frac{rad}{s}]$.

Finally, observing the last figure 6.8 with piston close to the end position, it is seen that response resembles the first order system. It could be explained looking at the figure A.22 the real pole is moved closer to origin and has a dominant affect on system dynamics. This results in higher damping and significantly less oscillatory response. This demonstrates that analysis is without an error, both numerical and analytical method showed the same results.

6.2 Coupling Analysis

In this section an analysis of the coupling in the system is carried out, to observe any couplings there may be, in spite of having already decided on using a MIMO control strategy. Along with the interest of finding out how severe the hydraulic system is coupled, the RGA (Relative Gain Array) can be used to determine how conservative the controllers have to be adjusted to avoid possible errors that occur as a result of the system couplings. The interest in doing RGA is also to gain an understanding of how different system parameters affect the couplings and which parameters have the most impact. In doing the coupling analysis, RGA will be conducted for different operating conditions. Another measure used in the coupling analysis is SVD (Singular Value Decomposition) which all together tells about the interaction between the I/O couplings and the feasibility of implementing control.

6.2.1 Relative Gain Array

A consequence in MIMO systems where there are multiple inputs and corresponding outputs is that an input may have an indirect effect on other outputs, where ideally an input would only effect the corresponding output. In the SMISMO system analysed an indirect effect would be if opening the piston side valve to allow flow to enter the cylinder, then it would result in a change in the rod side pressure which is not directly controlled by the piston side valve, ergo an indirect effect. The RGA contains the relative gain between input (j) and output (i) for all frequencies, and from the RGA it can be determined which I/O pairings would be most suited when applying control. In regards to the system, analysed inputs are the valve openings on both piston and rod side, and the controlled states are the piston and rod side pressure as well as the velocity.

The RGA, in the case where there are two I/O pairings, is expressed as:

$$RGA(G) = G \circ (G^{-1})^T = \begin{bmatrix} \lambda_{1,1} & \lambda_{1,2} \\ \lambda_{2,1} & \lambda_{2,2} \end{bmatrix}_{i \times j} = \begin{bmatrix} \lambda_{1,1} & 1-\lambda_{1,1} \\ 1-\lambda_{1,1} & \lambda_{1,1} \end{bmatrix}_{i \times j} \tag{6.1}$$

Where, $\circ$ denotes the Hadamard product or element-by-element multiplication and $\lambda_{i,j}$ is the relative gain between the various I/O pairings. Due to algebraic properties in the RGA it can be rewritten such that the diagonal entries can be defined as the I/O pairing between input 1 and output 1 (i.e. $\lambda_{1,1}$) and the off-diagonal is 1 subtracted from ($\lambda_{1,1}$). This is possible as the rows and columns of the RGA summed is equal to one. This gives that the RGA of a perfectly decoupled system would be the identity on either the diagonal or off-diagonal, which indicates there is no cross-coupling present, assuming that all dynamics are accounted for in the model. From the entries in the RGA it can be determined which coupling would be more prudent to apply when designing control. If the RGA is identity on the diagonal then the best I/O coupling to control would be $y_1(u_1)$,$y_2(u_2)$ and conversely if the RGA is identity on the off-diagonal then $y_1(u_2)$,$y_2(u_1)$ should be the I/O couplings that are used when designing controllers [Sigurd Skogestad, 2005].

As coupling in the system is dependent on frequency and control state it is essential to investigate the system under different operating conditions and parameters variations. When observing the RGA for different conditions a starting point is established that will serve as a reference when changing the different linearisation points. From the reference values, one linearisation point is changed at a time to see the effect it has on the coupling and the cross-over frequency. The variables that are going to be varied to see the affect on coupling, and system dynamics are: force load, inertia, piston position, velocity, the rod side pressure. The starting point values for RGA analysis are: $F_{ext} = 100[kN]$, $x_p = 0.985[m]$, $\dot{x}_p = 0.03[\frac{m}{s}]$, $M = 12 \times 10^3[kg]$, $P_r = 20[bar]$. The fitting parameter such as viscous friction used in analysis for all simulations is chosen to be $B_v = 45 \times 10^3[\frac{Ns}{m}]$. The starting point values for each parameter are chosen to be an average of maximum capabilities of the modelled system, and varied close to their extremes.

The RGA analysis is conducted considering cylinder in two positions: horizontal, vertical, and can be found in Appendix - A.3, A.4 respectively. In many hydraulic applications cylinder is placed in between these two positions, and contribution from gravitational force has a significant affect on the system, and has to be accounted. Furthermore, the effect of moving both directions: positive, and negative is considered in order to investigate change of coupling. The interaction between I/O pairings when primary control state is changed to a secondary is examined to decide which of the states would result in better controllability.

In Appendix - A.4 when cylinder is placed in vertical position, figures with parameters that have the most impact on the system are presented. Since it was observed that parameter variation in horizontal position have similar tendency in the effect it imposes on system dynamics. Additionally, in both appendixes secondary control state, P_p, is presented only for one position of the piston under certain operating conditions, considering that it showed the same performance for other parameter variations.

The observations from the RGA analysis are presented in order of having highest affect on coupling, and listing the effect of each change in a specific parameter on the coupling and system dynamics:

- **Position of the Piston, $\mathbf{x_p}$**: The change of position of the piston have highest affect on the system dynamics and coupling. Based on disposition of the piston the volume in the chambers varies significantly affecting natural frequency, and damping ratio, which was discussed in the section above 6.1. Depending on operating parameters the coupling varies but in the most cases the system is less coupled in the beginning of operation when the volume in the chamber is lowest. With piston moving towards the end position severe coupling appears, where diagonal, and off-diagonal intersect indicating coupled dynamics and control difficulty in certain frequency range. This can be seen in figures below for three different piston operating positions.
- **External Force Load, $\mathbf{F_{ext}}$**: The external force load in horizontal position is varied from $F_{ext} = 0[kN]$ to $F_{ext} = 270[kN]$. The increase of force load resulted in higher RGA number and element, and a stronger coupling in all frequency range. This can be seen in figures presented below for horizontal position. From observation when the

cylinder is placed in vertical position it is slightly harder to control, due to increased forces in the system this can be seen in figures A.101, A.107. Examining the system moving negative direction coupling appears to be more severe, RGA elements and numbers are significantly higher indicating control difficulty, figures with the coupling results are provided in Appendix A.3.

Horizontal position change of Force Load

Parameters	p_p [bar]	p_r [bar]	F_{ext} [kN]	x_{vp} [%]	x_{vr} [%]	$\dot{x}_p[\frac{m}{s}]$	m [kg]
Values	77.7	20	100	0.356	0.583	0.03	12 $\times 10^3$
Values	188.1	20	270	0.876	0.583	0.03	12 $\times 10^3$

Table 6.6: Parameters used in RGA analysis

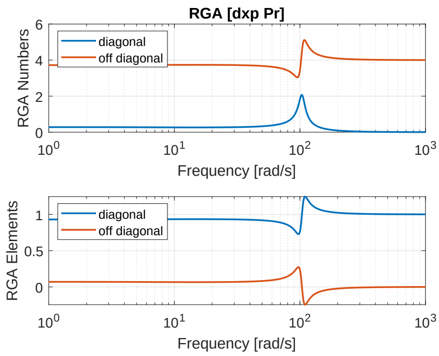

Figure 6.9: RGA for x_p=0.185m, $F_{ext} = 100kN$

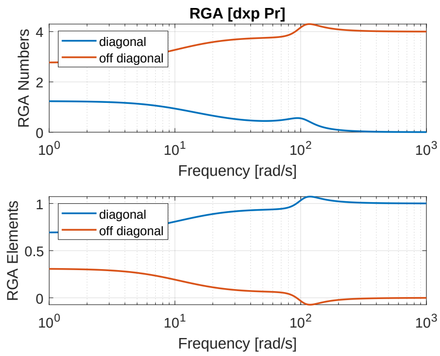

Figure 6.10: RGA for x_p=0.185m, $F_{ext} = 270kN$

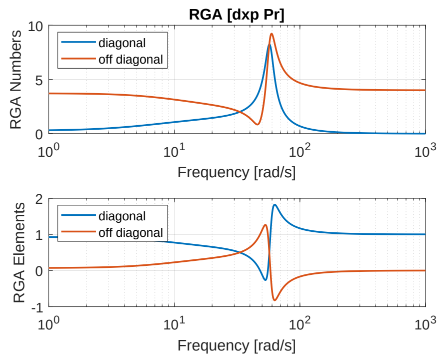

Figure 6.11: RGA for x_p=0.928m, $F_{ext} = 100kN$

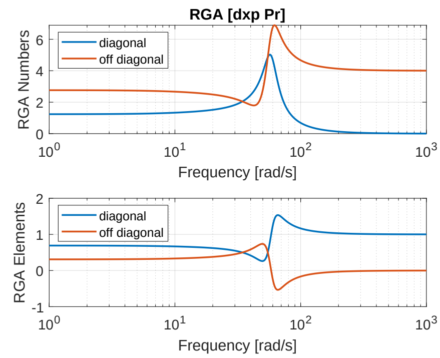

Figure 6.12: RGA for x_p=0.928m, $F_{ext} = 270kN$

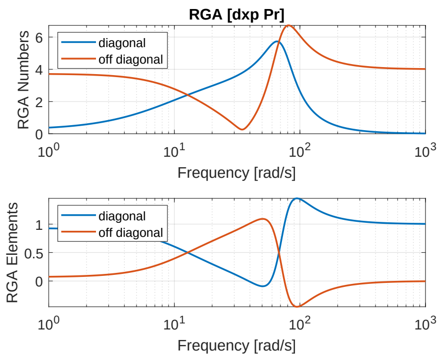

Figure 6.13: RGA for x_p=1.67m, $F_{ext} = 100kN$

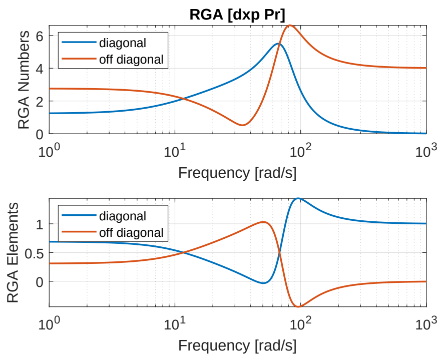

Figure 6.14: RGA for x_p=1.67m, $F_{ext} = 270kN$

- **Mass, m**: The change of mass from $m = 1 \times 10^3[kg]$ to $m = 20 \times 10^3[kg]$ affected the natural frequency and damping ratio. In regards to coupling the RGA elements and numbers more or less remained the same in magnitude, however with higher mass system is much slower, and the intersection of diagonal, off-diagonal appeared earlier. Considering cylinder in vertical position the affect of mass would exhibit the same effect on system dynamics, and therefore not presented in the report. The figures with observations are presented below 6.15, 6.16.

Horizontal position change of Mass

Parameters	p_p [bar]	p_r [bar]	F_{ext} [kN]	x_{vp} [%]	x_{vr} [%]	$\dot{x}_p[\frac{m}{s}]$	m [kg]
Values	80.6	25	100	0.36	0.51	0.03	1 $\times 10^3$
Values	80.6	25	100	0.36	0.51	0.03	20 $\times 10^3$

Table 6.7: Parameters used in RGA analysis

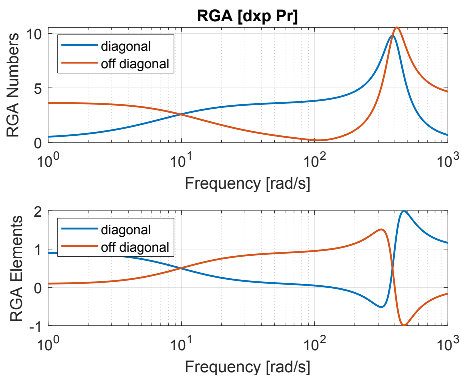

Figure 6.15: RGA for x_p=0.928m, $m = 1 \times 10^3$

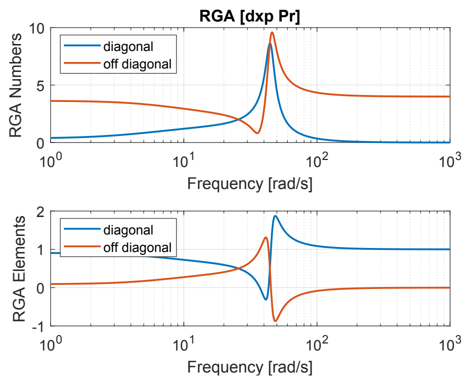

Figure 6.16: RGA for x_p=0.928m, $m = 20 \times 10^3$

- **Rod Side Pressure, $\mathbf{p_r}$**: The rod side pressure is set constant and varied from $p_r = 20[bar]$ to $p_r = 30[bar]$, from observations the change of pressure does not have significant affect on the coupling. With higher pressure the RGA numbers and elements increase marginally, the damping ratio is affected, and increase with higher pressure. This tendency of rising damping ratio can be seen in Appendix 6.2.1 from pole/zero map, when the real pole is moving closer to origin.

Horizontal position change of Rod Side Pressure

Parameters	p_p [bar]	p_r [bar]	F_{ext} [kN]	x_{vp} [%]	x_{vr} [%]	$\dot{x}_p[\frac{m}{s}]$	m [kg]
Values	77.7	20	100	0.356	0.583	0.03	12 $\times 10^3$
Values	83.5	30	100	0.364	0.462	0.03	12 $\times 10^3$

Table 6.8: Parameters used in RGA analysis

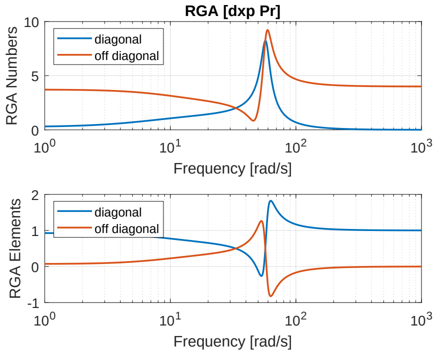

Figure 6.17: RGA for x_p=0.928m, $p_r = 20bar$

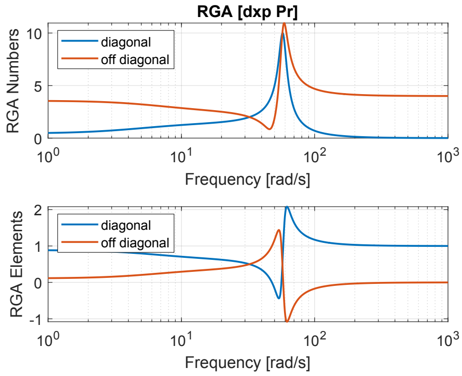

Figure 6.18: RGA for x_p=0.928m, $p_r = 30bar$

- **Velocity, $\dot{\mathbf{x}}_\mathbf{p}$**: From observation it is found out that it is harder to control for low velocity, which results in higher RGA numbers and elements. When applying negative velocity the coupling changes as the system dynamics, in this case controlling for negative velocity is more difficult as it results in more severe coupling 6.21, 6.22. In vertical position the change of velocity showed the similar manner.

Horizontal position change of Velocity

Parameters	p_p [bar]	p_r [bar]	F_{ext} [kN]	x_{vp} [%]	x_{vr} [%]	$\dot{x}_p[\frac{m}{s}]$	m [kg]
Values	77.1	20	100	0.118	0.194	0.01	12 $\times 10^3$
Values	78.2	20	100	0.595	0.971	0.05	12 $\times 10^3$

Table 6.9: Parameters used in RGA analysis

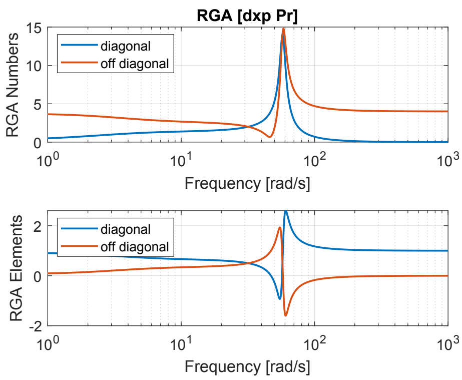

Figure 6.19: RGA for x_p=0.928m, $\dot{x}_p = 0.01\frac{m}{s}$

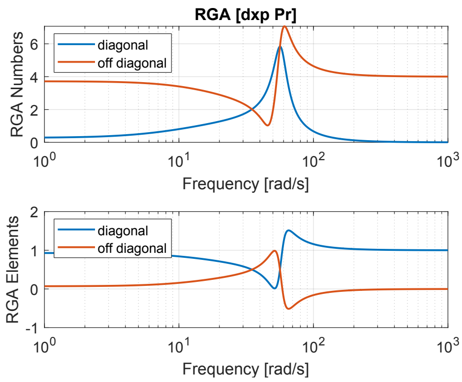

Figure 6.20: RGA for x_p=0.928m, $\dot{x}_p = 0.05\frac{m}{s}$

The increased difficulty in control is a result of the contribution from the external force load, as for the negative velocity it is along the motion of the piston.

Horizontal position Negative Velocity

Parameters	p_p [bar]	p_r [bar]	F_{ext} [kN]	x_{vp} [%]	x_{vr} [%]	$\dot{x}_p[\frac{m}{s}]$	m [kg]
Values	80	26.3	100	-0.15	-0.06	-0.01	12 $\times 10^3$
Values	80	28.3	100	-0.78	-0.29	-0.05	12 $\times 10^3$

Table 6.10: Parameters used in RGA analysis

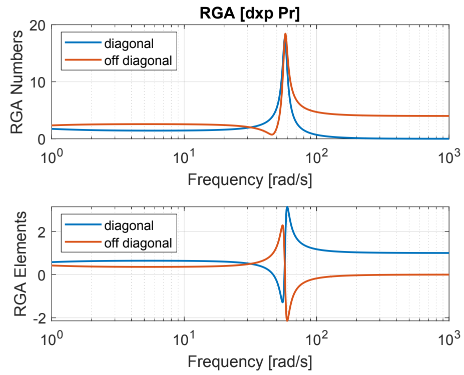

Figure 6.21: RGA for x_p=0.928m, $\dot{x}_p = -0.01[\frac{m}{s}]$

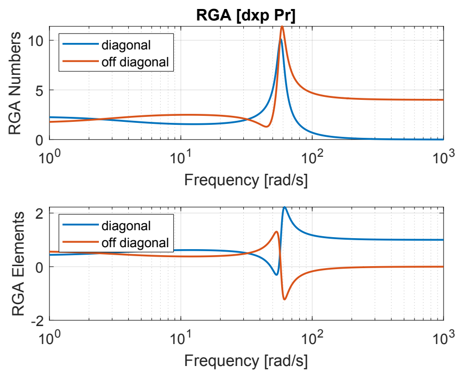

Figure 6.22: RGA for x_p=0.928m, $\dot{x}_p = -0.05[\frac{m}{s}]$

Based on the findings in sections 6.1 & 6.2.1 the linearisation points considered for the middle operating conditions are presented, and explained below, table 6.11.

Chosen linearisation points

Parameters	p_p $[bar]$	p_r $[bar]$	F_{ext} $[kN]$	x_p $[m]$	x_{vp} [%]	x_{vr} [%]	$\dot{x}_p[\frac{m}{s}]$	m $[kg]$
Values	77.7	20	100	0.928	0.356	0.583	0.03	12 $\times 10^3$

Table 6.11: Linearisation points

Based on analysis the change of rod side pressure has minor effect on the coupling. The effect of the increased pressure is a slight change in the damping of the system, based on observation seen in pole/zero maps 6.2.1. The reason for having rod side pressure, $p_r = 20[bar]$, is made in order to make the system more efficient, by keeping the back-pressure as low as possible without affecting the stiffness of the oil too much, where the relation between pressure and bulk modulus can be seen in figure 4.3. A force load of $F_{ext} = 100[kN]$ is chosen since it is close to the average load that the system can handle, and would be interesting to investigate under moderate operating conditions. A position of the piston is chosen $x_p = 0.928[m]$, as most of the coupling appears there, and operation may occur more frequently around the middle position rather the fully extended and retracted positions. The velocity is set to $\dot{x}_p = 0.03[\frac{m}{s}]$, which is again an average of what the system can achieve, in order to have rod side pressure of $20[bar]$. With the same consideration mentioned the mass was chosen to be $m = 12 \times 10^3[kg]$.

The RGA analysis figures with the chosen linearisation points are presented for both control states to evaluate coupling more detailed.

Chosen linearisation points

Parameters	p_p [bar]	p_r [bar]	F_{ext} [kN]	x_{vp} [%]	x_{vr} [%]	$\dot{x}_p[\frac{m}{s}]$	m [kg]
Values	77.7	20	100	0.356	0.583	0.03	12 $\times 10^3$

Table 6.12: Parameters used in RGA analysis for both control states

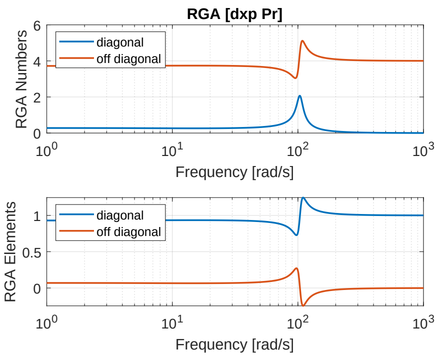

Figure 6.23: RGA at x_p=0.185m

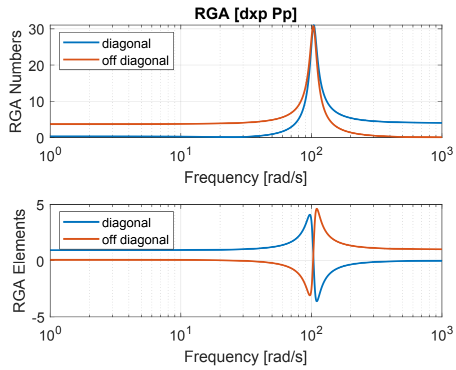

Figure 6.24: RGA at x_p=0.185m

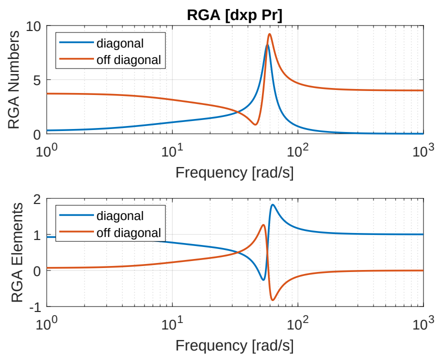

Figure 6.25: RGA at x_p=0.928m

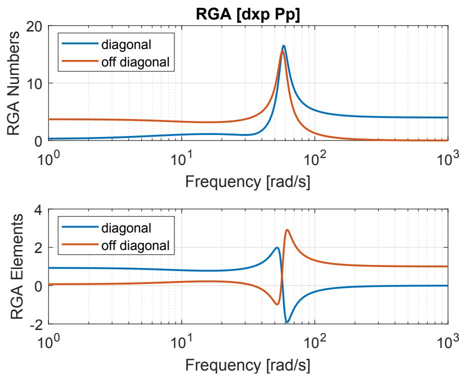

Figure 6.26: RGA at x_p=0.928m

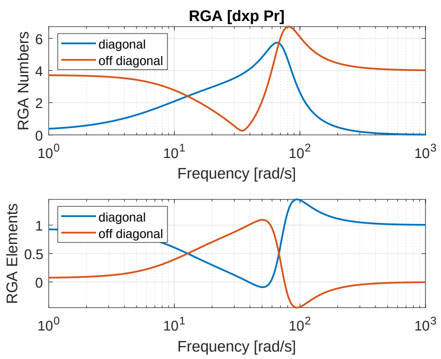

Figure 6.27: RGA at x_p=1.67m

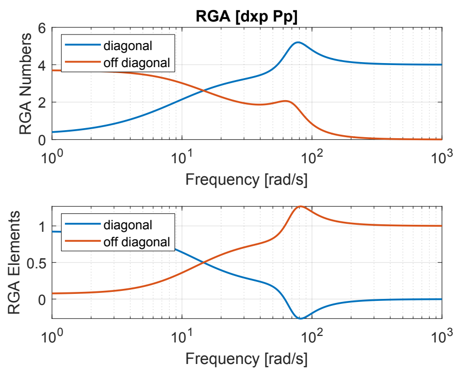

Figure 6.28: RGA at x_p=1.67m

From observation it is seen that at the start position of the piston the coupling is more severe for secondary control state, the RGA number at frequency around 100 $[\frac{rad}{s}]$ is above

30 indicating that it will be difficult to control the system. While the RGA elements of diagonal, off-diagonal intersect, and switched places indicating that input would affect different output. The primary control state at the same frequency is less coupled and would result in better controllability.

At the middle position the coupling for both control states is severe, and it is difficult to argue which state would be the better choice. Since in both cases the pre-compensator would be applied to remove unwanted coupling. The primary control state have lower RGA number below 10, while the secondary state have around 16, which still indicates difficulty in controlling for both states. However, the coupling appears at lower frequencies with the intersection around $30[\frac{rad}{s}]$, while the secondary state is mostly decoupled until $60[\frac{rad}{s}]$, which makes the bandwidth higher. In addition, the secondary control state results in cross-coupled dynamics which is always unwanted, while the primary state is only coupled. Finally, at the end position coupling is still severe, and appears approximately at the same $13[\frac{rad}{s}]$ frequencies for both states, which indicates that system response becomes slower. For control purpose of keeping back-pressure constant the primary state is chosen, since it has no cross-coupling and for both cases the pre-compensator has to be applied.

In the next subsection 6.2.2 the singular value decomposition analysis is conducted and presented.

6.2.2 Singular Value Decomposition

As discussed previously, in MIMO systems the input and output are vectors with corresponding magnitude and direction. What is of note, is that the input changes as a function of frequency and by definition so does the gain of the system. To determine the degree of directional dependence between the input and output vectors, SVD is applied to the system matrix G, expressing it as:

$$G = W \Sigma V^H \tag{6.2}$$

The maximum and minimum singular values are of special interest, and can be found by the following expression:

$$\bar{\sigma} = \sqrt{\lambda_{max}(G^H G)} \quad , \quad \underline{\sigma} = \sqrt{\lambda_{min}(G^H G)} \tag{6.3}$$

Where, the maximum singular value can be said to describe the amplification of an input and conversely the minimum singular value attenuates the input. Finding the maximum and minimum singular values is important in that the degree of directional dependency can be found in the ratio between the two, also known as the condition number expressed by:

$$\gamma = \frac{\bar{\sigma}}{\underline{\sigma}} \tag{6.4}$$

Where ideally the condition number is $= 1$, and if $\bar{\sigma} >> \underline{\sigma}$ the system is ill-conditioned, and measures may be needed to counteract the directional dependence. The figure with the maximum and minimum singular values as a function of the frequency is presented below 6.29.

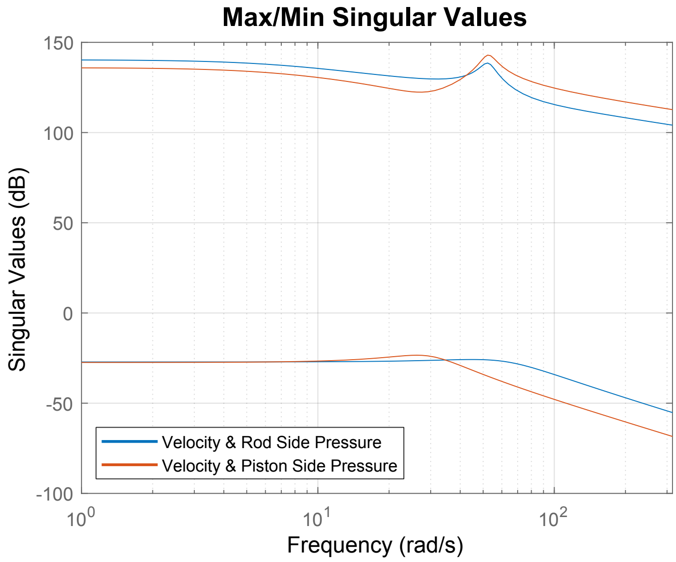

Figure 6.29: Singular values for velocity & piston/rod side pressure

From the SVD it is seen that when operating in the lower frequency range, $[0 - 100\frac{rad}{s}]$, it is difficult to conclude on which control state to control for since the difference in condition number is low.

7 | Controller Design

In this chapter the design of the chosen MIMO controllers along with the results showing their respective reference tracking capabilities is presented and ultimately compared to attain which of these show the best tracking ability. In section 7.1, the criteria in which the comparison between the controllers is based on are outlined. In section 7.2 the considerations regarding the tuning of the controllers and what factors that may influence this. Then between sections 7.3-7.9 the design procedures and results for each controller is presented, and lastly they are compared in the linear model. Then from sections 7.10-7.10.2 the controllers obtaining the best performance are compared for the non-linear model.

7.1 Criteria used for Controller Comparison

In this section the controller criteria used when evaluating and comparing the designed controllers is outlined. These are chosen based on the performance criteria used in SISO control, such as: Rise time, settling time, steady state error, overshoot. Furthermore, the criteria are also based on the controllers ability to handle disturbances, and its sensitivity to parameter changes. There are no specifications regarding how the controllers should perform, as this project focuses on the comparison of the controllers and not necessarily achieving excellent results, but merely to see how the controllers perform for the given system. Tests are conducted with emphasis on comparing the controllers in respect to each criteria stated below:

1. Overall performance of the controller for velocity tracking
2. Disturbance rejection
3. Sensitivity to parameter changes

In regards to how the controller are compared, the tracking capabilities of each controller is shown for the linear model. Then the 2-3 controllers showing the best tracking ability in the linear model, are tested and results are presented for the controller performance in the dynamic model for both the horizontal and vertical case. Lastly, the controllers showing the best performance are then tested in a sensitivity analysis where the parameters that have the most effect on the system performance are varied to see whether the controllers are aptly tuned to handle the effects thereof.
The input reference for the valve is a combination of steps in both positive and negative direction as well as a sine wave. The limits of the reference are set between $\pm 0.03[\frac{m}{s}]$, as this should be well within the physical limitations of the system.
The velocity is chosen as the primary state to control for, meaning the controller is tuned based on how well the velocity follows the reference and that the pressure tracking ability is given less priority. Lastly, the observability and controllability of the system should be confirmed as this is a necessary criterion for ensuring that all states are known and that

observers can be implemented.
In regards to the testing of the controllers, they are first tested on the linear model to see which controllers perform the best under near ideal circumstances for the sake of limiting the number of controllers that are compared in the non-linear model, as it is believed the chosen controllers would perform better in the non-linear model as well.

7.2 Controller Design Considerations

The considerations presented are based on what may effect the tuning of the LQ controllers and placement of poles in FSF control, such as: the effect of the weighting parameters on LQ controller performance, the operating conditions of the system, whether FSF or LQ control appear more applicable for the given system which includes considerations regarding robustness.

Increasing the weight of a state or input relative to each other, prioritizes the respective effort needed to drive the reference to its given value. Meaning, If a state is weighted less relative to the other states then it will converge onto the reference at a slower rate and vice versa, as the controller would conserve or spend more actuator/valve energy trying to adjust for the tracking error. When determining the starting value for the weights of each state and input, their respective units and how they scale in comparison should be considered when tuning the LQ controllers. So, in this case where the states are in the units: $[\frac{m}{s}]$ and $[Pa]$, a change of $1[\frac{m}{s}]$ in the velocity would not correspond to a change of 1 $[Pa]$. Furthermore, when tuning the LQ controllers it should be noted whether saturation occurs in the system. This can be determined if say, the inputs to the system exceed the normalised limits, (e.g. a valve cannot open more than [1;-1]), if this occur for extended periods of time it would degrade system performance. So if the valve inputs exceed this limit after the preliminary tuning of the controllers, it indicates that the controllers are tuned to aggressively and would have to be de-tuned.

For the FSF controllers, there are also considerations regarding saturation when placing the poles, and as with the LQ controllers saturation would be seen if the inputs exceed the limits described in the above paragraph. This could occur if the poles of the system are faster than the poles determining the valve dynamics which means the valve cannot respond to the changes in the system, in other words it goes beyond the physical capabilities of the spool. Furthermore, a consequence of placing the system poles at a high frequency is it could amplify signal noise which could degrade the performance.

The system may experience different operating conditions, namely due to internal and external disturbances, where the internal disturbances considered are the measurement and process noise, which granted is not inherent in the system due to it being a simulation study but for a sense of realism is injected into the states and outputs. Measurement noise in a physical system arise out of the sensors and the process noise could in a physical system be due to variations in the friction as a result of the lubrication of the surfaces changing [Sören Andersson, 2006]. The external disturbance considered include variations in the load force. If excitations, in the form of external disturbances to the system occur they would introduce frequency content that excite the system, where the worst case scenario would be if the system is excited near or at the natural frequency which may in turn cause decreased performance of the system if not properly accounted for in the LQ controller design by changing the weighting matrices accordingly [Basu and Nagarajaiah, 2008].

Reference Generation

The controllers that are designed for the velocity and pressure control are presented in further sections. The reference for the velocity is generated in a way to resemble the behaviour that can occur in the "real life" applications. The reference shown in figure 7.1 is constructed with different step intervals and sinusoidal wave with a frequency of approximately $2[\frac{rad}{s}]$, in order to observe and compare performance of each controller. The steps and sinusoidal wave shows how well the controller can track the references under strenuous circumstances, by having rapid changes between the average velocity for the positive and negative movement. Furthermore, in section 6.2.1 it showed that the lower velocity the higher couplings are present, which as mentioned relates to how aggressive the controllers can be tuned, which indicates for the velocity being $0.03[\frac{m}{s}]$ or less that a more conservative approach to the tuning of the controllers should be considered. The figure 7.2 illustrates the reference for the constant rod side pressure.

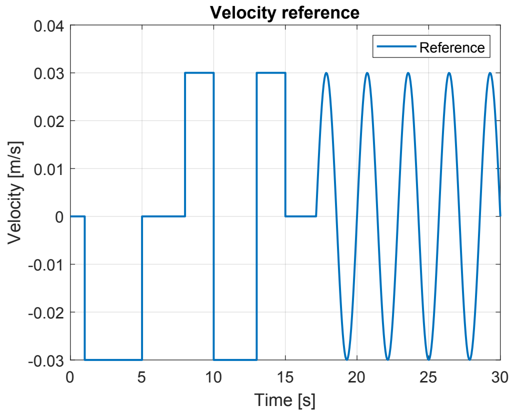

Figure 7.1: Velocity reference

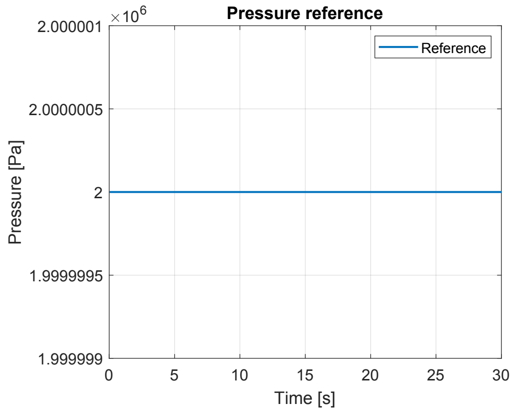

Figure 7.2: Rod side pressure reference

7.3 Full State Feedback Control

The FSF scheme is illustrated in the figure below:

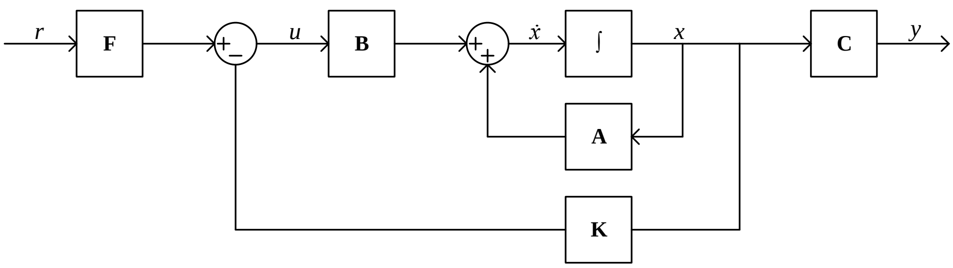

Figure 7.3: Full state feedback scheme

Where, F is the inverse DC gain of the plant, expressed by:

$$F = -(C(A - BK)^{-1}B)^{-1} \tag{7.1}$$

7.3.1 FSF Design Procedure

Full state feedback controllers allows the placing of the closed loop poles at desired locations. The way in which the poles are placed is through the control law:

$$\bar{u}(t) = -\mathbf{K}\bar{x}(t)$$

Where in the MIMO case, *u(t)* and *x(t)*, are vectors and K is a matrix. With the introduction of K in the system, the closed loop dynamics of the system change, where the closed loop definition of the system matrix A becomes:

$$\mathbf{A}_{cl} = \mathbf{A} - \mathbf{BK}$$

Where K is found through the comparison of the coefficients in the characteristic polynomial of the system with the coefficients of the desired characteristic polynomial, expressed by:

$$det(\lambda I - (\mathbf{A} - \mathbf{BK})) = \lambda^3 + a_2\lambda^2 + a_1\lambda + a_0 = \Lambda_a$$

$$\Lambda_a = \lambda^3 + \alpha_2\lambda^2 + \alpha_1\lambda + \alpha_0$$

Where, a_2 a_1 and a_0 are the polynomial coefficients of the actual characteristic polynomial that is compared with the coefficients of the desired characteristic polynomial, α_2 α_1 and α_0, which is how **K** is found, expressed by:

$$K = \alpha - a$$

Where **K** is then found for this system to be a 2x3 matrix, expressed by:

$$\mathbf{K} = \begin{bmatrix} K_{11} & K_{12} & K_{13} \\ K_{21} & K_{22} & K_{23} \end{bmatrix}$$

Provided that the system is controllable, then through tuning K the poles can theoretically be placed anywhere in the LHP [Charles L. Phillips, 2000]. A downside related to this method is it does not account for the couplings present in the system or parameter variations, where the effect of these can be difficult to account for when placing the poles.

7.3.2 FSF Results

In this subsection the results of the FSF controller are presented. Based on the design criteria and observations on the location of the open loop poles, it is desired to achieve a first order response, in order to avoid having any overshoot and longer settling time which in and of itself is not considered a problem but desirable in relation for easier interpretation when comparing controllers. Thus, the real pole is moved closer to origin to dominate the response of the system. The location of the old and new poles are noted in the table below:

Old Pole Locations	New Pole Locations
$s_1 = -6.834$	$s_1 = -9.23$
$s_2 = -3.66 \pm 52.4$	$s_2 = -15.32 \pm 52.4$

The achieved response of the linear model is presented below.

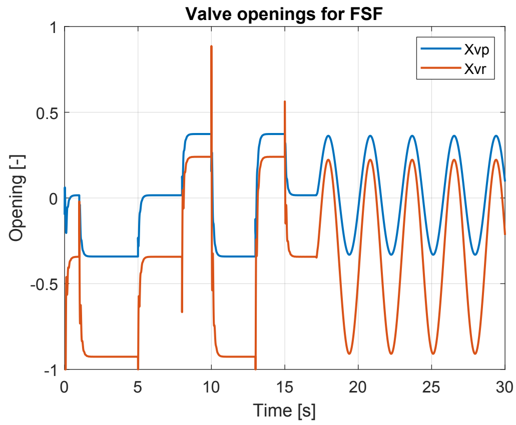

Figure 7.4: Valve openings

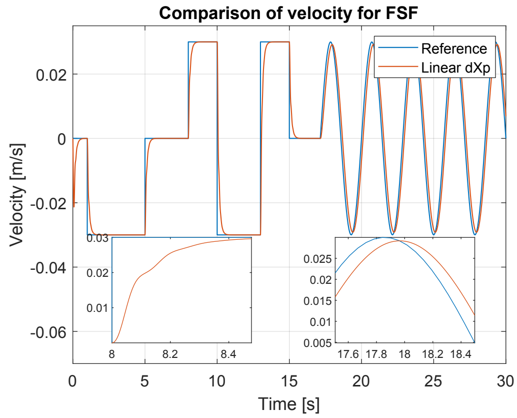

Figure 7.5: Comparison of velocity

From the figure 7.4 it is noted that rod side valve have spikes that appear when velocity is given a negative reference, this may happen due to a sudden switch from the tank to the supply line. The dive in the value seen in the initial velocity is caused by the rod side valve, which is most likely due to the velocity being zero but the rod side pressure is demanded to have 20[bar] in the chamber. This situation is not desirable as the pressure drop across the valve would be significant for all cases where the rod side pressure is kept low when connected to the supply line and similarly for when the piston side pressure is the working pressure.

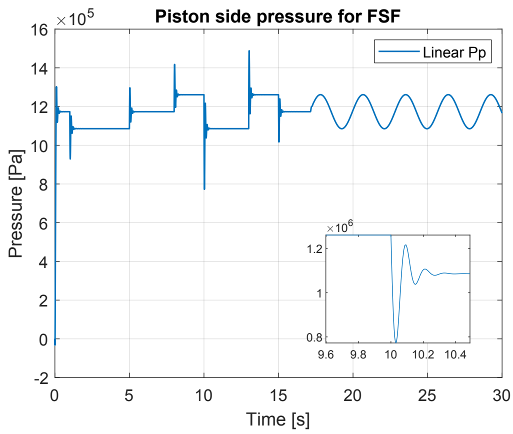

Figure 7.6: Piston side pressure

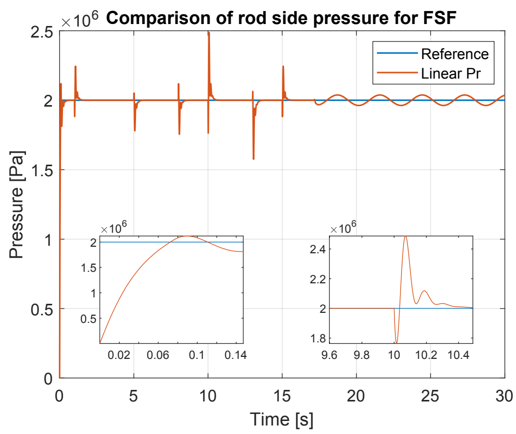

Figure 7.7: Comparison of rod side pressure

Both pressures are performing as expected as the main control focus is towards improving the velocity reference tracking by penalising the pressure performance.

7.4 Full State Feedback with Integral Action

In this section the FSF with integral action is presented. In order to achieve a correct steady state response of the signal, the general approach is to introduce an integrator to eliminate the error. The idea is to augment the system with a new state to include the error term, which is viewed as an integral error from the reference to the output the augmentation procedure is presented below [Feng et al., 2007] [Schmidt and Johansen, 2019]. The general structure of the controller is presented below figure 7.8.

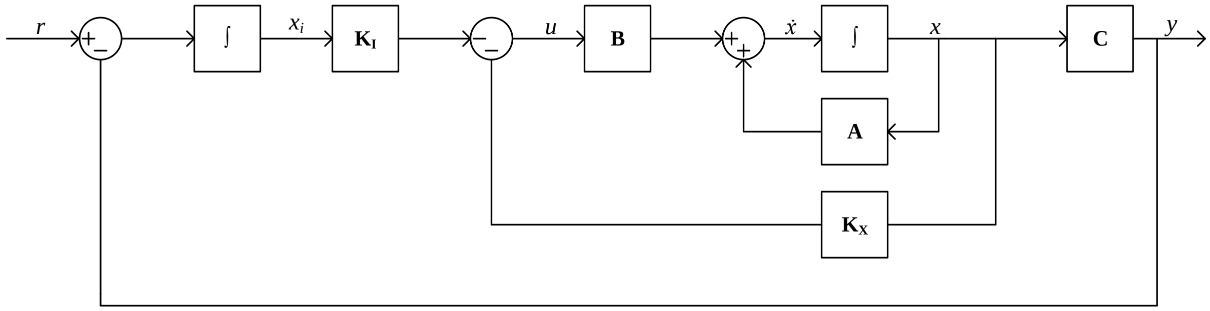

Figure 7.8: Full state feedback with integral action

Similarly to the FSF control law is given

$$\bar{u} = -\mathbf{K}\begin{bmatrix}\bar{x}\\ \bar{x}_i\end{bmatrix}$$

Where,

$$\dot{\bar{x}}_i = \bar{r} - \bar{y} = \bar{r} - \mathbf{C}\bar{x}$$

This augmentation changes the state space representation which is expressed as, [Feng et al., 2007]:

$$\begin{bmatrix}\dot{\bar{x}}\\ \dot{\bar{x}}_i\end{bmatrix} = \begin{bmatrix}\mathbf{A} & 0\\ -\mathbf{C} & 0\end{bmatrix}\begin{bmatrix}\bar{x}\\ \bar{x}_i\end{bmatrix} + \begin{bmatrix}\mathbf{B}\\ 0\end{bmatrix}\bar{u} + \begin{bmatrix}0\\ \mathbf{I}\end{bmatrix}\bar{r}$$

The location of the moved poles are noted in the table below, the old poles being the same as with FSF.

New Poles
$s_1 = -9.23$
$s_2 = -15.32 \pm 52.4$
$s_3 = -20 \pm 52.4$

The integrator poles ($s_3 = -20 \pm 52.4$) are moved twice further away from the dominant pole , so as to not affect the dominant system poles.
The results are very similar to the ones presented above, however some changes are present. From the figure 7.9 the spikes in the valve openings that caused an error between reference and output are eliminated due to the introduction of the integrator which serves to reduce the error. The velocity tracking is considered to be good and initial error is also practically eliminated comparing with figure 7.5.

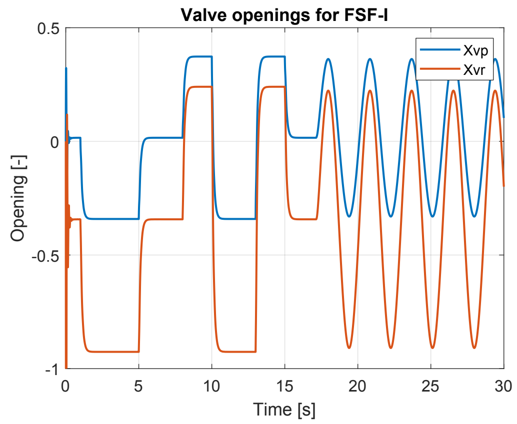

Figure 7.9: Valve openings

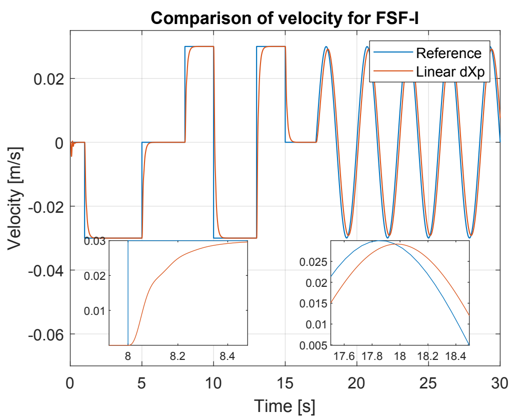

Figure 7.10: Comparison of velocity

From the figures 7.11,7.12 it is observed that undesired spikes in the pressures are also seen to be lower along the operating range, which is a positive improvement.

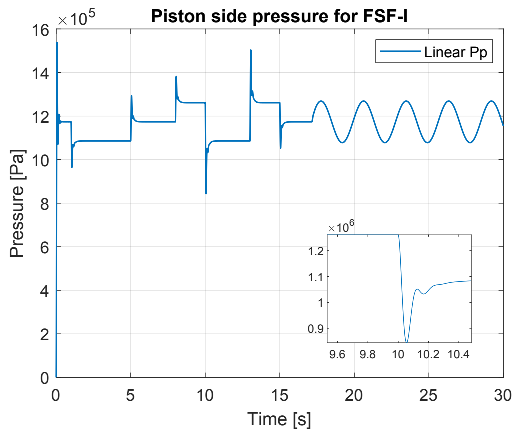

Figure 7.11: Piston side pressure

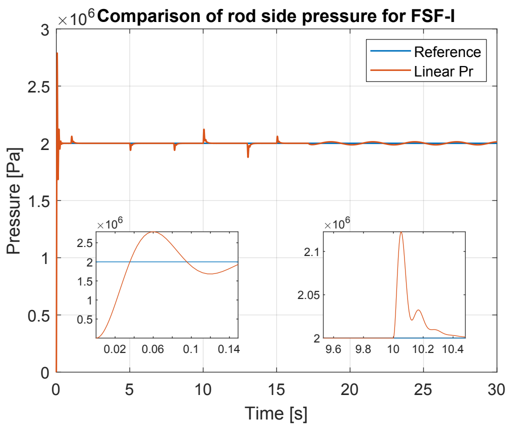

Figure 7.12: Comparison of rod side pressure

7.5 Linear Quadratic Control

LQ controllers are considered a part of optimal controllers. This is due to the nature of the controllers wherein the purpose is to minimize a quadratic cost function that ensures that the states are driven to the desired reference [Sigurd Skogestad, 2005], [Razmjooy et al., 2014]. If the system is controllable and observable implementing LQ control ensures that the system is asymptotically stable, and that the LQ controllers have guaranteed stability margins where the gain margin is infinity and a minimum phase margin of 60°, provided that R is chosen to be diagonal [Sigurd Skogestad, 2005] [Jaen et al., 2006] [Rocha et al., 2012]. The cost function is as follows:

$$J = \int_0^\infty (\bar{x}^T(t)\mathbf{Q}\bar{x}(t) + \bar{u}^T(t)\mathbf{R}\bar{u}(t))dt$$

Where, bold denotes matrices and a bar denotes vectors. Finding the optimal solution that minimises the cost function depends on the control law which for LQR/LQG controllers is as follows:

$$\bar{u}(t) = -\mathbf{K}\bar{x}(t)$$

Which is similar to the control law seen for FSF, where the difference is that the feedback gain is now found through optimisation instead of pole placement. The feedback gain that ensures the optimal solution for $u(t)$ and hence J is expressed by:

$$\mathbf{K} = -\mathbf{R}^{-1}\mathbf{B}^T\mathbf{P}$$

Where the matrix P is the unique solution to the Ricatti equation, expressed by:

$$\mathbf{A}^T\mathbf{P} + \mathbf{P}\mathbf{A} - \mathbf{P}\mathbf{B}\mathbf{R}^{-1}\mathbf{B}^T\mathbf{P} + \mathbf{Q} = 0$$

Putting the theory covered into the perspective of designing the controllers, the LQR design procedure is outlined below. The LQR controller discussion will serve as a base for discussing the LQI/LQG controllers, where the augmentations to the system that occur due to the controller structure is covered under their respective section. The process for designing a LQR controller is as follows:

1.
Select design parameter matrices $\mathbf{Q}$ and $\mathbf{R}$.

2.
Solve the algebraic Riccati equation for $\mathbf{P}$.

3.
Find the optimal value for the feedback by using the control law, where $\mathbf{K} = -\mathbf{R}^{-1}\mathbf{B}^T\mathbf{P}$.

Considering the objective of the controllers tested which is to follow a reference, the controllers needs to have a pre-filter implemented. As this takes it from a regulator to a servo problem as the LQR/LQG controllers are in their base form regulators, driving the states to zero, the implementation of the pre-filter would enable the possibility of having the states converge at a setpoint [Sigurd Skogestad, 2005] [Razmjooy et al., 2014].

Tuning of Q and R

The $\mathbf{Q}$ and $\mathbf{R}$ matrices are diagonal matrices with each entry being a weighting parameter corresponding to each of the states for the $\mathbf{Q}$ matrix, and for the respective inputs in the $\mathbf{R}$ matrix, as described below:

$$\mathbf{Q} = \begin{bmatrix} q_1 & 0 & 0 \\ 0 & q_2 & 0 \\ 0 & 0 & q_3 \end{bmatrix} \quad , \quad \mathbf{R} = \begin{bmatrix} \mu & 0 \\ 0 & \mu \end{bmatrix}$$

The challenges featured with this type of controller is that it relies on finding the best ratio between the weighing matrices. As mentioned previously, a good starting point would be to consider the scales of the respective states in relation to one another. In this case where the states controlled for are the velocity and backside pressure, the scaling between $[\frac{m}{s}]$ and [Pa] should be taken into account when making initial guesses. To account for the scaling between $1[\frac{m}{s}]$ and 1[bar], the initial guess for the tuning parameters is set so this is taken into account, yielding:

$$q_{1,ini} = 1 \quad , \quad q_{2,ini} = 1e^{-5} \quad , \quad q_{3,ini} = 1e^{-5}$$

In relation to the cost function, this means that the contribution from the pressures and velocity is on the same scale. From the initial guess, the weighting parameters should be changed accordingly to how it is desired that the controllers should penalize the velocity and pressure tracking effort. Having a high weighting parameter means that the allowable error between the present value and setpoint is smaller and vice versa. In this case it is desired to achieve good velocity tracking, so to ensure this the weighting parameter for the velocity should be set at a higher value than for the pressures. It is difficult to determine the relation of the weighting parameters that gives the desired performance, and it is here a trial and error procedure for finding the final tuning parameters is employed. In regards to the **R** matrix, it similarly penalises the actuation effort of the valves. Setting the weights at a low value means restricting the valves energy expenditure is of less concern, referred to as cheap control, and opposite when increasing the weights to a high value, referred to as expensive control.

7.6 Linear Quadratic Regulator

The LQR scheme, which is identical to the FSF scheme, is illustrated in the figure below:

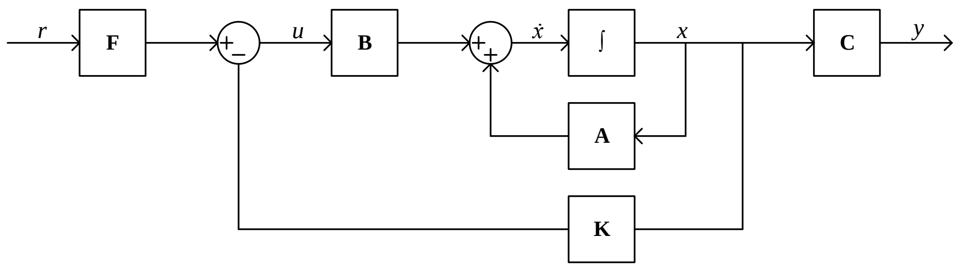

Figure 7.13: LQR scheme

Similarly, **F** is the pre-filter and **K** is the feedback gain matrix found here by tuning of the weighting matrices **Q** and **R** described in section 7.2 and further outlined in section 7.5.

Parameters	$q_1(\dot{x}_p)$	$q_2(p_p)$	$q_3(p_r)$	$\mu(x_{vp}, x_{vr})$
Values	$1e^5$	$1e^{-9}$	$1e^{-8}$	$1e^{-3}$

Table 7.1: Parameters used for the LQR

The value of the weights relative to one another indicates that the controller effort is primarily focused on driving the error for the velocity to zero, over the chamber pressures. From observing figure 7.14 it is noted that there are unwanted spikes in the rod side valve. The nature of these spikes could be related to the numerical problems as there are practically no visible changes at the rod side pressure when the spike occurs, due to the very short duration in which the spikes occur. The initial spike in the velocity is due to initialisation problem, despite that the velocity exhibits smooth first order characteristics as opposed to the slight oscillations seen for the velocity when using the FSF and FSF-I controllers.

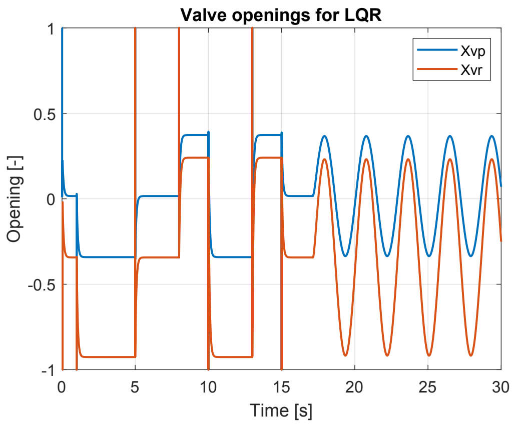

Figure 7.14: Valve openings

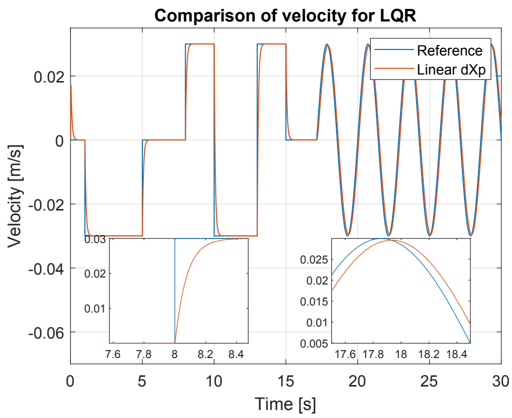

Figure 7.15: Comparison of velocity

The piston side pressure figure 7.16 have some large spikes at the time when switching from tank to supply and vice versa. This could be explained by the highly coupled system dynamics as the spikes seen in the rod side valve input corresponds to peaks seen in the piston side pressure.

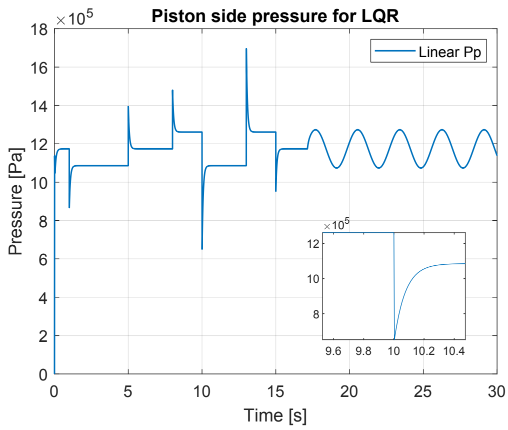

Figure 7.16: Piston side pressure

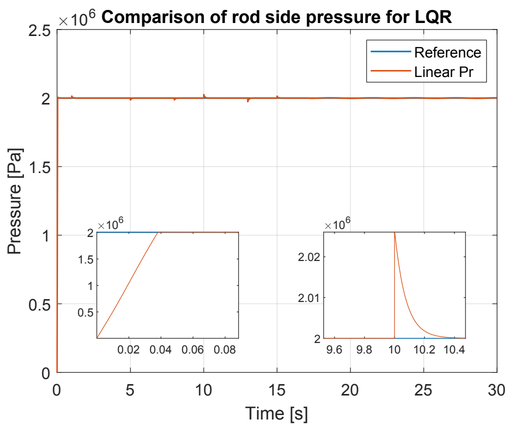

Figure 7.17: Comparison of rod side pressure

7.7 Linear Quadratic Integrator

In this section the design of linear quadratic integrator, LQI, is presented. The LQI scheme is illustrated in figure 7.18, which is similar to that of FSF-I.

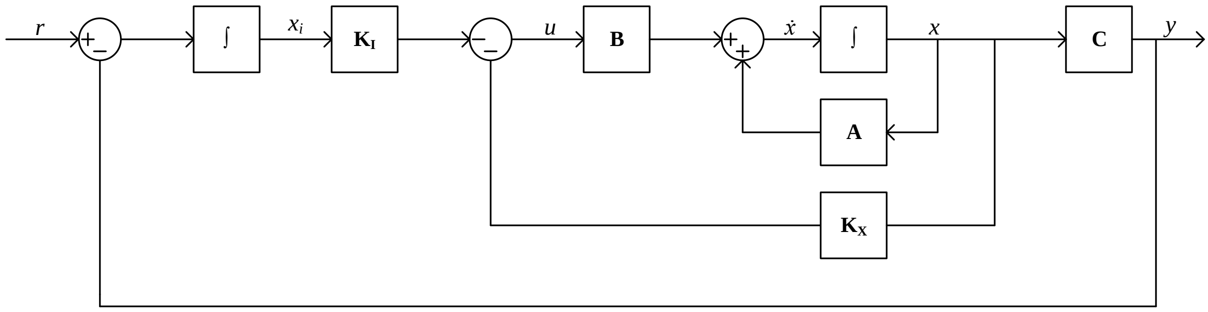

Figure 7.18: Linear Quadratic Integrator

7.7.1 LQI Design Procedure

In LQI the control law is similarly found through the Ricatti equation. The main difference from the LQR controller is that an integral state is introduced, where the control law is expressed by:

$$\bar{u} = -\mathbf{K}\begin{bmatrix}\bar{x}\\ \bar{x}_i\end{bmatrix}$$

Where,

$$\dot{\bar{x}}_i = \bar{r} - \bar{y} = \bar{r} - \mathbf{C}\bar{x}$$

This augmentation changes the state space representation which is expressed as, [Feng et al., 2007]:

$$\begin{bmatrix}\dot{\bar{x}}\\ \dot{\bar{x}}_i\end{bmatrix} = \begin{bmatrix}\mathbf{A} & 0\\ -\mathbf{C} & 0\end{bmatrix}\begin{bmatrix}\bar{x}\\ \bar{x}_i\end{bmatrix} + \begin{bmatrix}\mathbf{B}\\ 0\end{bmatrix}\bar{u} + \begin{bmatrix}0\\ \mathbf{I}\end{bmatrix}\bar{r}$$

Similarly with the non-zero set-point variation of the LQR controller, the LQI controller attempts to drive the error dynamics towards zero, where instead of applying a pre-filter an integrator is used. Therefore a benefit of LQI over LQR is that it does not rely on the implementation of a pre-filter when following a non-zero reference, where a property of the integrator is it ensures zero steady state error. [Rocha et al., 2012].

7.7.2 LQI Results

The parameters used to minimize the quadratic cost function are presented in table 7.2. Where the q_4 is a weighting parameter for the velocity error state and q_5 is used to penalise the pressure error state, μ is used to penalise both inputs.

Parameters	$q_1(\dot{x}_p)$	$q_2(p_p)$	$q_3(p_r)$	$q_4(\dot{x}_{err})$	$q_5(p_{err})$	$\mu(x_{vp}, x_{vr})$
Values	0	0	0	$3e^5$	$1e^{-9}$	1

Table 7.2: Parameters used for the LQI

By augmenting the system some improvement in reducing the error can be observed in figure 7.19 where the initial spikes from initialisation are partly removed. The tracking of the velocity got a bit slower due to properties of the integrator, however the steady state error is completely eliminated [Charles L. Phillips, 2000].

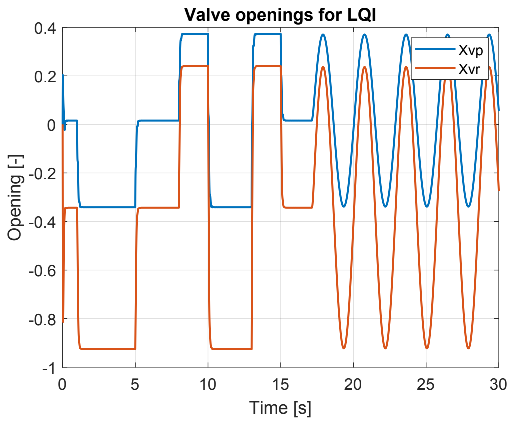

Figure 7.19: Valve openings

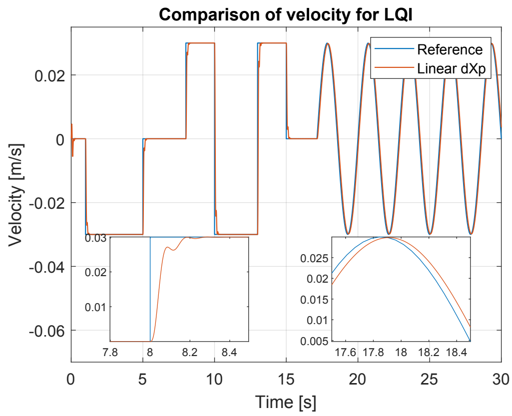

Figure 7.20: Comparison of velocity

The spikes in both figures for the pressures 7.21, 7.22 could again be explained by the high penalty on these and heavily coupled dynamics.

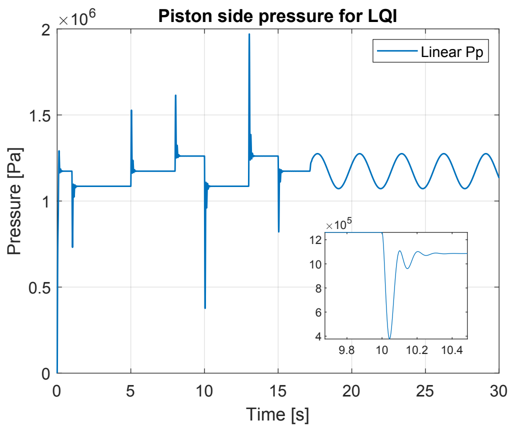

Figure 7.21: Piston side pressure

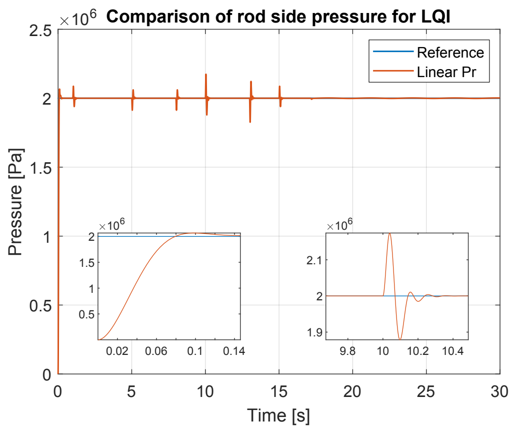

Figure 7.22: Comparison of rod side pressure

In the next section the comparison of the controllers is presented and discussed.

7.8 Linear Quadratic Gaussian Controller

The LQG scheme with integral action is illustrated in figure 7.23, with the addition of process and measurement noise.

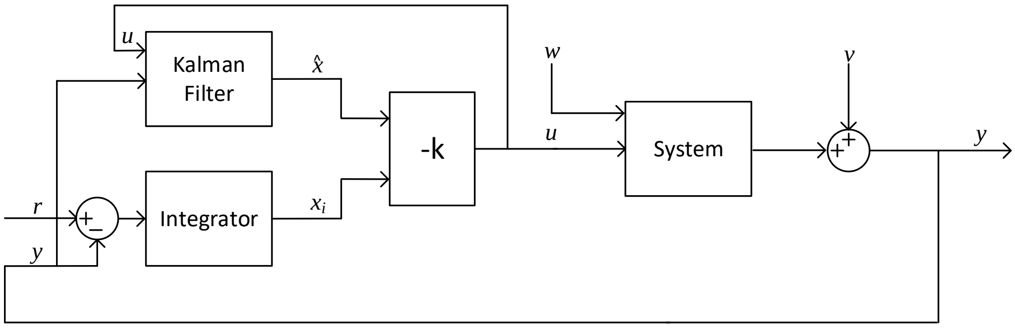

Figure 7.23: Linear Quadratic Gaussian servo controller with integral action, made with inspiration from [MATLAB]

7.8.1 LQG Design Procedure

LQG control is similar to that of LQR, the difference being that now a Kalman filter is added to the control structure. A Kalman filter is an observer that will estimate the states based on previous measurements of the states together with the presumed covariance matrices for the process and measurement noise, which is used in tuning the Kalman filter gain. In LQG control the control law is the same as with LQR, the difference being that now that instead of the system states, the optimal state estimates are found through the use of a Kalman filter and substituting these with the actual states, yielding the following control law, [Sigurd Skogestad, 2005] [Schmidt and Johansen, 2019]:

$$\bar{u} = -\mathbf{K}\hat{\bar{x}}$$

K is found through the Ricatti equation. The state space model now also includes the process and measurement noise, which then gives:

$$\begin{aligned} \dot{\bar{x}}(t) &= \mathbf{A}\bar{x}(t) + \mathbf{B}u(t) + \mathbf{G}\bar{w}(t) \\ \bar{y}(t) &= \mathbf{C}\bar{x}(t) + \bar{v}(t) \end{aligned}$$

Where, $\bar{w}(t)$ is the process noise and $\bar{v}(t)$ is the measurement noise. The state space equation for the Kalman filter is expressed by:

$$\dot{\hat{\bar{x}}} = \bar{\mathbf{A}}\hat{\bar{x}}(t) + \bar{\mathbf{B}}\bar{u}(t) + L(y(t) - \bar{C}\hat{x})$$

Where, L, is the Kalman gain found through the following expression:

$$L = (P_0\bar{C}^T + GR_{vw})R_v^{-1}$$

Where the additional tuning parameters for finding L is seen below:

$$\begin{bmatrix} R_w & R_{wv} \\ R_{wv}^T & R_v \end{bmatrix}$$

Here, the tuning parameters are: R_v and R_w, which corresponds to the intensity of the noise variables w(t) and v(t). As with the **Q** and **R**, the values for R_w and R_v are relative to each other. When tuning the parameters it can be viewed as whether to trust the model or the measurements, if setting the parameter R_v to a low value then from the Kalman gain expression it can be seen that it would have a large value. This means that the observer states are being driven mainly by the Kalman gain and not by the model. The applicability of the LQG in a physical system should especially be considered in cases where there is no full state feedback, as the Kalman filter based on knowledge of the states and noise estimate any unknown states. Seeing as all the states are available, and the white noise amplitude is known beforehand it is decided to tune the Kalman filter such that it relies on the measurements. This is also decided in relation to the implementation in a physical SMISMO system, where there may be model inaccuracies in relation to namely friction and bulk modulii, then it may be taking the more cautious approach to trust the measurements over the process model.

7.8.2 LQG-I Results

In this section the results of LQG-I controller are presented. The penalty parameters are shown in table 7.3 and selected to be the same as for the LQI controller for the purpose of comparison, observation in performance.

Parameters	$q_1(\dot{x}_p)$	$q_2(p_p)$	$q_3(p_r)$	$q_4(\dot{x}_{err})$	$q_5(p_{err})$	$\mu(x_{vp}, x_{vr})$
Values	0	0	0	$3e^5$	$1e^{-9}$	1

Table 7.3: Parameters used for the LQG-I

Figure 7.24 illustrates convergence of the observer states to the linear ones. The velocity and rod side pressure are controlled for, and their states are available at all times this is seen in their corresponding plots. The state that is being estimated is the piston side pressure and it takes observer approximately 4 seconds to converge to the real value.

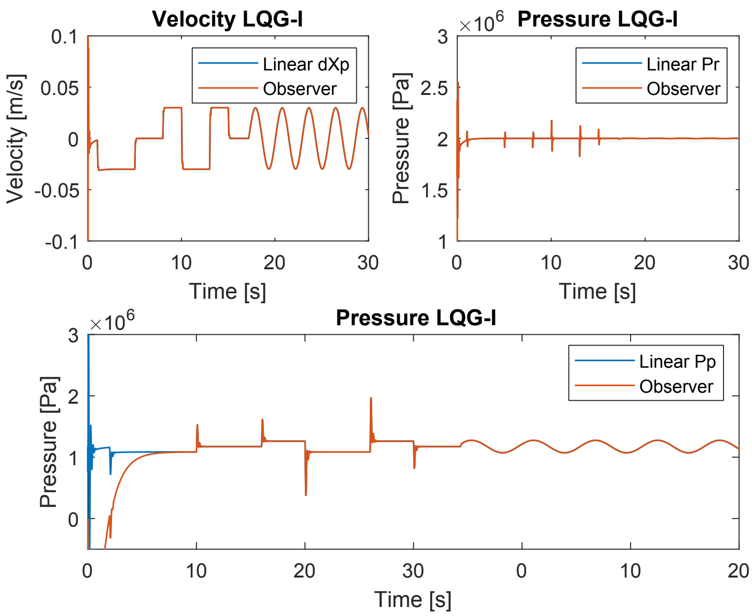

Figure 7.24: Convergence of the observers to the linear states

From the results of the simulation it is observed that response of the LQG-I controller is very similar to the LQI which is expected as it utilises the same core structure and penalty matrices. Some deviations from the LQI are seen in the figure 7.26 the velocity converges to the reference after period of time, this is due to including the observer which converges to reference with a delay, thus pressure in the piston side is not sufficient to propel the movement resulting in deviation from the reference value.

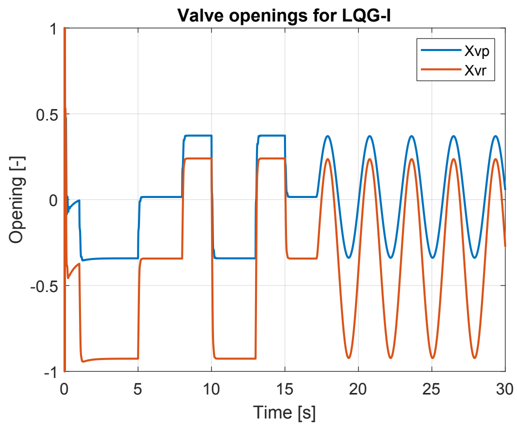

Figure 7.25: Valve openings

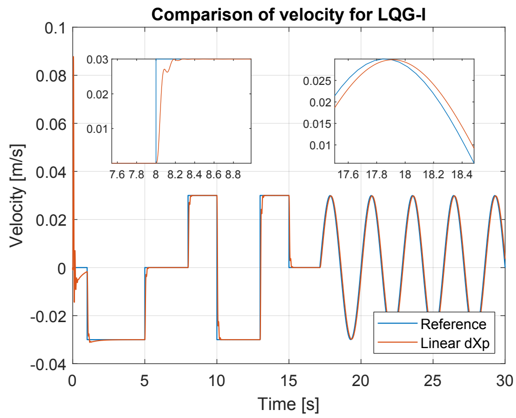

Figure 7.26: Comparison of velocity

The effect of including the observer also seen in rod side pressure, the explanation is the same as for the case with velocity described above. The pressure spikes exhibit the same behaviour as for the LQI controller.

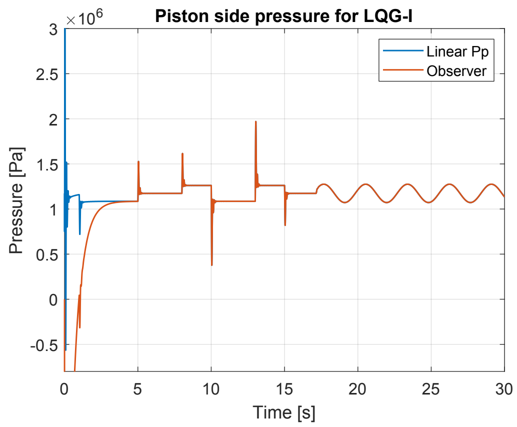

Figure 7.27: Piston side pressure

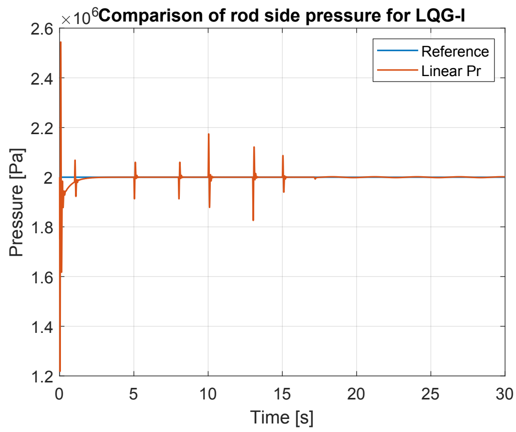

Figure 7.28: Comparison of rod side pressure

In the next section the performance of the controllers is presented and evaluated.

7.9 Controller Performance Evaluation

Throughout the design of controllers the performance of each of them is noted and presented in the table 7.4. Based on overall performance in different characteristics and considerations for the further testing against non-linear model 2-3 controllers are going to be selected.

Characteristic	**FSF**	**FSF-I**	**LQR**	**LQI**	**LQG-I**
e_{ss} [%]	< 0.1	0	< 0.1	0	0
Overshoot [%]	0	0	0	0	0
t_s [s]	0.36	0.44	0.24	0.2	0.2
t_r [s]	0.2	0.22	0.16	0.15	0.088
τ [s]	0.09	0.11	0.06	0.05	0.056
RMSE [-]	0.0119	0.0114	0.0145	0.0098	0.0116

Table 7.4: Performance of the controllers

The performance characteristics are presented for the velocity as it was chosen as a primary state and is the main focus of an investigation for the selected control strategy. From the table 7.4 it is observed that the steady state error is eliminated only for the controllers that have an integrator which is expected and is a desirable property which in addition helps to deal with the disturbances[M.Gopal, 2002]. All of the controllers have no overshoot as it was taken into consideration when designing. The settling, rise time and as well a time constant are better for the LQ controllers as they utilise the cost function and Riccati equation to place the poles at the optimal location based on the chosen weighting parameters. The interpretation of the achieved results from RMSE indicates that the controllers with integral action result in a better absolute fit of the velocity reference to the actual value.

Based on the achieved results from the linear model the 3 controllers selected are the FSF-I, LQI, and LQG-I as all of them have an integral action which would help to reduce deviations from the reference in presence of noise and disturbance. Furthermore, the performance of controllers are relatively close to each other, besides FSF-I which is slightly slower. However, with the interest of investigating how well FSF-I can perform against more advanced controllers in a non-linear environment it is selected.

7.10 Comparing Controllers against Non-Linear Model

In this section the controllers are tested in the non-linear model to observe their performance in the presence of noise, disturbance and parameter variations. Figures 7.29, 7.30 represents the external force load profile and white noise respectively that is applied to the system.

Disturbance and Noise applied to the system

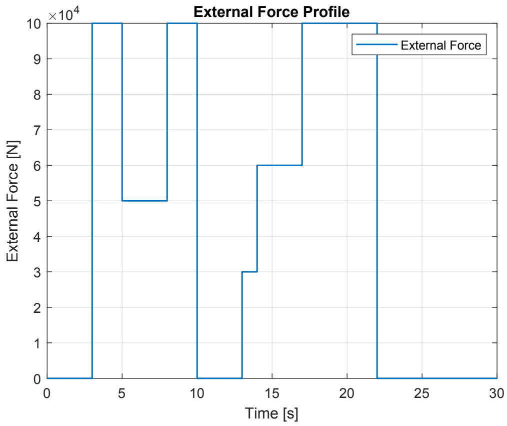

Figure 7.29: External force reference

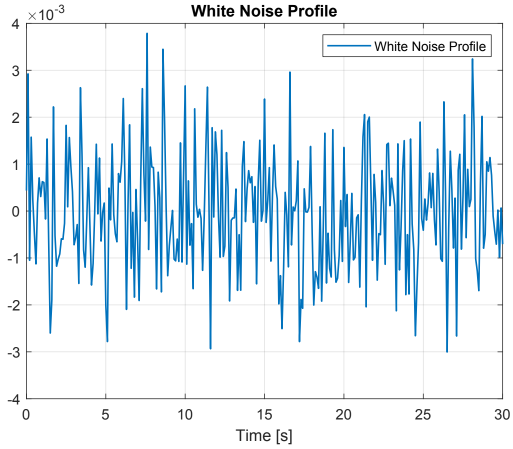

Figure 7.30: White noise reference

The disturbance profile is generated in way to test how would the designed controllers perform away from linearisation point. The white noise profile is generated to represent the measurement noise in the figure 7.30. Illustrated white noise is applied to the velocity state with an amplitude of 10 % from the chosen value. The same noise profile with a consideration of 10 % is applied to the pressure state which figure is for convenience not presented.

7.10.1 Comparison in Horizontal position of the cylinder

Firstly, the controllers are going to be tested in the horizontal position of the cylinder when no gravitational force is present. The table 7.5 with linearisation points is presented below.

Linearisation points for controllers in horizontal position

Parameters	p_p [bar]	p_r [bar]	F_{ext} [kN]	x_{vp} [%]	x_{vr} [%]	$\dot{x}_p[\frac{m}{s}]$	m [kg]
Values	77.7	20	100	0.356	0.583	0.03	12 $\times 10^3$

Table 7.5: Linearisation points used for both controllers

From the comparison of velocity it is observed that the LQI controller performs better at reference tracking both when there is no force load and in the presence of force load. In addition to that, there are less visible oscillations and pressure spikes appear to have lower amplitude than the rest of the controllers. The performance of LQI surpasses FSF-I mainly because of the utilisation of the optimal algorithm, and the LQG is performing slightly worse since it has to estimate the state that is already available in the simulation, only causing a delay in both pressures and velocity.

Further explanation of the achieved results is generalised for all the controllers, since they exhibit corresponding behaviour. From observing figure 7.31 the value of velocity is below the reference until 3 seconds due to low pressure level in piston side chamber as the force profile is set equal to 0 and there is not enough force to accelerate the movement of the piston. The second and third spike from 3 to 10 seconds relate to increase of force load, where after settling the tracking of velocity is improved, since the parameters are closer to the linearisation points. Furthermore, all the consequent spikes are explained with the reasoning just described.

Comparison in Horizontal Position

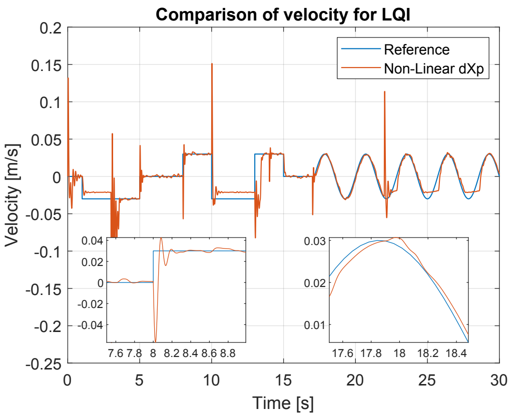

Figure 7.31: Velocity of LQI controller

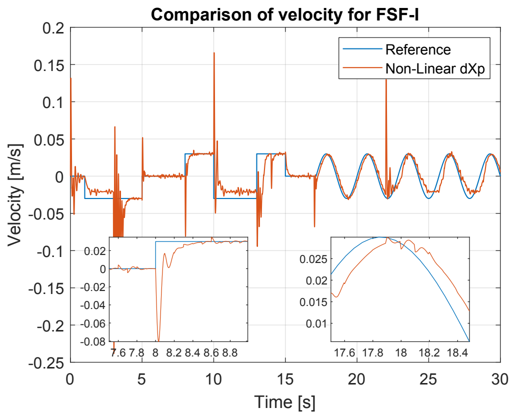

Figure 7.32: Velocity of FSF-I controller

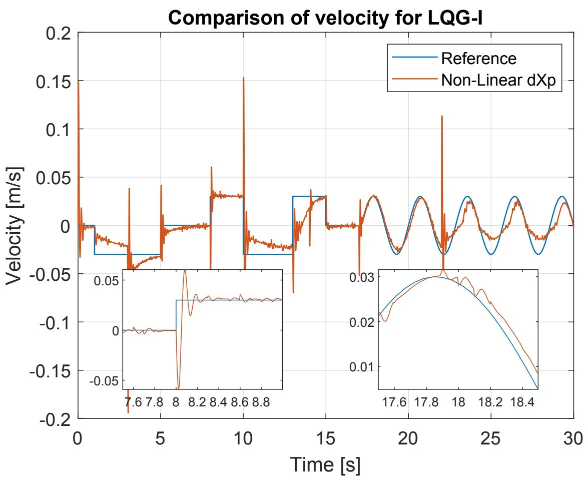

Figure 7.33: Velocity of LQG-I controller

From the figures with rod side pressure it is evident that LQI and FSF-I are performing better at keeping the back pressure constant. The oscillations in the pressures are seen in both controllers, however the FSF-I seems to be more sensitive to the change of external force load and oscillations last a bit longer. On the other hand, the LQI controller struggles to converge to the reference at times, when velocity is stepped in the negative direction. This could be due to the low penalty on the pressure weighting parameter which means the allowable error between the actual value and reference is relatively high.

From figure 7.33 with the LQG-I controller it is seen that pressure is constantly fluctuating around its reference value. The possible explanation for achieved results could be due to the frequent excitation to the system for which the observer is not able to account for in a timely fashion as was also seen in the linear model in figures 7.26, 7.27 and 7.28 when initially the pressures converge only after ∼ 2-4 seconds.

Comparison in Horizontal Position

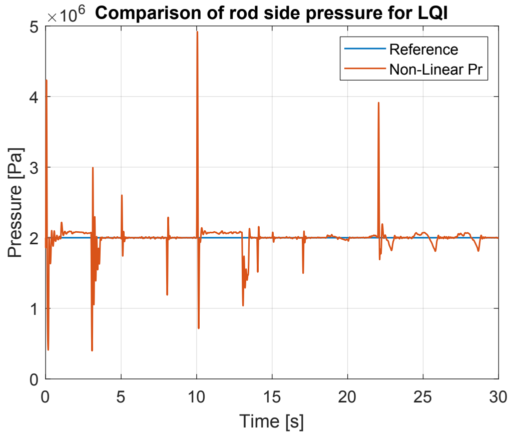

Figure 7.34: Rod side pressure of LQI controller

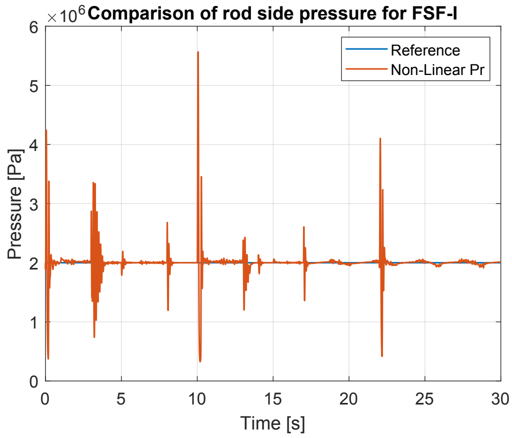

Figure 7.35: Rod side pressure of FSF-I controller

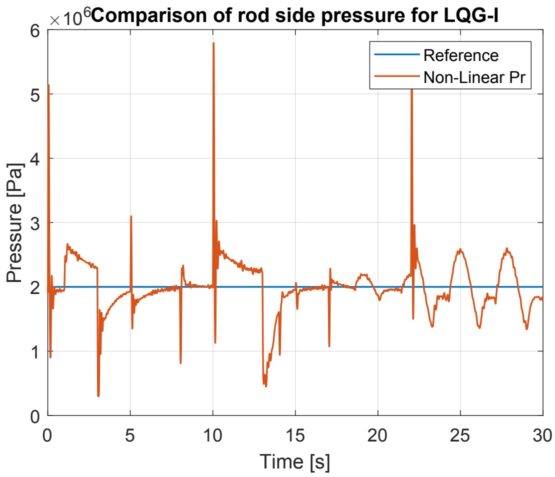

Figure 7.36: Rod side pressure of LQG-I controller

Figures with piston side pressure are presented below. It is evident that piston side pressure is highly dependant on the external force load, and its profile changes accordingly. Pressures in all controllers exhibit expected behaviour without any anomalies.

Comparison in Horizontal Position

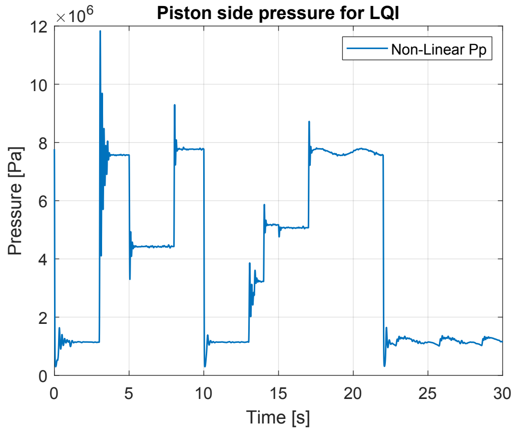

Figure 7.37: Piston side pressure of LQI controller

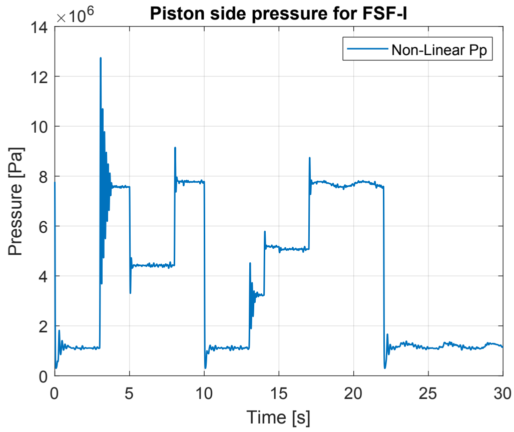

Figure 7.38: Piston side pressure of FSF-I controller

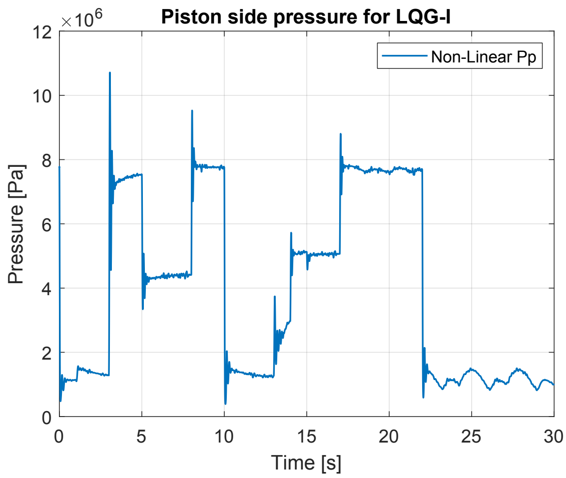

Figure 7.39: Piston side pressure of LQG-I controller

From the figures 7.40, 7.41 it is seen that valves are saturated for a long period of time this effect appears when system reaches physical limits. The system reaches its limit when there is no force load and velocity is set higher that it is possible to achieve, this is evident from plots presented above 7.31, 7.40. The saturation effect is not desirable as there is no way to apply any control effort over the system as it behaves like an open loop system. Furthermore, once the input saturates the integrator keeps adding the error and causes a delay in the response. Anti-windup has to be implemented to avoid having the integrator continuously increasing the error which prolongs the saturation effect. The valve openings for the LQG-I controller is seen to have a smaller amount of saturation, but for relatively short periods of time, as this the case it is not assumed to have a significant impact.

Comparison in Horizontal Position

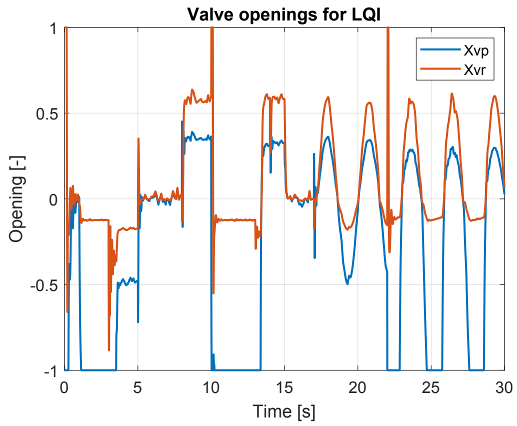

Figure 7.40: Valve openings of LQI controller

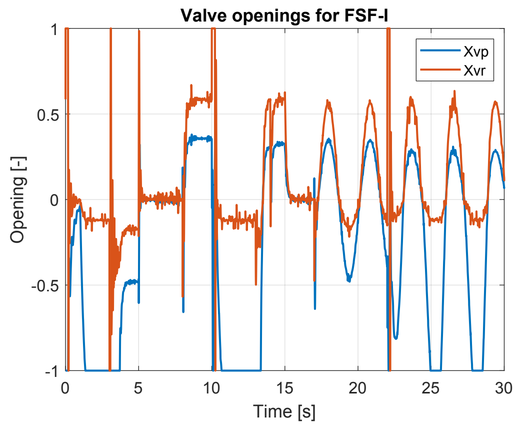

Figure 7.41: Valve openings of FSF-I controller

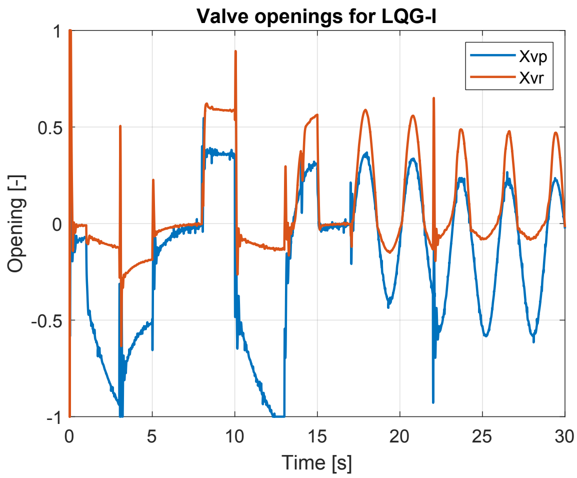

Figure 7.42: Valve openings of LQG-I controller

The table 7.6 with performance parameters is presented below. The values for comparison are taken when velocity is stepped at 8 seconds.

Performance of the controllers in horizontal position

Characteristic	FSF-I	LQI	LQG-I
Overshoot [%]	0	40	100
Undershoot[%]	266	183	193
t_s [s]	0.8	0.2	0.32
t_r [s]	0.37	0.06	0.064
τ [s]	0.2	0.05	0.059
RMSE [-]	0.0293	0.0245	0.0273

Table 7.6: Performance of the controllers

The overall comparison shows that LQI controller for the horizontal case is performing better than the rest controllers. This is further elaborated in the 8 chapter. In the next section controllers are tested in the vertical position.

7.10.2 Comparison in Vertical position of the cylinder

Table 7.8 shows the parameter values in the linearisation point and is presented below. The structure of the presented controllers is the same as for the horizontal position of the cylinder.

Linearisation points for controllers in vertical position

Parameters	p_p [bar]	p_r [bar]	F_{ext} [kN]	x_{vp} [%]	x_{vr} [%]	$\dot{x}_p[\frac{m}{s}]$	m [kg]
Values	154.7	20	100	0.55	0.583	0.03	12 $\times 10^3$

Table 7.7: Linearisation points used for both controllers

The observations of achieved results are generalised for all the controllers, similarly to the horizontal case. The reference tracking of all controllers is significantly improved, the main reason for this is due to the gravitational force which increase the pressure level in the system allowing to accelerate the movement of the piston. Besides that, the system parameters are closer to the linearisation points which also indicates improvement in the performance.

The spikes which are present in all velocity figures display the same behaviour as was described above in horizontal position of the cylinder, and no abnormal behaviour is noted. The LQG-I is performing slightly better than the rest of controllers in disturbance rejection and reference tracking but shows a slightly more oscillatory response due to the noise.

Comparison in Vertical Position

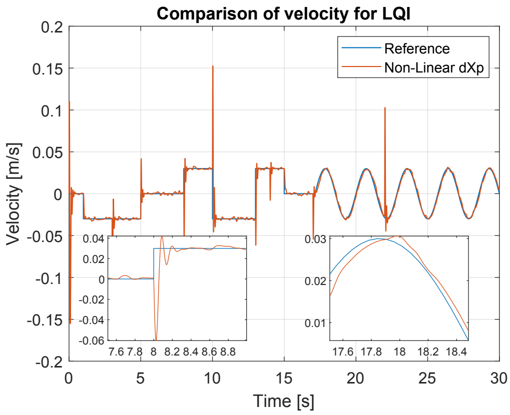

Figure 7.43: Velocity of LQI controller

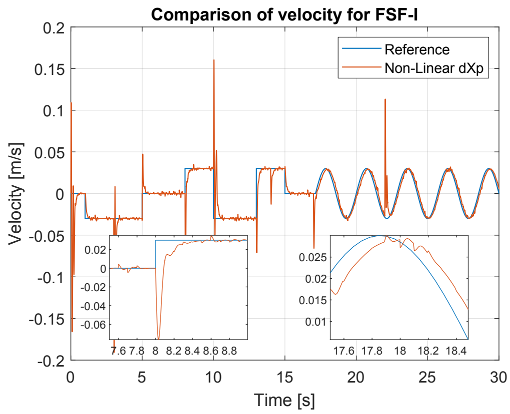

Figure 7.44: Velocity of FSF-I controller

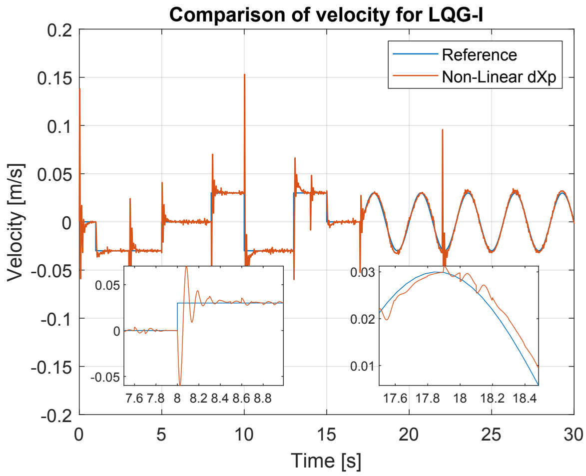

Figure 7.45: Velocity of LQG-I controller

From the figures with a constant back-pressure it is seen that response and reference tracking is improved. The LQI and FSF-I controllers are performing better than the LQG-I the reasoning for this is the same as for the horizontal case, likely due to the introduction of the Kalman filter to the system.

Comparison in Vertical Position

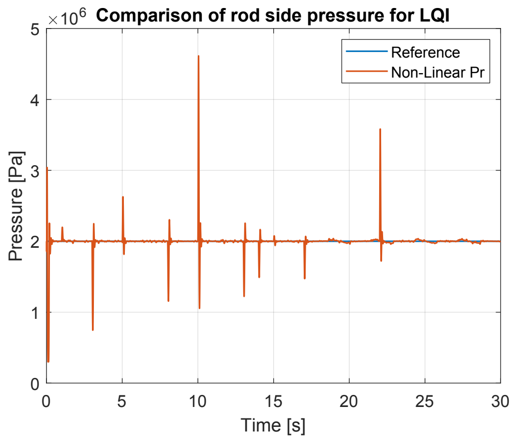

Figure 7.46: Rod side pressure of LQI controller

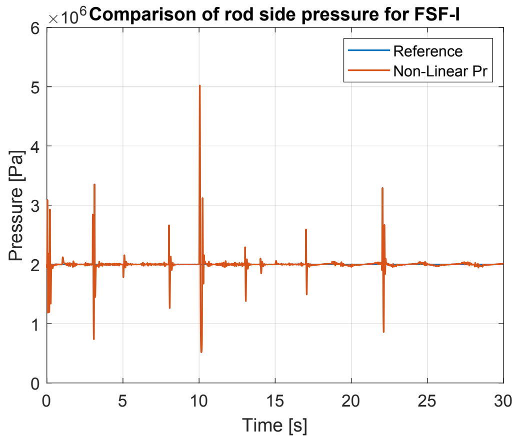

Figure 7.47: Rod side pressure of FSF-I controller

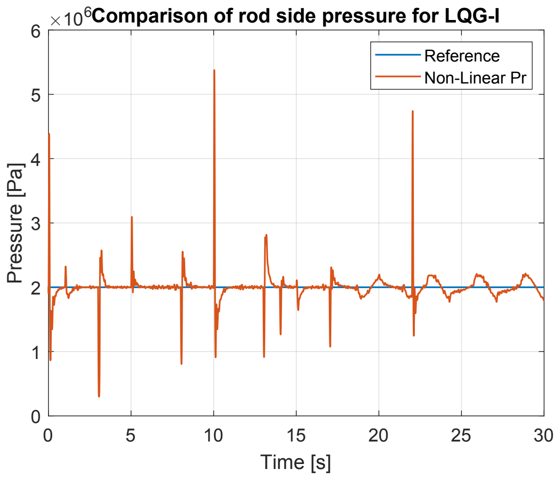

Figure 7.48: Rod side pressure of LQG-I controller

The figures with piston side pressure are presented in below, where no abnormalities are noted.

Comparison in Vertical Position

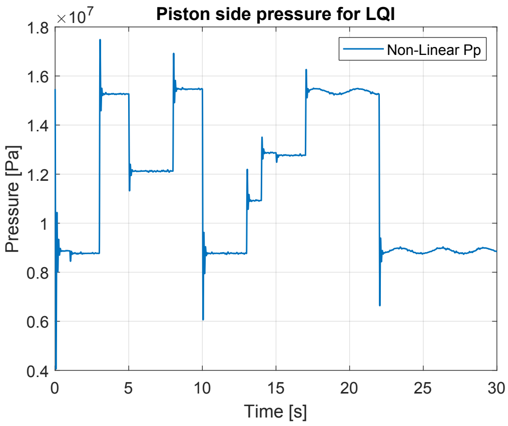

Figure 7.49: Piston side pressure of LQI controller

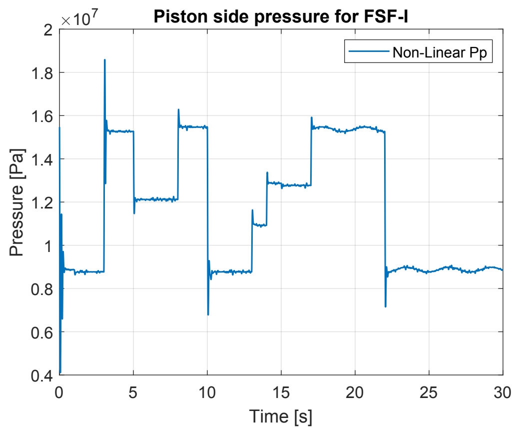

Figure 7.50: Piston side pressure of FSF-I controller

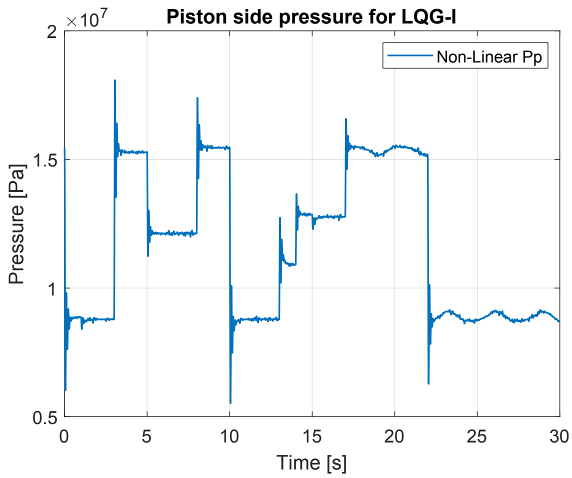

Figure 7.51: Piston side pressure of LQG-I controller

Figures with valve openings are presented below, where the unwanted saturation effect is virtually non existent. Valves for all of the controllers show normal behaviour, without any anomalies.

Comparison in Vertical Position

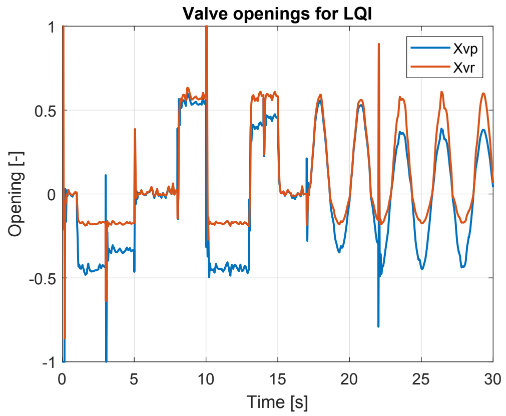

Figure 7.52: valve openings of LQI controller

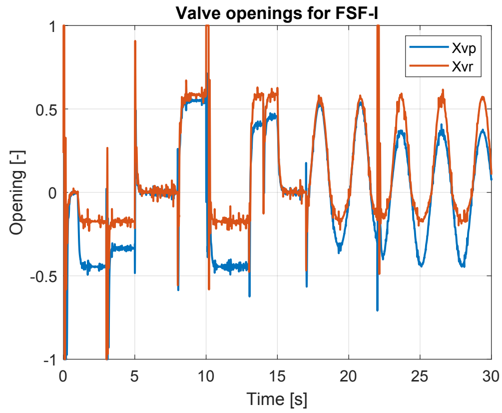

Figure 7.53: Valve openings of FSF-I controller

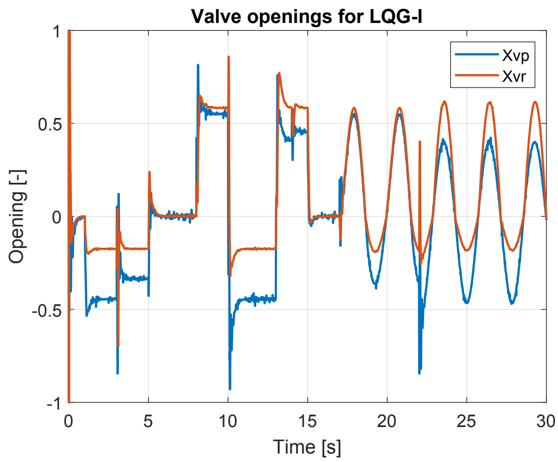

Figure 7.54: Valve openings of LQG-I controller

The table 7.8 with noted performance parameters is presented below.

Performance of the controllers in vertical position

Characteristic	FSF-I	LQI	LQG-I
Overshoot [%]	0	33	133
Undershoot[%]	253	200	195
t_s [s]	0.8	0.36	0.37
t_r [s]	0.24	0.072	0.06
τ [s]	0.2	0.067	0.058
RMSE [-]	0.0276	0.0258	0.0195

Table 7.8: Performance of the controllers

The overall comparison showed that LQG-I and LQI controllers in vertical position of the cylinder are performing better in terms of tracking the velocity reference. This is further elaborated in chapter 8.

8 Discussion

This chapter provides a discussion of achieved findings, considerations and results throughout the report.

Assumptions

A few noted assumptions are discussed in relation to how they may effect the results in an experimental setting.
Firstly, leakage throughout the system should be considered as it is an inevitability and would likely increase after a prolonged period of operation as the components would wear over time. The leakage can be difficult to determine, and can in a mathematical model be introduced as a fitting parameter for when comparing simulation results with experimental data.
Secondly, the volumes were assumed constant around the linearisation point and as a result the order of the model was reduced as the position state was disregarded. In order to obtain a more accurate model the position may need to be included as part of the linear model, as the volumes heavily impact the dynamics of the system.

Results and Considerations for the Controller Tracking

A number of things is discussed which is believed to have a significant effect on how the controllers tracked the reference.
Firstly, the chosen force profile had the benefit that it showed how the controllers would track the reference under extreme conditions, so that if they performed well for the chosen profile they would most likely also perform well under less strenuous conditions. However a disadvantage might have been that the chosen profile was operating mainly away from the linearisation point, which may have had an negative impact on the controllers ability to track the reference. So, in the interest of testing the controllers around the linearisation point which would make it easier to relate to the results of the linear model, the average value for the chosen profile should lie around the 100[kN] as was chosen in the linearisation point.
Secondly, for the results in the non linear model it was seen that saturation in the valves occurred. This was likely due to the chosen velocity reference profile, as this in combination with the force profile which gave extreme variations in the external force caused the controllers to drive the valves to their physical limit. This may give need for further analysis into the system limitations when the rod side pressure is set to a constant value.

Thirdly, it was shown that the controllers tracked the reference better for the vertical case than the horizontal case. This is most likely due to the pressure in the piston side increasing due to the increase in the force exerted onto the cylinder due to the contribution from the gravity. To achieve better results for the horizontal case, it may be necessary to consider different linearisation points, which may be done by using a new linearisation point to design the controllers or to employ the use of gain scheduling.
Fourthly, the LQG-I controller showed a more oscillatory response than the other controllers with integral action. This is most likely due to the tuning process in which the controller was tuned to accept the measurements without much regard for the relative amplitude of the noise. This could be verified by tuning the controller such that it does not trust the measurements and relies more on the accuracy of the model, in which it should be seen that the response from the controller should smoothen.

The results from the table 7.6 of the controller comparison in regards to testing in the non-linear show that the LQI controller for the horizontal case show better performance and tracking of velocity reference then the other controllers, although not by a considerable margin. This relates both to the over-and undershoot which is seen to be considerably less for the LQI controller. However, the LQI also exhibits saturation of the valves which negatively impacts the controllers ability to track the reference. The negative impact is not shown to be severe in the simulations as the controller is still able to track the reference for both the velocity and pressure without a delay that would arise due to issues with wind-up.

Considering the comparison for the vertical case it is seen from the table 7.8 that LQG-I is performing better that other controllers, however the response of velocity and pressure is more oscillatory due to the white noise injected to the states and the tuning being weighted towards trusting the measurements. In addition to that the LQI controller could be argued to be a better choice, since it is slightly under performing but the transient response is more smooth under the presence of white noise. In order to fully conclude which controller is more feasible, it is recommended that the LQG-I controller be tuned in a way that it relies on the accuracy of the model by increasing the related weight R_v.

Finally, in regards to the implementation in the setup it might be necessary to consider, whether the states can be measured through sensors, as if they are not readily available for the given experimental setup, it may be more prudent to consider the implementation of LQG-I as it has the ability to estimate the states, even though they are not measured. Then the Kalman filter may need to be configured such that is recursively updates the states based on previous data instead of applying the steady state Kalman filter.

In the next chapter the conclusion on the finding throughout report are presented.

9 Conclusion

The initial focus of this Master's Thesis was to investigate which controllers had not been implemented prior for a SMISMO system and compare their performance. A literature review was conducted to avoid implementing the same combination of control strategy and controllers as seen in prior research. From the control strategy analysis carried out in [Berthing, 2019], it was decided to make use of a pressure/velocity control strategy, which lead to the final problem statement:

"For a pressure/velocity control strategy, how does the chosen MIMO controllers compare in relation to performance when tracking a pre-defined reference set for the rod side pressure and piston velocity, when subjected to disturbance and noise."

In order to answer the raised question the methodology was outlined with the procedure of how to approach the problem.
Firstly, the assumptions and considerations were applied based on engineering knowledge and prior research on SMISMO hydraulic system in order to simplify the modelling. Based on those assumptions the non-linear model was developed and validated in the simulation without the experimental data. Afterwards the non-linear model was linearised and compared against the linear model. As the linear model was validated it is used in the system analysis to investigate system dynamics and couplings.

System analysis was conducted, showing the RGA for different linearisation points to attain how severe the coupling was for all operating conditions, and observing which parameters bore the most significant effect on these. The piston position was seen to have the most significant impact on the couplings as they relate to the chamber volumes. From the RGA it was seen that there was no clear indications as to which pressure was better to control for, it was decided however to control for the rod side pressure as this showed slightly less coupling, compared to when controlling for the piston side pressure, and no cross couplings. Analysis of the system poles showed how the system dynamics change as a result of the change in volume for different velocities. The increase in velocity showed a slight increase in the natural frequency for the real pole and an increase in the damping.

The design of FSF, FSF-I, LQR, LQI, LQG-I was specified and considered to be a good initial step into investigating whenever MIMO controllers are feasible. The controllers were first tuned and tested in the linear model. Afterwards FSF-I, LQI and LQG-I controllers were selected for the comparison against the non-linear model to investigate the performance and robustness towards noise and disturbance. From the investigation it is found that for horizontal case the LQI performs better, and for the vertical case the LQG-I controller is better. In both the horizontal and vertical case the FSF-I controller performed slightly worse than the LQ controllers.

10 | Future Work

This chapter presents the possible improvements that could be accomplished in the near future, to enhance the performance of the system.

Experimental Validation

As a result of the AAU laboratory being closed, this project is only focused on simulation study without practical implementation. Firstly, the developed non-linear model of the system should be validated against the experimental data. Secondly, experiments can be carried out to determine the magnitude of fitting parameters such as viscous and Coulomb friction. Furthermore, the designed MIMO controllers should be tested and validated in the laboratory as well.

Different Controllers and Control Strategies

It would be interesting to investigate different MIMO controllers such as gain scheduling, H^{∞} and H_2, which were presented in the literature review but showed poor performance results. The implementation of non-linear controllers such as sliding mode control and extended Kalman filter would be an interesting consideration due to high nonlinearities in the system and the stochastic nature of noise. Therefore, applying non-linear controllers could improve the overall performance of the system.

Testing different control strategies such as slave function and pressure/flow would be a valid choice. The slave function reduces control effort in a way that by controlling one state of the valve the other valve is controlled as well. While the pressure/flow strategy is similar to pressure/velocity and is used for at least one case in a SMISMO setup as shown in the literature review in [Hansen et al., 2011].

Reducing assumption, simplifications in the system

Throughout the report the assumptions are made in order to simply the model and they are deemed to be reasonable. However, by reducing the amount of assumptions it would definitely increase the accuracy of the model by an unknown amount as it depends on the experimental results.

Bibliography

A. Baratta and J. Rodellar. Structural control. volume 13, 1997. ISBN 978-981-4546-56-0.

B. Basu and S. Nagarajaiah. A wavelet-based time-varying adaptive lqr algorithm for structural control. *Engineering Structures*, 30:2470–2477, 09 2008. doi: 10.1016/j.engstruct.2008.01.011.

D. H. Bendtsen, S. Zubarev, S. Hovda, and S. B. Vedel. Controller design for a hil test bench for pitch systems. PDF, 2019.

A. Berthing. Investigation of separate meter-in separate meter-out control strategies. Technical report, Aalborg University, 2019.

J. M. P. Charles L. Phillips. *Feedback Control Systems*. Pearson Education Inc., 5th ed. edition, 2000. ISBN-13: 978-0-13-186614-0.

Z. Feng, J. Zhu, and R. Allen. Design of continuous and discrete lqi control systems with stable inner loops. *Journal of Shanghai Jiaotong University (Science)*, 12, 12 2007.

A. Hansen, H. Pedersen, T. Andersen, and L. Wachmann. Design of energy efficient smismo-els control strategies. In *Proceedings of the 2011 International Conference on Fluid Power and Mechatronics*, pages 522–527. IEEE Press, 2011. ISBN 978-1-4244-8449-2. 2011 International Conference on Fluid Power and Mechatronics (FPM) ; Conference date: 17-08-2011 Through 20-08-2011.

R. B. G. S. Hossein Gholizadeh, Doug Bitner. Modeling and experimental validation of the effective bulk modulus of a mixture of hydraulic oil and air. 10 2014. URL https://www.semanticscholar.org/paper/Modeling-and-Experimental-Validation-of-the-Bulk-of-Gholizadeh-Bitner/3f62d870de2a48f0ea69250ab596595670002fe4.

C. Jaen, J. Pou, R. Pindado, V. Sala, and J. Zaragoza. A linear-quadratic regulator with integral action applied to pwm dc-dc converters. pages 2280 – 2285, 12 2006. doi: 10.1109/IECON.2006.347726.

A. Jansson and J.-O. Palmberg. Separate controls of meter-in and meter-out orifices in mobile hyraulic systems. 1990.

A. Jansson, P. Krus, and J.-O. Palmberg. Decoupling of response and pressure level in a hydraulic actuator. 01 1992.

H. Y. Jing Wang, Guofang Gong. Control of bulk modulus of oil in hydraulic systems. 06 2008. URL https://ieeexplore.ieee.org/document/4601865.

J.-O. P. Kim Heybroek. Applied control strategies for a pump controlled open circuit solution. 2008.

S. Liu and B. Yao. Energy-saving control of single-rod hydraulic cylinders with programmable valves and improved working mode selection. *49th National Conference on Fluid Power*, 06 2004. doi: 10.4271/2002-01-1343.

L. Lu and B. Yao. Energy-saving adaptive robust control of a hydraulic manipulator using five cartridge valves with an accumulator. *Industrial Electronics, IEEE Transactions on*, 61:7046–7054, 12 2014. doi: 10.1109/TIE.2014.2314054.

MATLAB. Linear-Quadratic-Gaussian (LQG) design. https://se.mathworks.com/help/control/ref/ss.lqg.html. [Online; downloaded 24-05-2020].

M.Gopal. *Control systems principles and design*. Tata McGraw-Hill Education, 2nd edition, 2002. ISBN 0070482896.

MOOG. Servovalves direct drive servovalves d633/d634. PDF, 2019.

B. Nielsen. *Controller Development for a Separate Meter-In Separate Meter-Out Fluid Power Valve for Mobile Applications*. PhD thesis, 2005.

C. Nyberg. Flowmeter Accuracy Matters. https://www.flowcontrolnetwork.com/instrumentation/flow-measurement/turbine/article/15560770/flowmeter-accuracy-matters, 2014. [Online; downloaded 4-May-2020].

H. Pedersen, T. Andersen, T. Skoubo, and M. Jacobsen. Investigation and comparison of separate meter-in separate meter-out control strategies. In *"Proceedings of the ASME/BATH 2013 Symposium on Fluid Power & Motion Control, FPMC2013"*, pages "1–10", "United States", 2013. "American Society of Mechanical Engineers". ISBN "978-0-7918-5608-6". doi: "10.1115/FPMC2013-4480". "ASME/BATH 2013 Symposium on Fluid Power & Motion Control, FPMC2013 ; Conference date: 06-10-2013 Through 09-10-2013".

N. Razmjooy, M. A., H. Alikhani, and M. Mohseni. Comparison of lqr and pole placement design controllers for controlling the inverted pendulum. *journal of world electrical engineering and technology*, 3, 07 2014.

R. Rocha, J. Silvino, and P. Resende. Lqr with integral action for the control of variable speed induction generator connected to ac grid. pages 1061–1066, 10 2012. doi: 10.1109/IECON.2012.6388573.

L. Schmidt and P. Johansen. Multivariable control course. PDF, 2019.

I. P. Sigurd Skogestad. *Multivariable Feedback Control Analysis and design*. Wiley, 2nd ed. edition, 2005. ISBN-13: 978-0-470-01168-3.

S. B. Sören Andersson, Anders Söderberg. Friction models for sliding dry, boundary and mixed lubricated contacts. 01 2006. URL https://www.sciencedirect.com/science/article/pii/S0301679X05003154.

Yingjie Liu, Bing Xu, Huayong Yang, and Dingrong Zeng. Modeling of separate meter in and separate meter out control system. In *2009 IEEE/ASME International Conference on Advanced Intelligent Mechatronics*, pages 227–232, 2009.

A Validation and Analysis

A.1 Validation of Linear Model

In this section the validation of linear model moving opposite direction is presented. The method of validation is the same as described above, the hydraulic valves are stepped from initial values of $x_{vp} = -0.25$, $x_{vr} = -0.5$, which is seen in figure A.2. The validation of the model is conducted under given operating parameters which are presented in table A.1. The results of model comparison are presented below:

Parameters	F_{ext} $[kN]$	m $[kg]$	x_{vp} $[\%]$	x_{vr} $[\%]$	B_v	F_c $[N]$	x_p $[m]$
Values	100	12 $\times 10^3$	-0.25	-0.5-0.55	45 $\times 10^3$	200	0.928

Table A.1: Parameters used in linear model validation

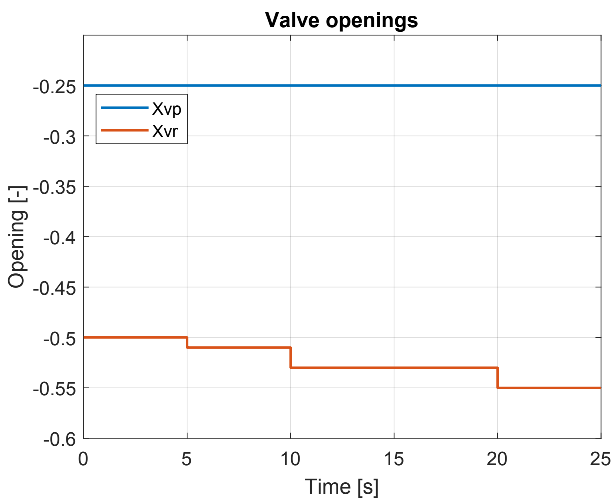

Figure A.1: Valve Opening

The comparison of position and velocity is shown in figures A.2, A.3.

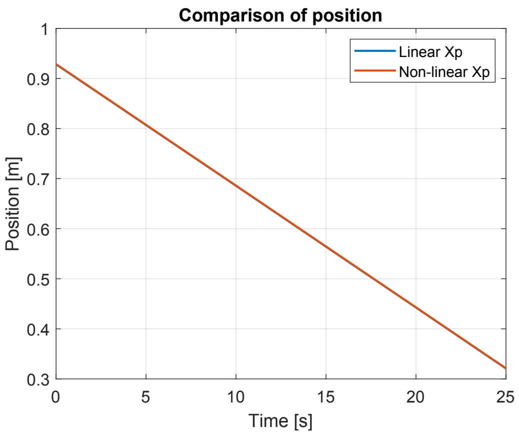

Figure A.2: Comparison of Position

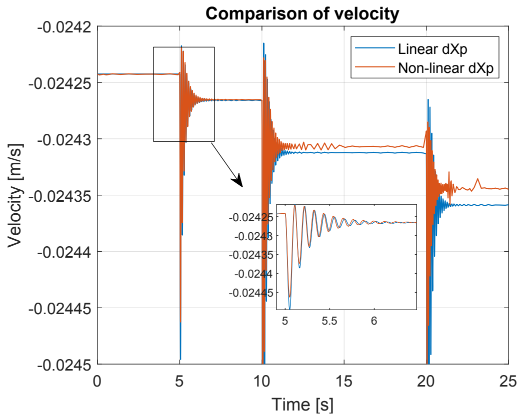

Figure A.3: Comparison of Velocity

As it is seen from position graph it fits very accurately, the change of velocity is minuscule to see the change in the slope. The velocity has some oscillations in the beginning of the step, and deviates from the actual value as valve opening increases.

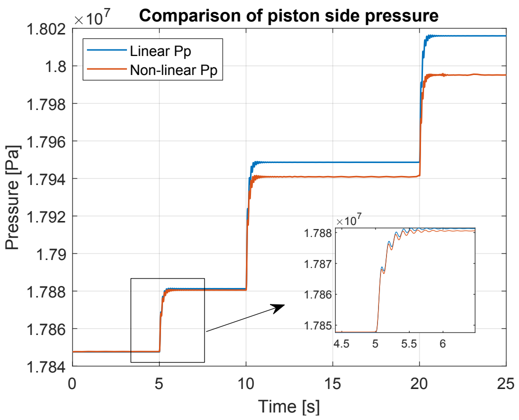

Figure A.4: Comparison of Piston side Pressure

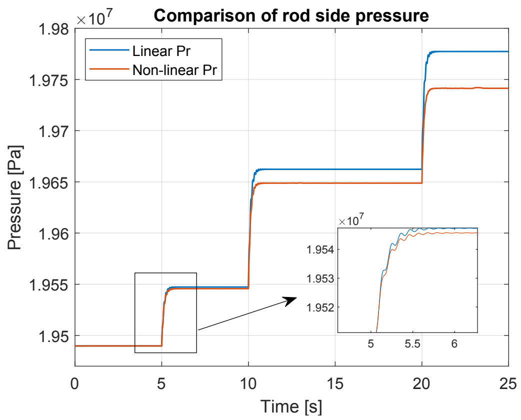

Figure A.5: Comparison of Rod side Pressure

As it is seen from figures A.4, A.5 both pressures have the same transient, and steady state value around the linearisation point. Therefore, it is concluded that linear model is valid when valves are given negative input signals.

A.2 Damping and Natural Frequency for Negative Direction

In this Appendix section the natural frequency and damping ratio are presented for the negative velocity for both cylinder's positions. The tables with parameters used to create the figures are presented above each of them.

Horizontal position

Parameters	p_p [bar]	p_r [bar]	F_{ext} [kN]	x_{vp} [%]	x_{vr} [%]	$\dot{x}_p[\frac{m}{s}]$	m [kg]
Values	80	27.3	100	-0.47	-0.18	-0.03	12 $\times 10^3$

Table A.2: Parameters used in analysis

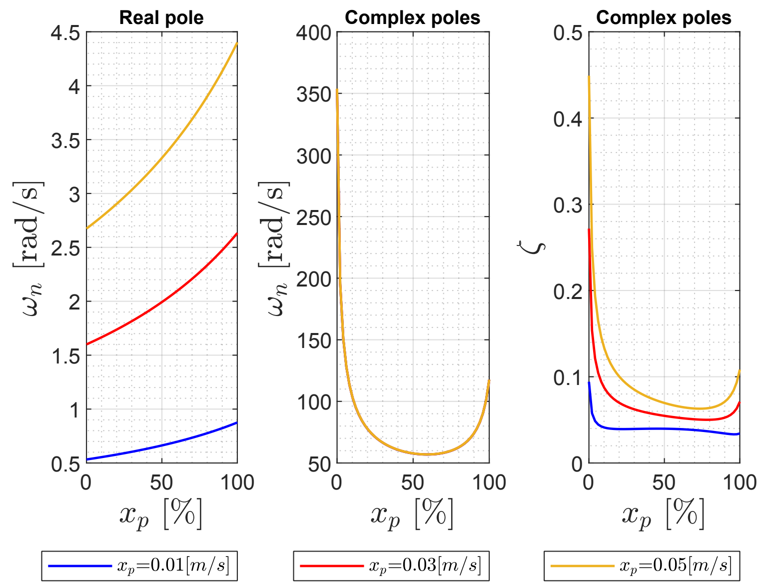

Figure A.6: Damping ratio and natural frequency of poles for whole piston stroke with $F_{ext} = 100kN$, $p_r = 27.3bar$, $p_p = 80bar$ in horizontal position moving negative direction

From the figure A.6 it is seen that natural frequency and damping ratio exhibit similar behaviour as for the positive direction with the change of magnitude. The major difference when moving negative is that force load is not opposing the motion, and in order to avoid cavitation in the rod side chamber the pressure in piston side has to be increased. From the analysis it is found that pressure in the piston side has to be increased to 80bar, to ensure that hydraulic fluid in the rod side has enough stiffness.

Vertical position

Parameters	p_p [bar]	p_r [bar]	F_{ext} [kN]	x_{vp} [%]	x_{vr} [%]	$\dot{x}_p[\frac{m}{s}]$	m [kg]
Values	155	24	100	-0.332	-0.176	-0.03	12 $\times 10^3$

Table A.3: Parameters used in analysis

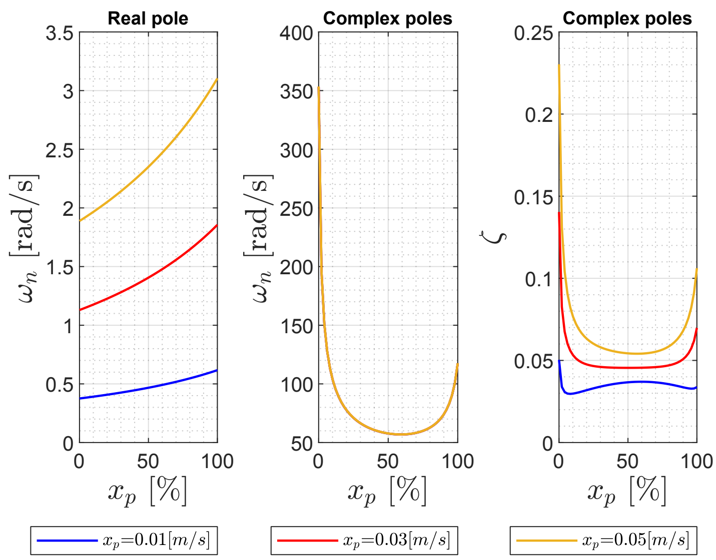

Figure A.7: Damping ratio and natural frequency of poles for whole piston stroke with $F_{ext} = 100kN$, $p_r = 24bar$ $p_p = 155bar$ in vertical position moving negative direction

In vertical position damping and natural frequencies follow the same trend discussed above.

Horizontal position with increased force load

Parameters	p_p [bar]	p_r [bar]	F_{ext} [kN]	x_{vp} [%]	x_{vr} [%]	$\dot{x}_p[\frac{m}{s}]$	m [kg]
Values	145	27.4	200	-0.343	-0.177	-0.03	12 $\times 10^3$

Table A.4: Parameters used in analysis

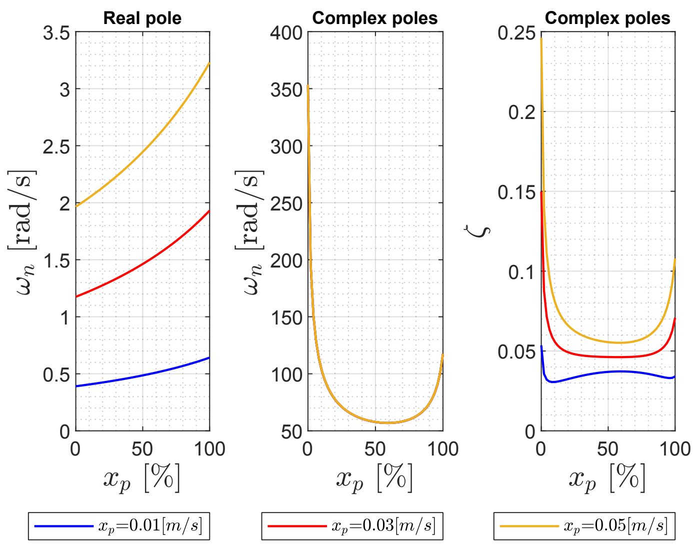

Figure A.8: Damping ratio and natural frequency of poles for whole piston stroke with $F_{ext} = 200kN$, $p_r = 27.4bar$ $p_p = 145bar$, in horizontal position moving negative direction

The increase of force load for the positive velocity is considered for $F_{ext} = 270kN$, however when moving negatively it is observed that the piston side pressure increases to 190bar, which is considerably large opposing force, and would result in loss of energy and inefficient control condition. For this case it is decided to investigate lower force load of $F_{ext} = 200kN$. From the figure A.8, A.92 it is seen that real poles are closer to origin, and would dampen the response. From investigation it is present that generally moving negative, and keeping the back pressure large enough dampens system dynamics.

Vertical position with increased force load

Parameters	p_p [bar]	p_r [bar]	F_{ext} [kN]	x_{vp} [%]	x_{vr} [%]	$\dot{x}_p[\frac{m}{s}]$	m [kg]
Values	185	19.7	150	-0.303	-0.174	-0.03	12 $\times 10^3$

Table A.5: Parameters used in analysis

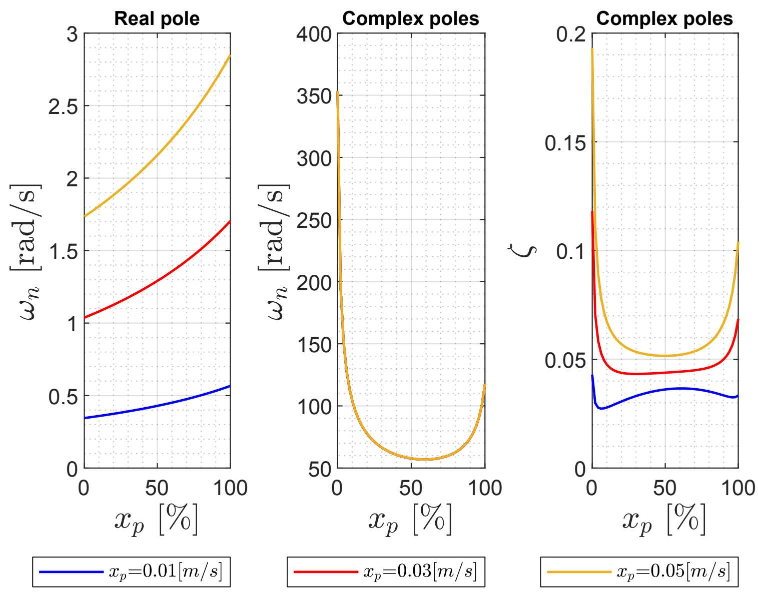

Figure A.9: Damping ratio and natural frequency of poles for whole piston stroke with $F_{ext} = 150kN$, $p_r = 19.7bar$ $p_p = 185bar$ in vertical position moving negative direction

Figure A.7 illustrates close to maximum force load that can be applied on the system in vertical position.

Step Response of the System

Figures below represent the dynamics response when applying negative velocity for the cylinder in horizontal position, this is done similarly to the positive velocity described above in section 6.1.

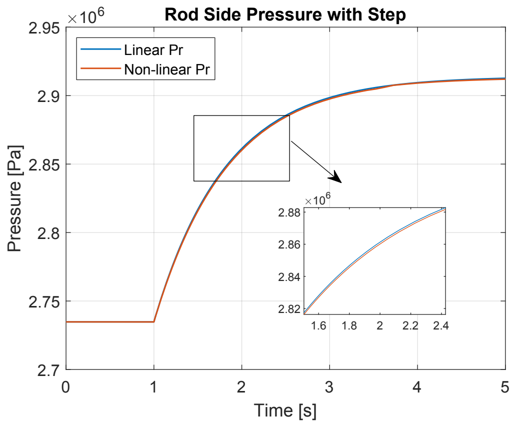

Figure A.10: Step with $x_p = 1.67m$

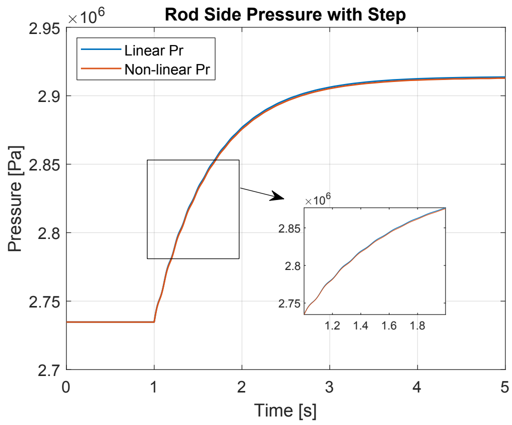

Figure A.11: Step with $x_p = 0.928m$

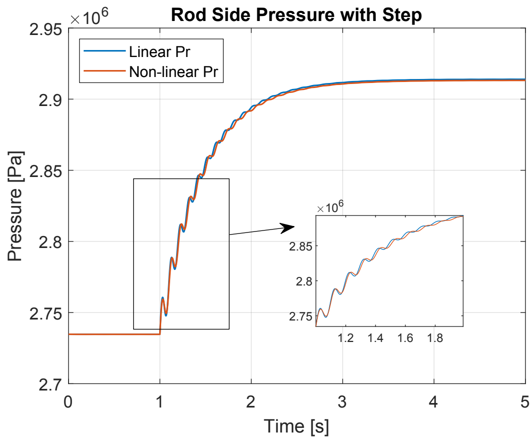

Figure A.12: Step with $x_p = 0.185m$

From the figures A.10, A.11, A.12 it is observed that oscillations are significantly lower than for positive movement, the same notion can be seen from figure A.80, A.82, A.90. The real poles for all figures are closer to origin, indicating higher damping in the system. The reason for this could be that in order to avoid cavitation the back-pressure is hold up higher creating an opposing force that dampens the system.

A.3 RGA Analysis for Horizontal Position

RGA and Pole/Zero figures for cylinder in Horizontal Position. Varying External Force Load and Controlling for p_r State

Parameters	p_p [bar]	p_r [bar]	F_{ext} [kN]	x_{vp} [%]	x_{vr} [%]	$\dot{x}_p[\frac{m}{s}]$	m [kg]
Values	12.7	20	0	0.291	0.583	0.03	12 $\times 10^3$

Table A.6: Parameters used in RGA analysis

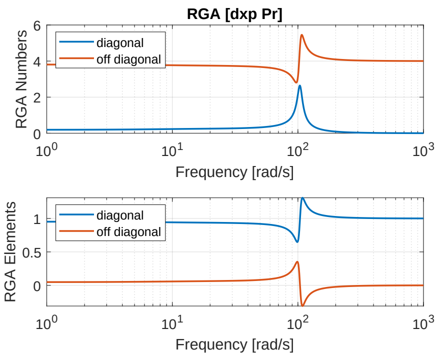

Figure A.13: RGA for x_p=0.185m

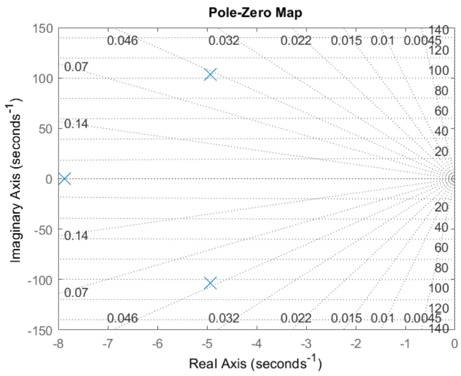

Figure A.14: Eigenvalues: -7.87, -4.93 $\pm$ 1.0375i

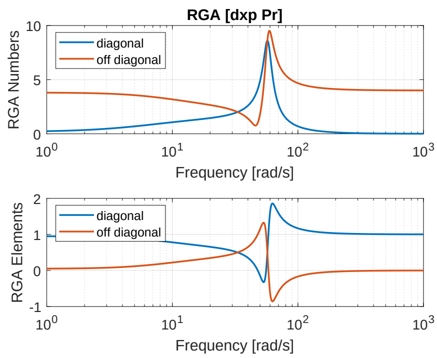

Figure A.15: RGA for x_p=0.928m

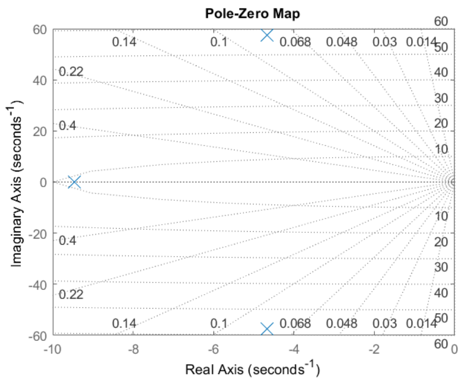

Figure A.16: Eigenvalues: -9.4674, -4.6765 $\pm$ 57.3737i

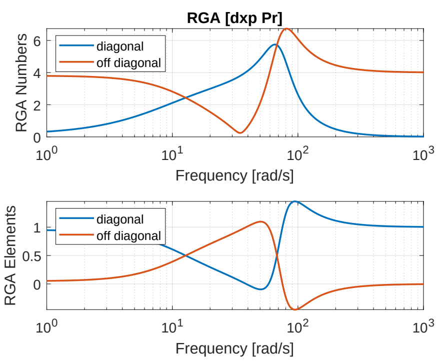

Figure A.17: RGA for x_p=1.67m

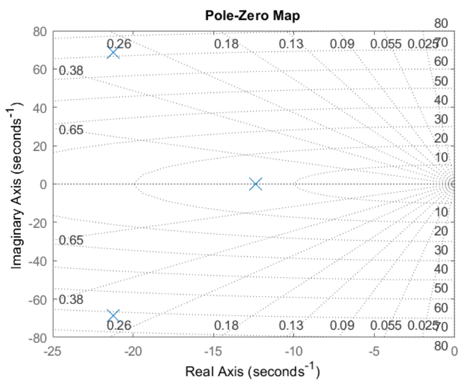

Figure A.18: Eigenvalues: -12.3797, -21.2547 $\pm$ 68.7876i

Parameters	p_p [bar]	p_r [bar]	F_{ext} [kN]	x_{vp} [%]	x_{vr} [%]	$\dot{x}_p[\frac{m}{s}]$	m [kg]
Values	77.7	20	100	0.356	0.583	0.03	12×10^3

Table A.7: Parameters used in RGA analysis

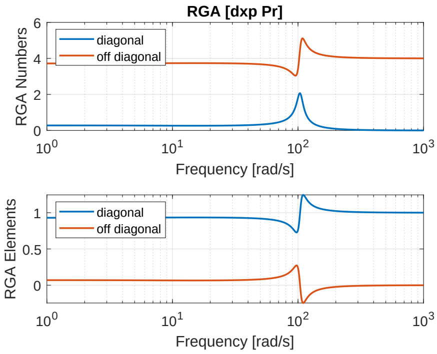

Figure A.19: RGA for x_p=0.185m

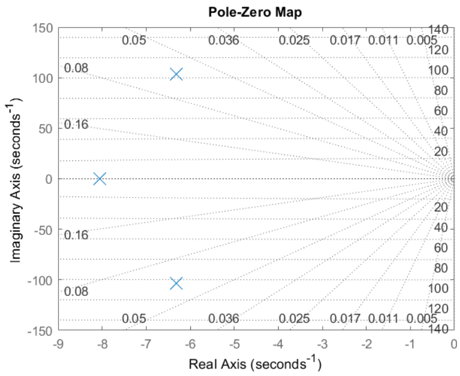

Figure A.20: Eigenvalues: -8.06, -6.32 ± 103.72i

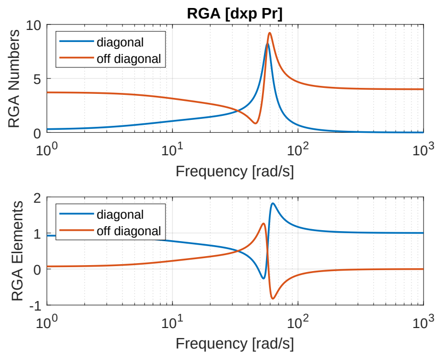

Figure A.21: RGA for x_p=0.928m

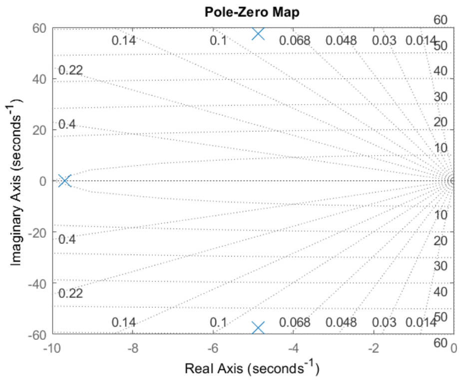

Figure A.22: Eigenvalues: -9.6857, -4.8835 ± 57.4003i

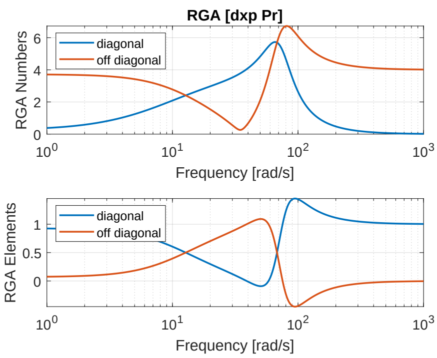

Figure A.23: RGA for x_p=1.67m

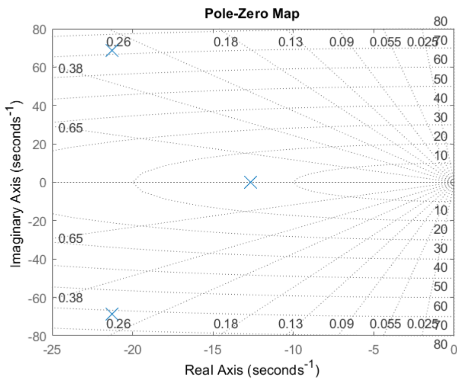

Figure A.24: Eigenvalues: -12.6697, -21.2867 ± 68.8215i

Parameters	p_p [bar]	p_r [bar]	F_{ext} [kN]	x_{vp} [%]	x_{vr} [%]	$\dot{x}_p[\frac{m}{s}]$	m [kg]
Values	188.1	20	270	0.876	0.583	0.03	12 $\times 10^3$

Table A.8: Parameters used in RGA analysis

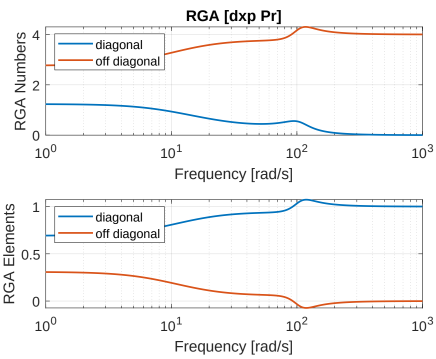

Figure A.25: RGA for x_p=0.185m

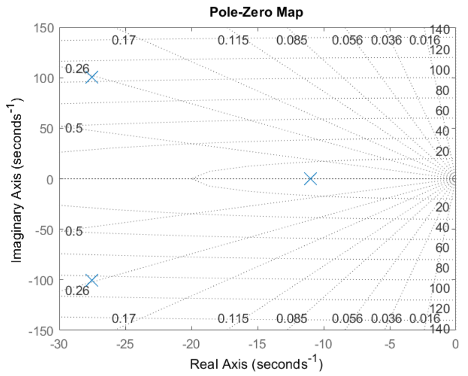

Figure A.26: Eigenvalues: -11, -27.52 $\pm$ 100.35i

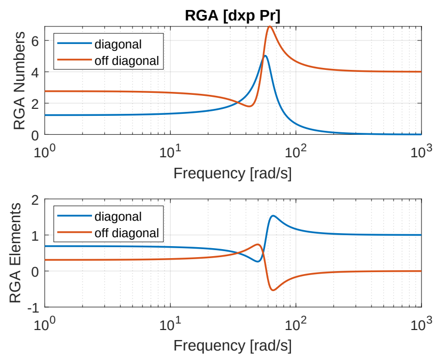

Figure A.27: RGA for x_p=0.928m

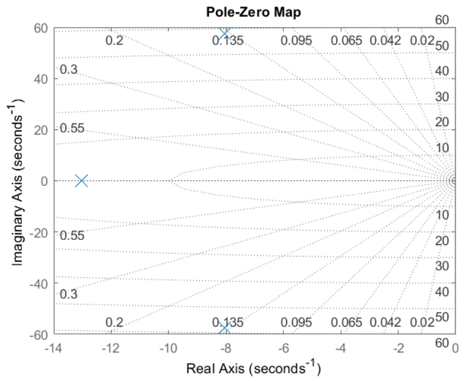

Figure A.28: Eigenvalues: -13.0412, -8.0553 $\pm$ 57.5178i

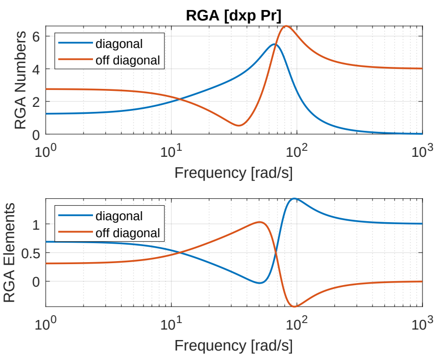

Figure A.29: RGA for x_p=1.67m

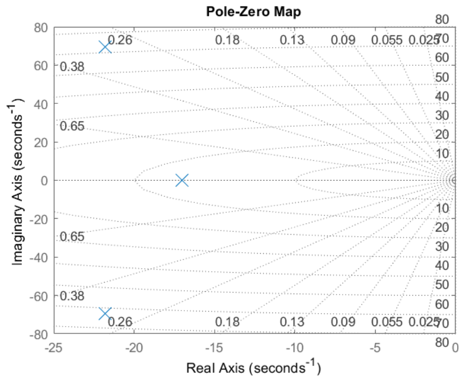

Figure A.30: Eigenvalues: -17.0440, -21.8149 $\pm$ 69.3078i

RGA and Pole/Zero figures for cylinder in Horizontal Position. Varying External Force Load and Controlling for $\mathbf{p_p}$ State

Parameters	p_p [bar]	p_r [bar]	F_{ext} [kN]	x_{vp} [%]	x_{vr} [%]	$\dot{x}_p[\frac{m}{s}]$	m [kg]
Values	12.7	20	0	0.291	0.583	0.03	12 $\times 10^3$

Table A.9: Parameters used in RGA analysis

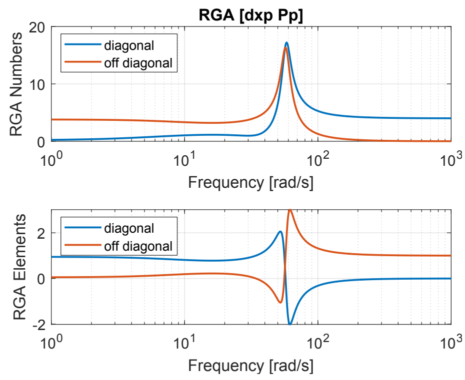

Figure A.31: RGA for x_p=0.928m

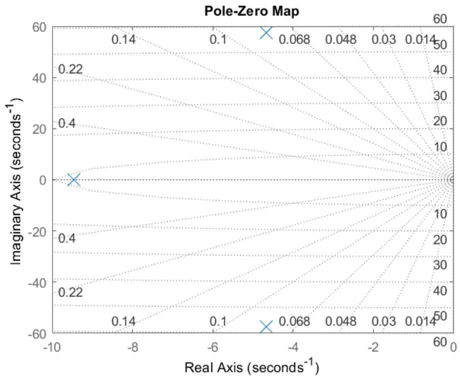

Figure A.32: Eigenvalues: -9.4674, -4.6765 ± 57.3737i

Parameters	p_p [bar]	p_r [bar]	F_{ext} [kN]	x_{vp} [%]	x_{vr} [%]	$\dot{x}_p[\frac{m}{s}]$	m [kg]
Values	77.7	20	100	0.356	0.583	0.03	12 $\times 10^3$

Table A.10: Parameters used in RGA analysis

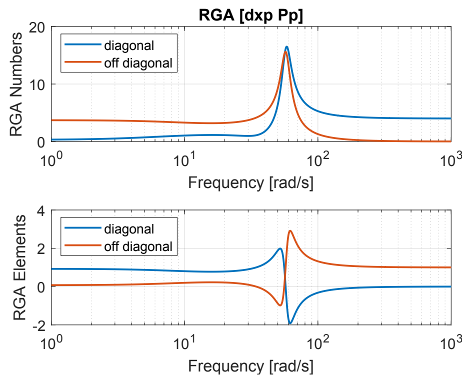

Figure A.33: RGA for x_p=0.928m

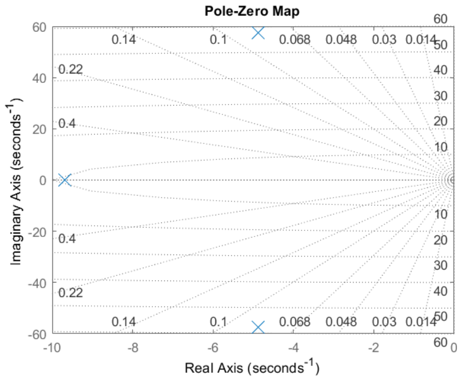

Figure A.34: Eigenvalues: -9.6857, -4.8835 ± 57.4003i

Parameters	p_p [bar]	p_r [bar]	F_{ext} [kN]	x_{vp} [%]	x_{vr} [%]	$\dot{x}_p[\frac{m}{s}]$	m [kg]
Values	188.1	20	270	0.876	0.583	0.03	12 $\times 10^3$

Table A.11: Parameters used in RGA analysis

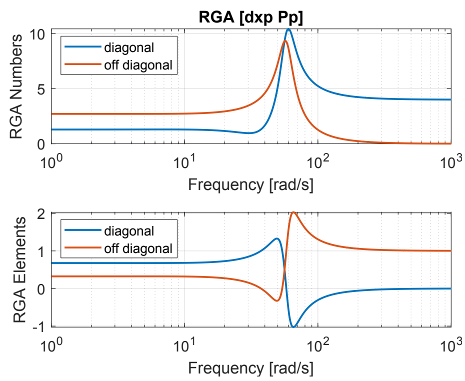

Figure A.35: RGA for x_p=0.928m

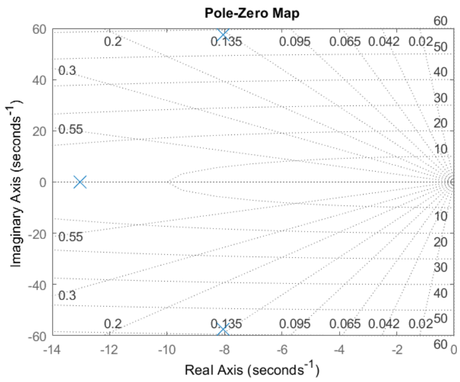

Figure A.36: Eigenvalues: -13.0412, -8.0553 ± 57.5178i

RGA and Pole/Zero figures for cylinder in Horizontal Position. Varying Rod Side Pressure and Controlling for $\mathbf{p_r}$ State

Parameters	p_p [bar]	p_r [bar]	F_{ext} [kN]	x_{vp} [%]	x_{vr} [%]	$\dot{x}_p[\frac{m}{s}]$	m [kg]
Values	80.6	25	100	0.36	0.512	0.03	12×10^3

Table A.12: Parameters used in RGA analysis

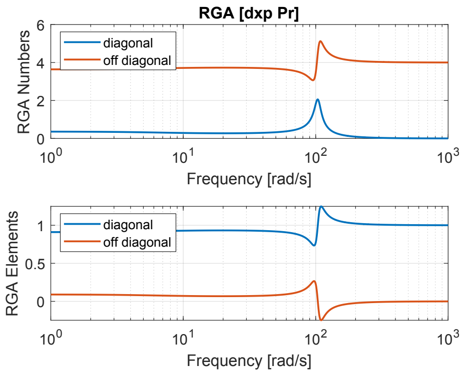

Figure A.37: RGA for x_p=0.185m

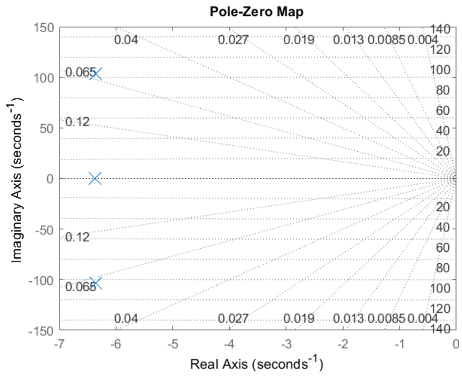

Figure A.38: Eigenvalues: -6.37, -6.36 ± 103.72i

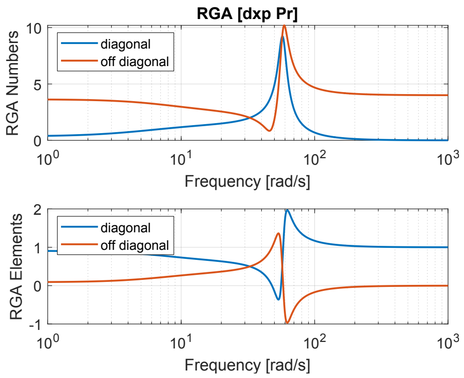

Figure A.39: RGA for x_p=0.928m

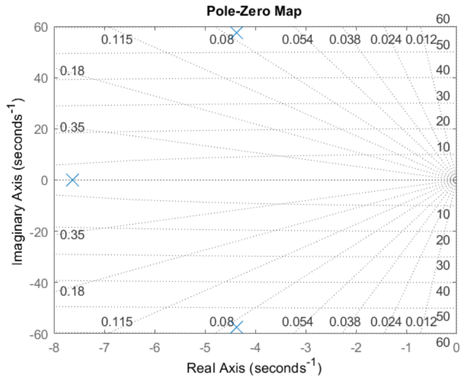

Figure A.40: Eigenvalues: -7.6291, -4.3646 ± 57.5370i

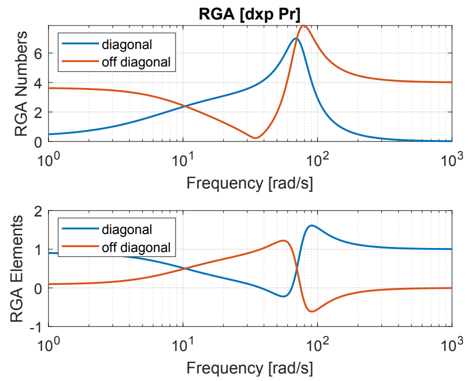

Figure A.41: RGA for x_p=1.67m

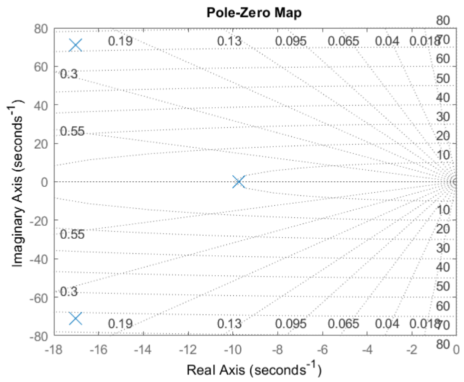

Figure A.42: Eigenvalues: -9.7237, -17.0398 ± 71.0859i

Parameters	p_p [bar]	p_r [bar]	F_{ext} [kN]	x_{vp} [%]	x_{vr} [%]	$\dot{x}_p[\frac{m}{s}]$	m [kg]
Values	83.5	30	100	0.364	0.462	0.03	12 $\times 10^3$

Table A.13: Parameters used in RGA analysis

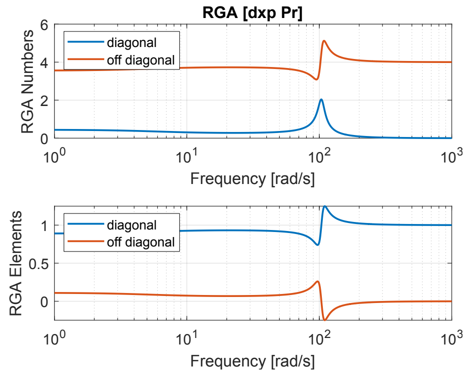

Figure A.43: RGA for x_p=0.185m

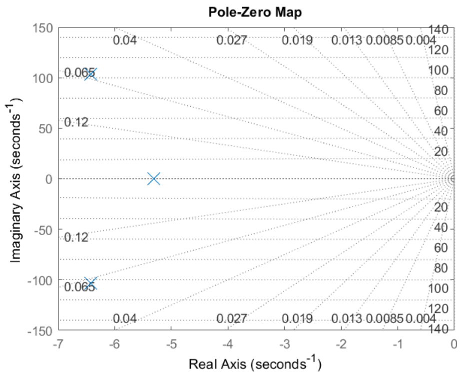

Figure A.44: Eigenvalues: -5.31, -6.42 $\pm$ 103.72i

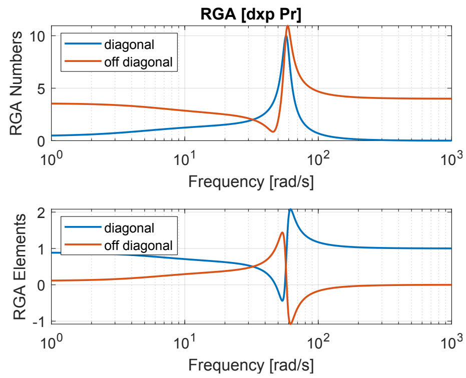

Figure A.45: RGA for x_p=0.928m

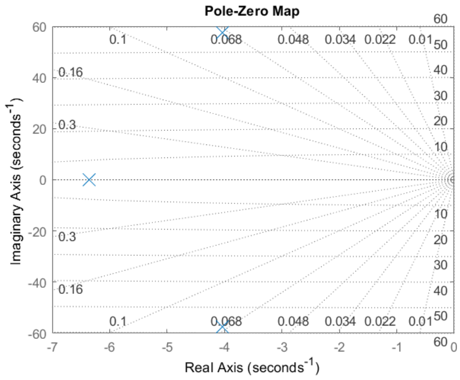

Figure A.46: Eigenvalues: -6.3517, -4.0381 $\pm$ 57.610i

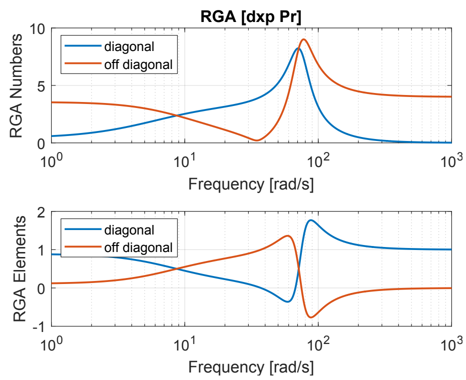

Figure A.47: RGA for x_p=1.67m

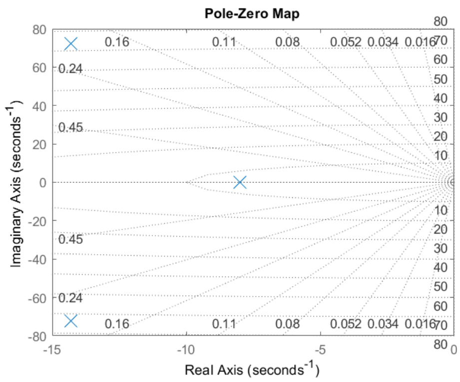

Figure A.48: Eigenvalues: -8.0043, -14.3031 $\pm$ 72.1627i

RGA and Pole/Zero figures for cylinder in Horizontal Position. Varying Rod Side Pressure and Controlling for $\mathbf{p_p}$ State

Parameters	p_p [bar]	p_r [bar]	F_{ext} [kN]	x_{vp} [%]	x_{vr} [%]	$\dot{x}_p[\frac{m}{s}]$	m [kg]
Values	80.6	25	100	0.36	0.512	0.03	12 $\times 10^3$

Table A.14: Parameters used in RGA analysis

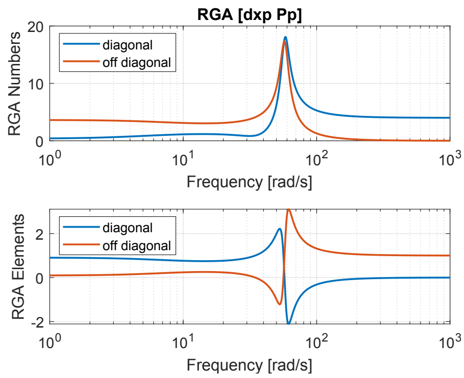

Figure A.49: RGA for x_p=0.928m

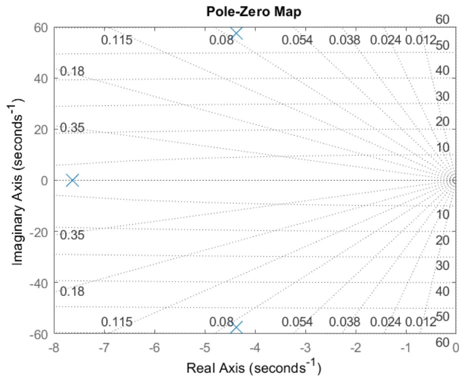

Figure A.50: Eigenvalues: -7.6291, -4.3646 $\pm$ 57.5370i

Parameters	p_p [bar]	p_r [bar]	F_{ext} [kN]	x_{vp} [%]	x_{vr} [%]	$\dot{x}_p[\frac{m}{s}]$	m [kg]
Values	83.5	30	100	0.364	0.462	0.03	12 $\times 10^3$

Table A.15: Parameters used in RGA analysis

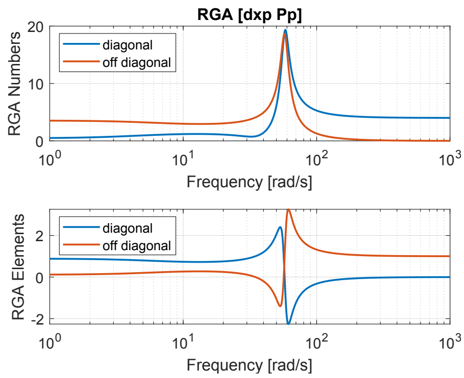

Figure A.51: RGA for x_p=0.928m

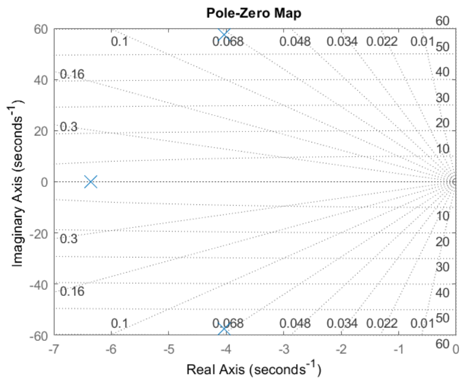

Figure A.52: Eigenvalues: -6.3517, -4.0381 $\pm$ 57.610i

RGA and Pole/Zero figures for cylinder in Horizontal Position. Varying Velocity and Controlling for p_r State

Parameters	p_p [bar]	p_r [bar]	F_{ext} [kN]	x_{vp} [%]	x_{vr} [%]	$\dot{x}_p[\frac{m}{s}]$	m [kg]
Values	77.1	20	100	0.118	0.194	0.01	12 $\times 10^3$

Table A.16: Parameters used in RGA analysis

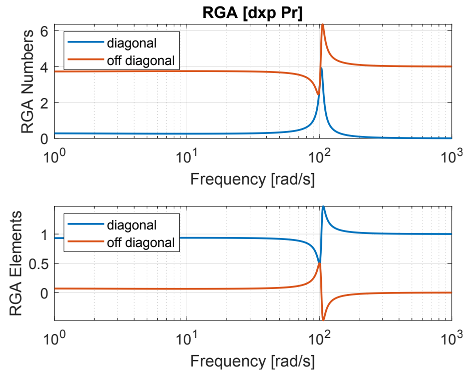

Figure A.53: RGA for x_p=0.185m

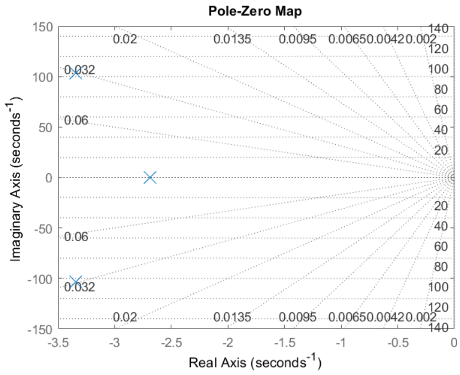

Figure A.54: Eigenvalues: -2.69, -3.34 $\pm$ 103.76i

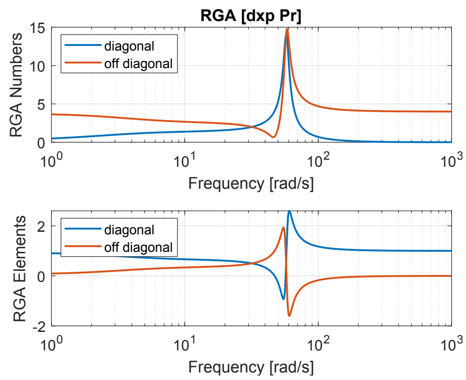

Figure A.55: RGA for x_p=0.928m

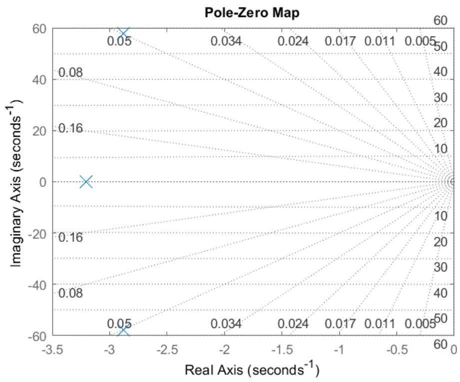

Figure A.56: Eigenvalues: -3.2079, -2.8785 $\pm$ 57.6527i

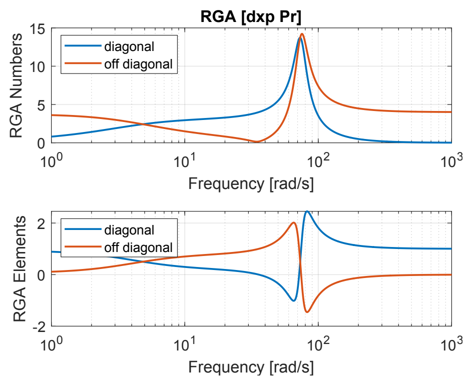

Figure A.57: RGA for x_p=1.67m

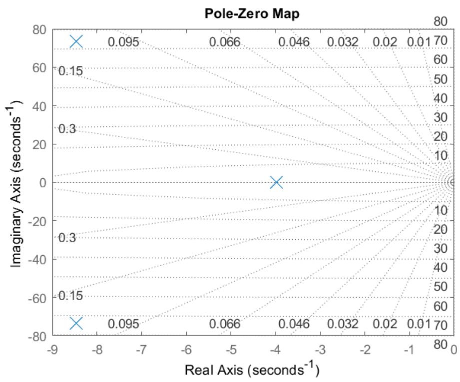

Figure A.58: Eigenvalues: -3.9861, -8.4551 $\pm$ 73.5789i

Parameters	p_p [bar]	p_r [bar]	F_{ext} [kN]	x_{vp} [%]	x_{vr} [%]	$\dot{x}_p[\frac{m}{s}]$	m [kg]
Values	78.2	20	100	0.595	0.971	0.05	12 $\times 10^3$

Table A.17: Parameters used in RGA analysis

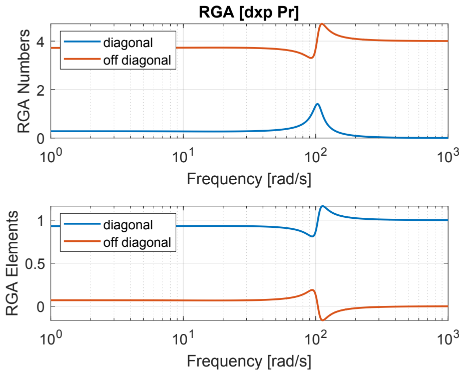

Figure A.59: RGA for x_p=0.185m

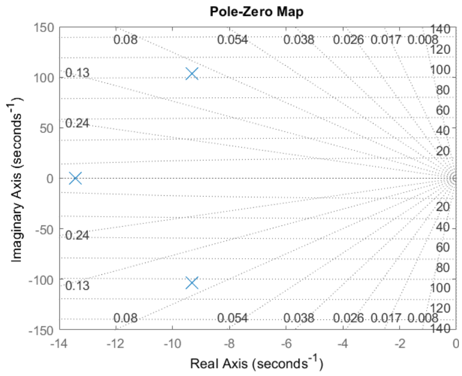

Figure A.60: Eigenvalues: -13.44, -9.32 $\pm$ 103.6i

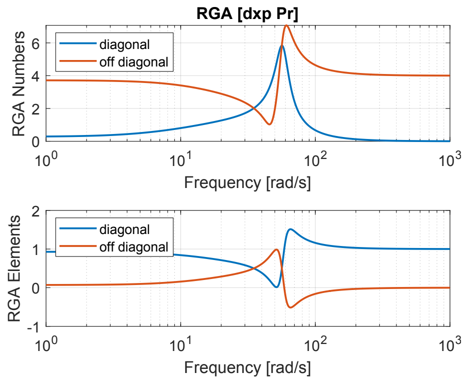

Figure A.61: RGA for x_p=0.982m

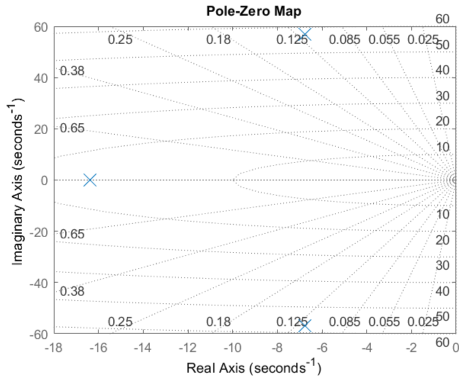

Figure A.62: Eigenvalues: -16.3844, -6.7838 $\pm$ 56.8463i

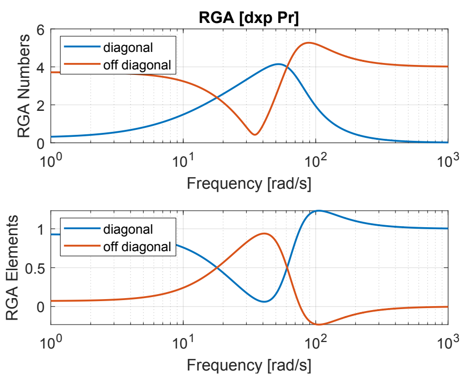

Figure A.63: RGA for x_p=1.67m

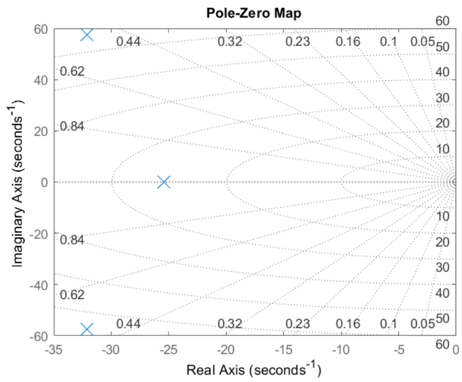

Figure A.64: Eigenvalues: -25.4091, -32.0937 $\pm$ 57.3849i

RGA and Pole/Zero figures for cylinder in Horizontal Position. Varying Velocity and Controlling for $\mathrm{p_p}$ State

Parameters	p_p [bar]	p_r [bar]	F_{ext} [kN]	x_{vp} [%]	x_{vr} [%]	$\dot{x}_p[\frac{m}{s}]$	m [kg]
Values	77.1	20	100	0.118	0.194	0.01	12 $\times 10^3$

Table A.18: Parameters used in RGA analysis

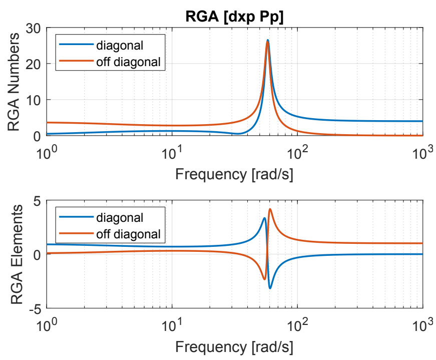

Figure A.65: RGA for x_p=0.982m

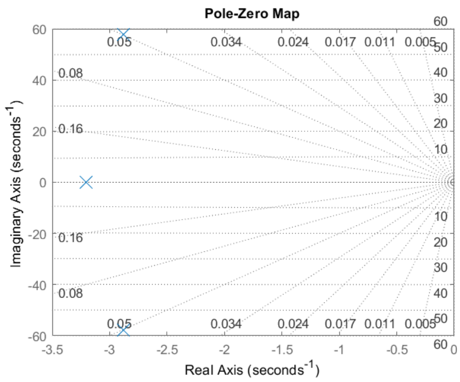

Figure A.66: Eigenvalues: -2.69, -3.34 ± 103.76i

Parameters	p_p [bar]	p_r [bar]	F_{ext} [kN]	x_{vp} [%]	x_{vr} [%]	$\dot{x}_p[\frac{m}{s}]$	m [kg]
Values	78.2	20	100	0.595	0.971	0.05	12 $\times 10^3$

Table A.19: Parameters used in RGA analysis

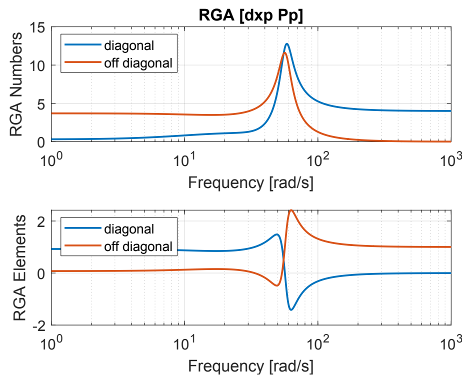

Figure A.67: RGA for x_p=0.982m

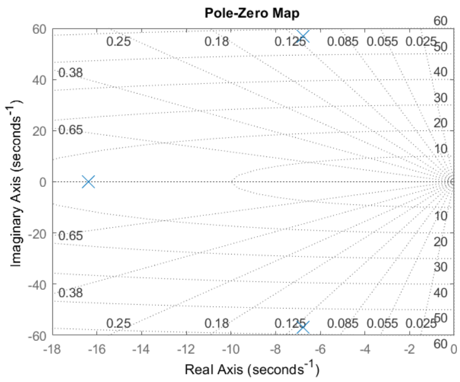

Figure A.68: Eigenvalues: -16.3844, -6.7838 ± 56.8463i

RGA and Pole/Zero figures for cylinder in Horizontal Position. Varying Mass of the System and Controlling for $\mathrm{p_r}$ State

Parameters	p_p [bar]	p_r [bar]	F_{ext} [kN]	x_{vp} [%]	x_{vr} [%]	$\dot{x}_p[\frac{m}{s}]$	m [kg]
Values	80.6	25	100	0.36	0.51	0.03	$1\ \times 10^3$

Table A.20: Parameters used in RGA analysis

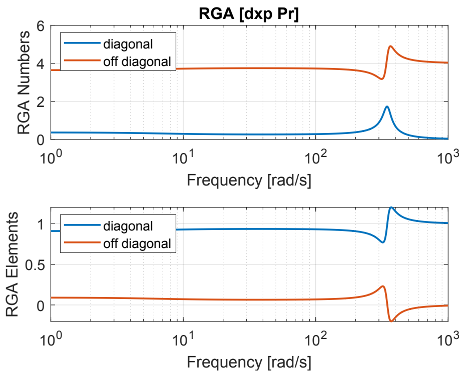

Figure A.69: RGA for x_p=0.185m

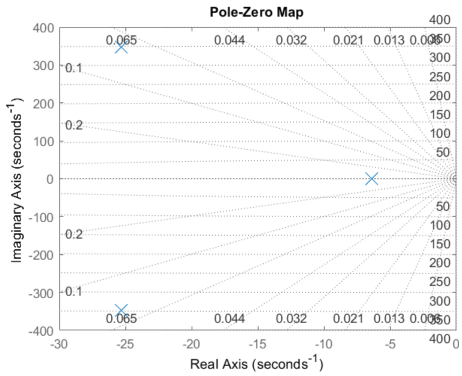

Figure A.70: Eigenvalues: -6.37, -25.33 ± 346.62i

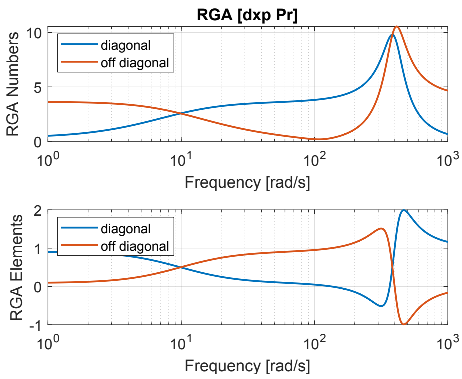

Figure A.71: RGA for x_p=0.928m

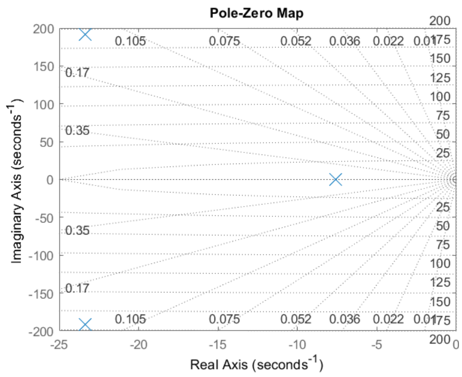

Figure A.72: Eigenvalues: -7.59, -23.35 ± 192.02i

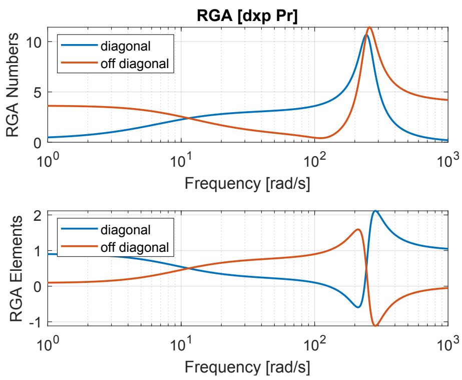

Figure A.73: RGA for x_p=1.67m

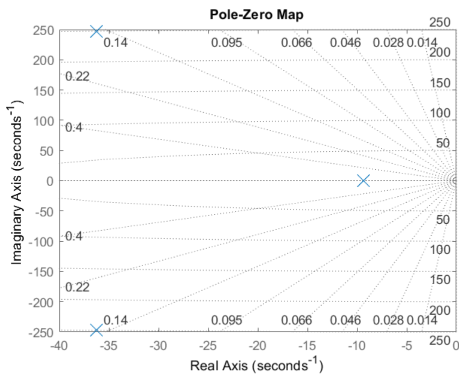

Figure A.74: Eigenvalues: -9.32 , -36.21 ± 247.09i

Parameters	p_p [bar]	p_r [bar]	F_{ext} [kN]	x_{vp} [%]	x_{vr} [%]	$\dot{x}_p[\frac{m}{s}]$	m [kg]
Values	80.6	25	100	0.36	0.51	0.03	20 $\times 10^3$

Table A.21: Parameters used in RGA analysis

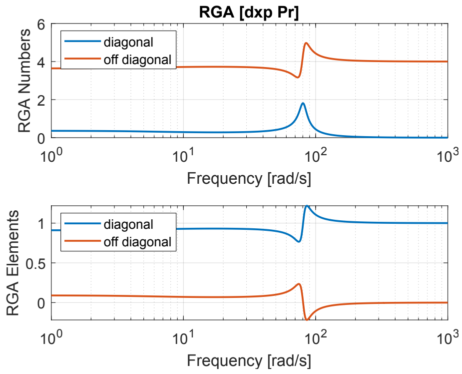

Figure A.75: RGA for x_p=0.185m

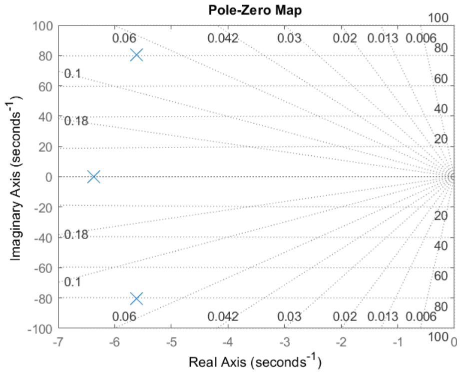

Figure A.76: Eigenvalues: -6.369, -5.6154 $\pm$ 80.4023i

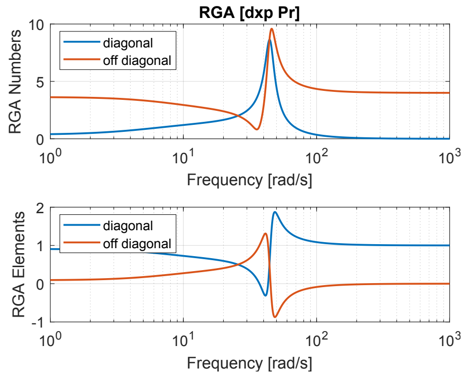

Figure A.77: RGA for x_p=0.928m

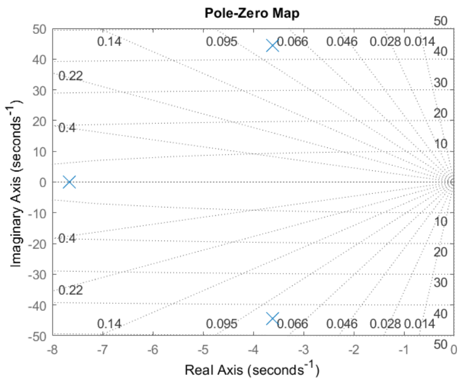

Figure A.78: Eigenvalues: -7.6552, -3.6094 $\pm$ 44.5327i

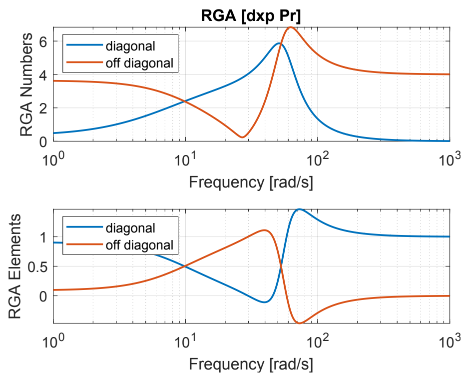

Figure A.79: RGA for x_p=1.67m

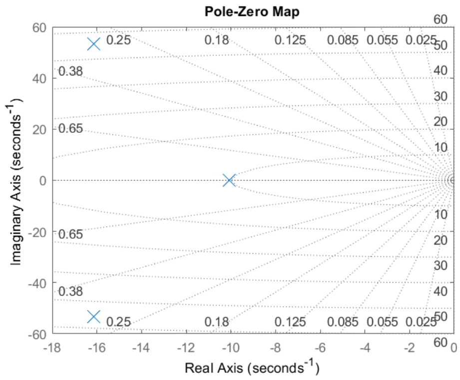

Figure A.80: Eigenvalues: -10.0622, -16.128 $\pm$ 53.3514i

RGA and Pole/Zero figures for cylinder in Horizontal Position. Varying Mass of the System and Controlling for $\mathbf{p_p}$ State

Parameters	p_p [bar]	p_r [bar]	F_{ext} [kN]	x_{vp} [%]	x_{vr} [%]	$\dot{x}_p[\frac{m}{s}]$	m [kg]
Values	80.6	25	100	0.36	0.51	0.03	1×10^3

Table A.22: Parameters used in RGA analysis

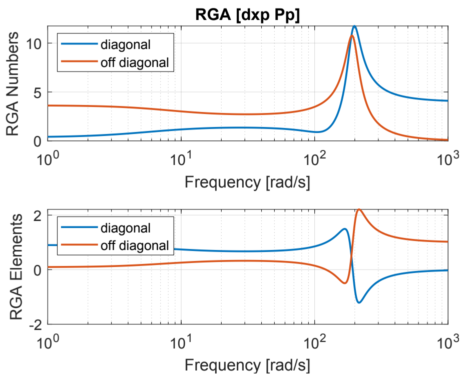

Figure A.81: RGA for x_p=0.928m

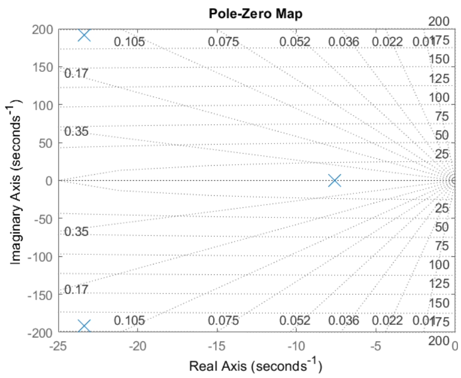

Figure A.82: Eigenvalues: -7.59, -23.35 $\pm$ 192.02i

Parameters	p_p [bar]	p_r [bar]	F_{ext} [kN]	x_{vp} [%]	x_{vr} [%]	$\dot{x}_p[\frac{m}{s}]$	m [kg]
Values	80.6	25	100	0.36	0.51	0.03	20×10^3

Table A.23: Parameters used in RGA analysis

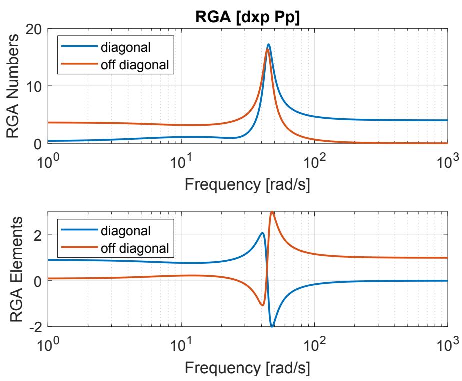

Figure A.83: RGA for x_p=0.928m

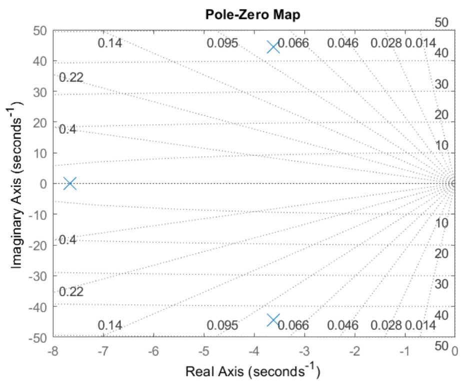

Figure A.84: Eigenvalues: -7.6552, -3.6094 $\pm$ 44.5327i

RGA and Pole/Zero figures for cylinder in Horizontal Position. Applying Negative Velocity, Varying Force Load and Controlling for $\mathrm{p_r}$ State

Parameters	p_p [bar]	p_r [bar]	F_{ext} [kN]	x_{vp} [%]	x_{vr} [%]	$\dot{x}_p[\frac{m}{s}]$	m [kg]
Values	80	27.3	100	-0.47	-0.18	-0.03	12×10^3

Table A.24: Parameters used in RGA analysis

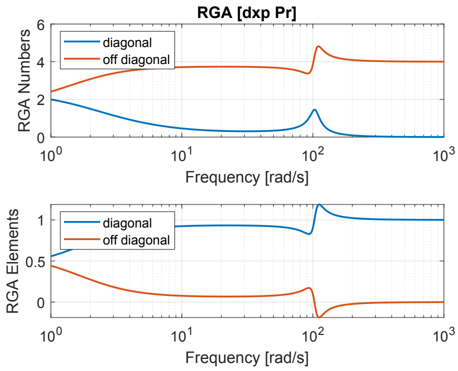

Figure A.85: RGA for x_p=0.185m

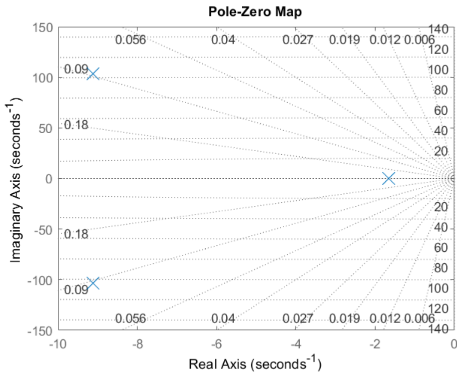

Figure A.86: Eigenvalues: -1.67, -9.11 ± 103.56i

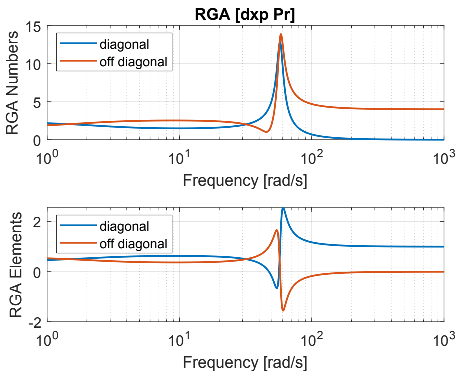

Figure A.87: RGA for x_p=0.928m

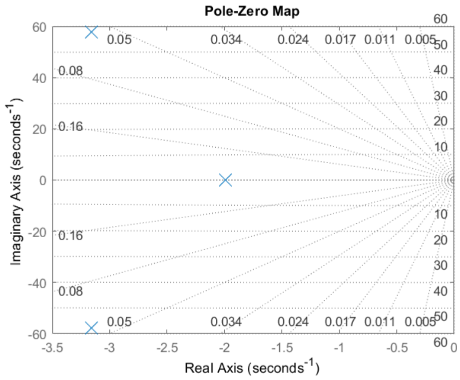

Figure A.88: Eigenvalues: -1.9926, -3.1584 ± 57.6792i

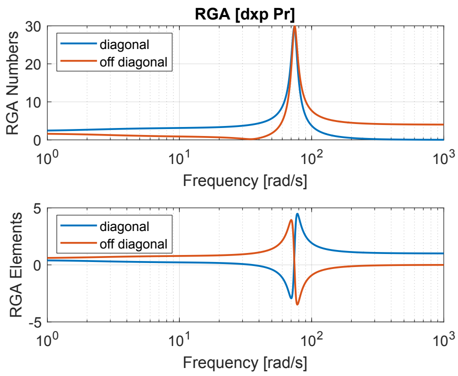

Figure A.89: RGA for x_p=1.67m

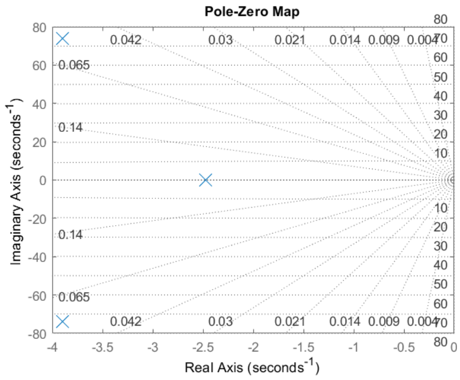

Figure A.90: Eigenvalues: -2.4745, -3.8964 ± 74.0362i

Parameters	p_p [bar]	p_r [bar]	F_{ext} [kN]	x_{vp} [%]	x_{vr} [%]	$\dot{x}_p[\frac{m}{s}]$	m [kg]
Values	145	27.4	200	-0.343	-0.177	-0.03	12 $\times 10^3$

Table A.25: Parameters used in RGA analysis

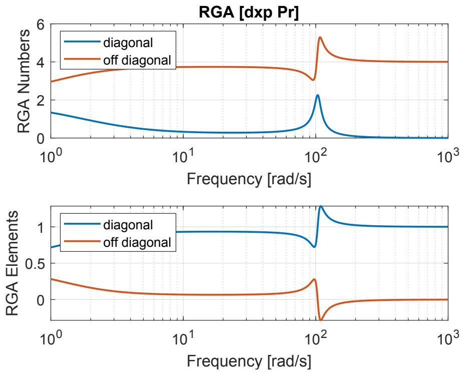

Figure A.91: RGA for x_p=0.185m

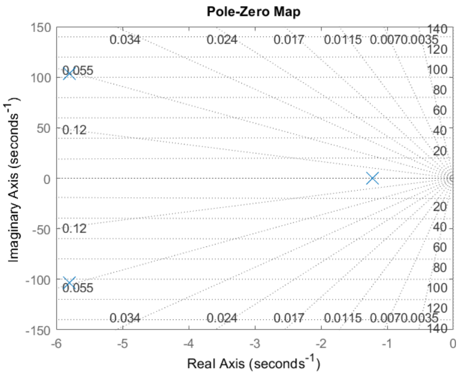

Figure A.92: Eigenvalues: -1.22, -5.8 ± 103.72i

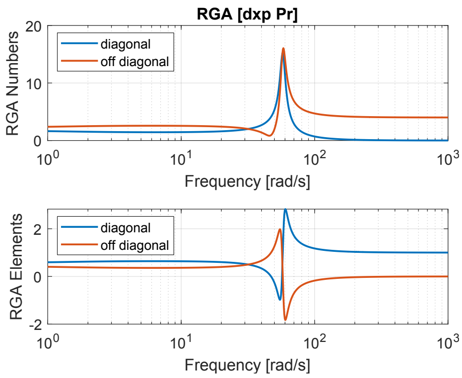

Figure A.93: RGA for x_p=0.928m

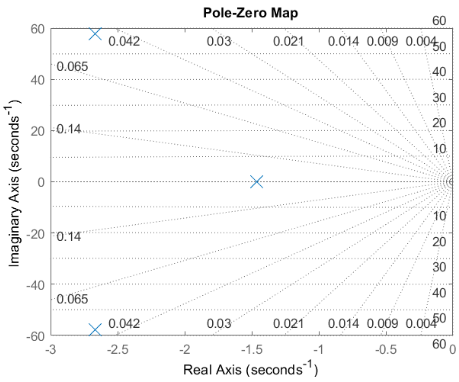

Figure A.94: Eigenvalues: -1.4625, -2.6686 ± 57.6799i

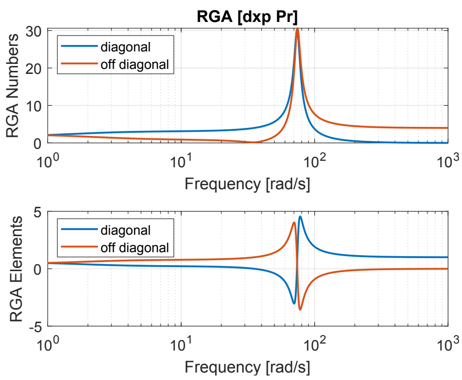

Figure A.95: RGA for x_p=1.67m

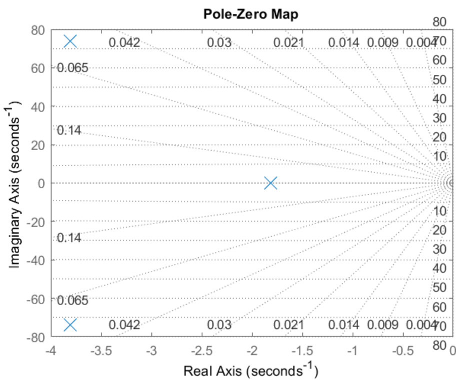

Figure A.96: Eigenvalues: -1.8152, -3.8041 ± 74.0299i

RGA and Pole/Zero figures for cylinder in Horizontal Position. Applying Negative Velocity, Varying Force Load and Controlling for $\mathbf{p_p}$ State

Parameters	p_p [bar]	p_r [bar]	F_{ext} [kN]	x_{vp} [%]	x_{vr} [%]	$\dot{x}_p[\frac{m}{s}]$	m [kg]
Values	80	27.3	100	-0.47	-0.18	-0.03	12 $\times 10^3$

Table A.26: Parameters used in RGA analysis

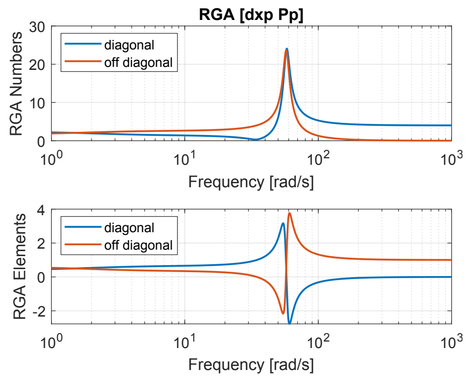

Figure A.97: RGA for x_p=0.928m

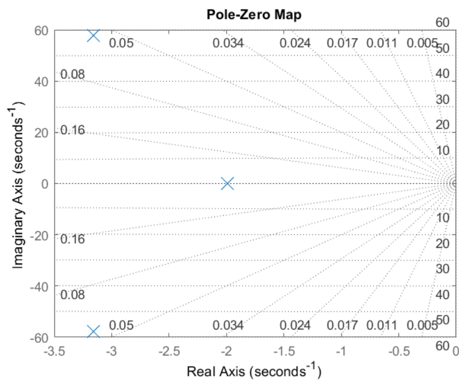

Figure A.98: Eigenvalues: -1.9926, -3.1584 ± 57.6792i

Parameters	p_p [bar]	p_r [bar]	F_{ext} [kN]	x_{vp} [%]	x_{vr} [%]	$\dot{x}_p[\frac{m}{s}]$	m [kg]
Values	145	27.4	200	-0.343	-0.177	-0.03	12 $\times 10^3$

Table A.27: Parameters used in RGA analysis

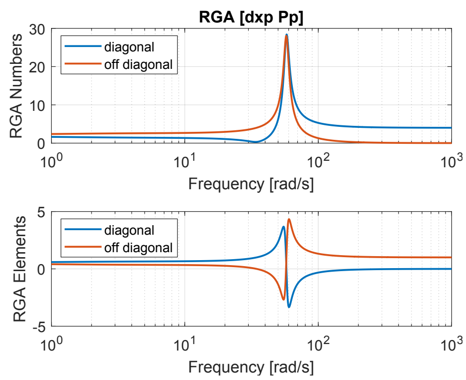

Figure A.99: RGA for x_p=0.928m

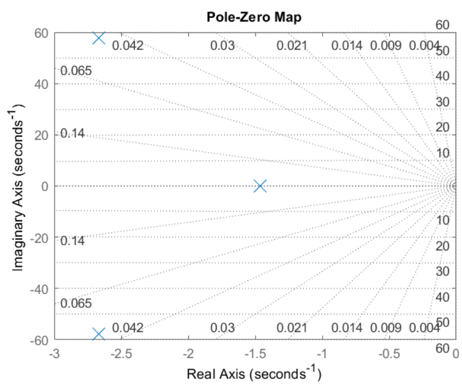

Figure A.100: Eigenvalues: -1.4625, -2.6686 ± 57.6799i

A.4 RGA Analysis for Vertical Position

RGA and Pole/Zero figures for cylinder in Vertical Position. Varying External Force Load and Controlling for $\mathbf{p_r}$ State

Parameters	p_p [bar]	p_r [bar]	F_{ext} [kN]	x_{vp} [%]	x_{vr} [%]	$\dot{x}_p[\frac{m}{s}]$	m [kg]
Values	154.7	20	100	0.55	0.583	0.03	12 $\times 10^3$

Table A.28: Parameters used in RGA analysis

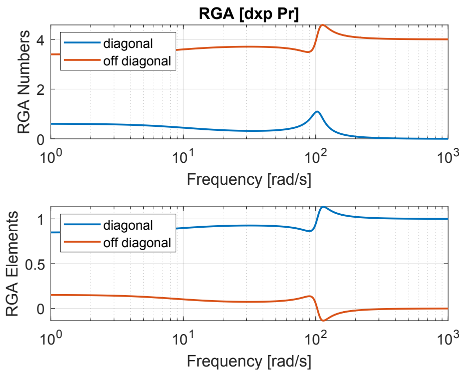

Figure A.101: RGA for x_p=0.185m

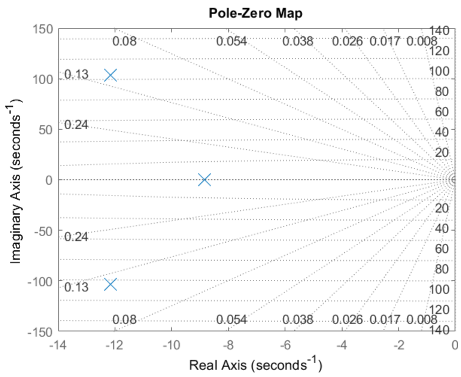

Figure A.102: Eigenvalues: -8.85, -12.17 ± 103.36i

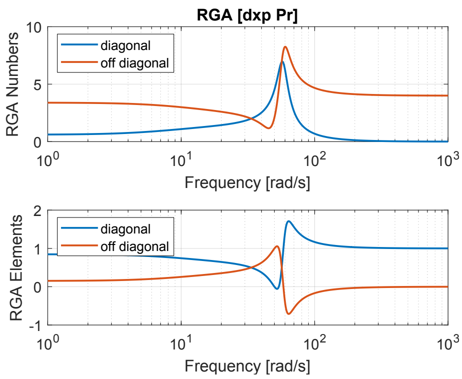

Figure A.103: RGA for x_p=0.928m

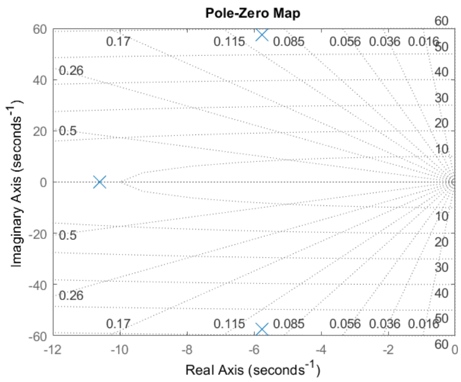

Figure A.104: Eigenvalues: -10.6077, -5.7587 ± 57.4870i

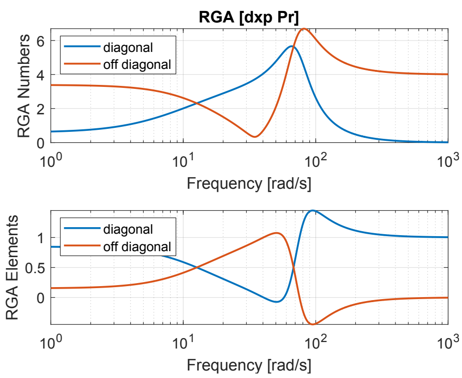

Figure A.105: RGA for x_p=1.67m

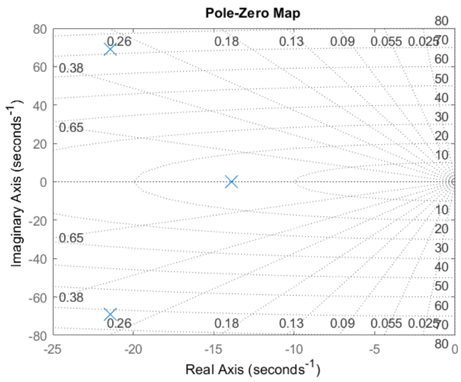

Figure A.106: Eigenvalues: -13.8886 , -21.4254 ± 68.9622i

Parameters	p_p [bar]	p_r [bar]	F_{ext} [kN]	x_{vp} [%]	x_{vr} [%]	$\dot{x}_p[\frac{m}{s}]$	m [kg]
Values	187.1	20	150	0.566	0.512	0.03	12 $\times 10^3$

Table A.29: Parameters used in RGA analysis

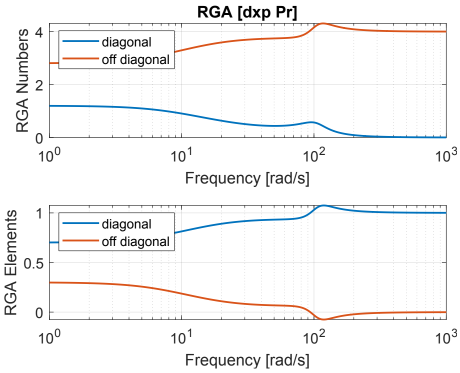

Figure A.107: RGA for x_p=0.185m

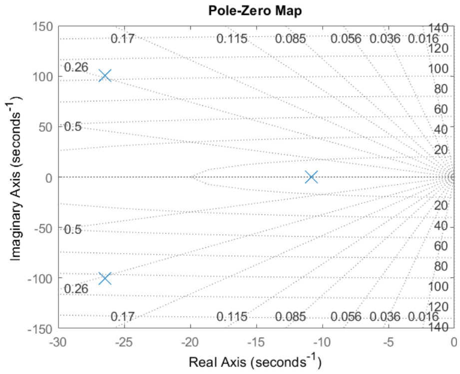

Figure A.108: Eigenvalues: -10.85, -12.17 ± 100.66i

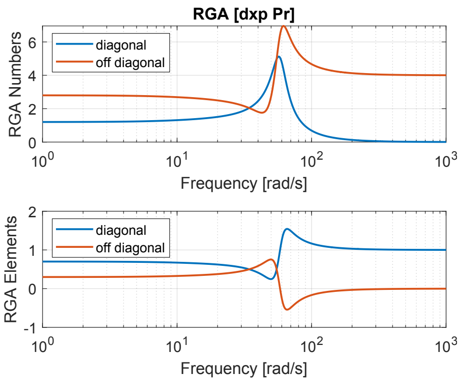

Figure A.109: RGA for x_p=0.928m

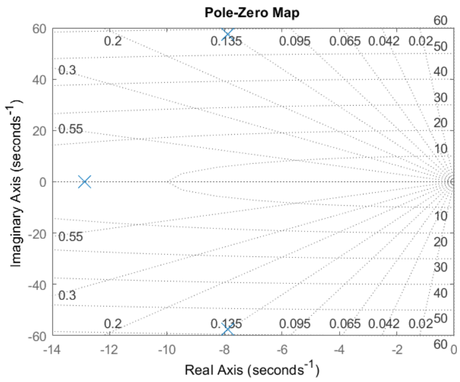

Figure A.110: Eigenvalues: -12.8689, -7.8943 ± 57.5250i

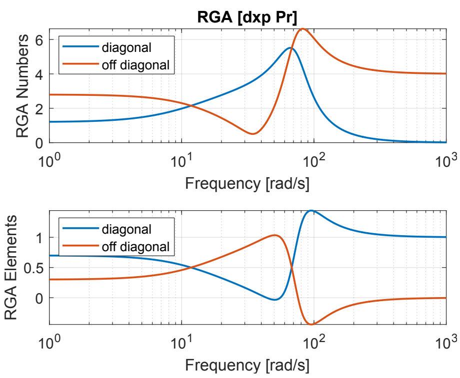

Figure A.111: RGA for x_p=1.67m

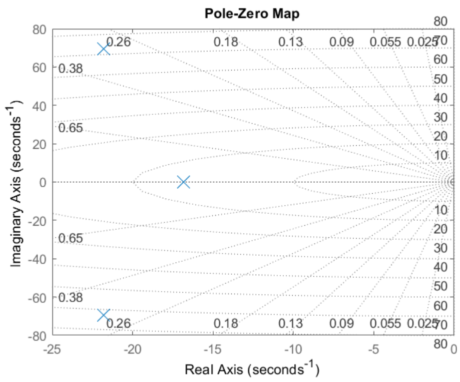

Figure A.112: Eigenvalues: -16.8242 , -21.7864 ± 69.2847i

RGA and Pole/Zero figures for cylinder in Vertical Position. Varying External Force Load and Controlling for $\mathbf{p_p}$ State

Parameters	p_p [bar]	p_r [bar]	F_{ext} [kN]	x_{vp} [%]	x_{vr} [%]	$\dot{x}_p[\frac{m}{s}]$	m [kg]
Values	154.7	20	100	0.55	0.583	0.03	12 $\times 10^3$

Table A.30: Parameters used in RGA analysis

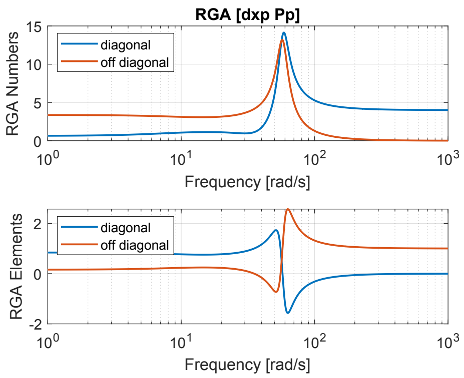

Figure A.113: RGA for x_p=0.928m

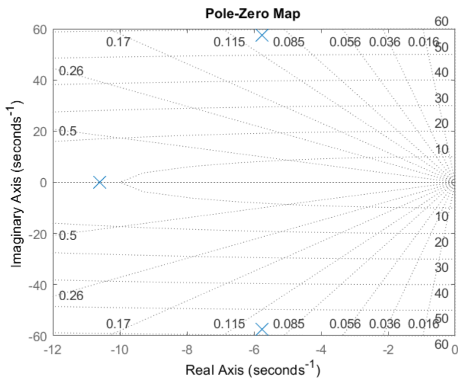

Figure A.114: Eigenvalues: -10.6077, -5.7587 $\pm$ 57.4870i

Parameters	p_p [bar]	p_r [bar]	F_{ext} [kN]	x_{vp} [%]	x_{vr} [%]	$\dot{x}_p[\frac{m}{s}]$	m [kg]
Values	187.1	20	150	0.566	0.512	0.03	12 $\times 10^3$

Table A.31: Parameters used in RGA analysis

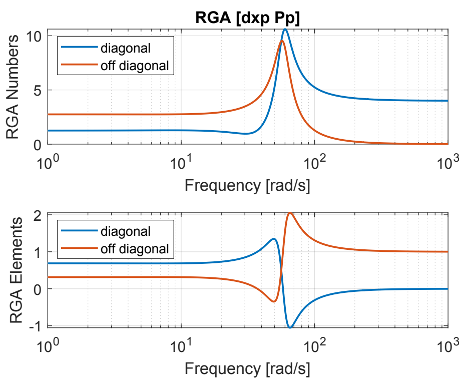

Figure A.115: RGA for x_p=0.928m

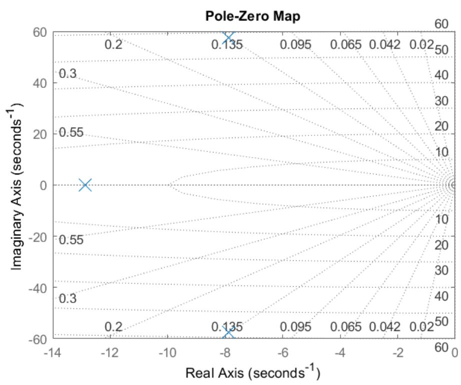

Figure A.116: Eigenvalues: -12.8689, -7.8943 $\pm$ 57.5250i

RGA and Pole/Zero figures for cylinder in Vertical Position. Applying Negative Velocity, Varying External Force Load and Controlling for $\mathbf{p_r}$ State

Parameters	p_p [bar]	p_r [bar]	F_{ext} [kN]	x_{vp} [%]	x_{vr} [%]	$\dot{x}_p[\frac{m}{s}]$	m [kg]
Values	155	24	100	-0.332	-0.176	-0.03	12 $\times 10^3$

Table A.32: Parameters used in RGA analysis

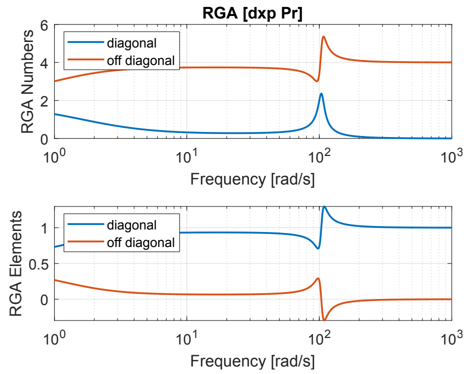

Figure A.117: RGA for x_p=0.185m

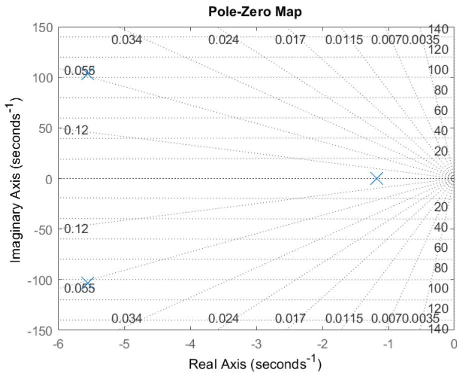

Figure A.118: Eigenvalues: -1.8, -5.55 $\pm$ 103.73i

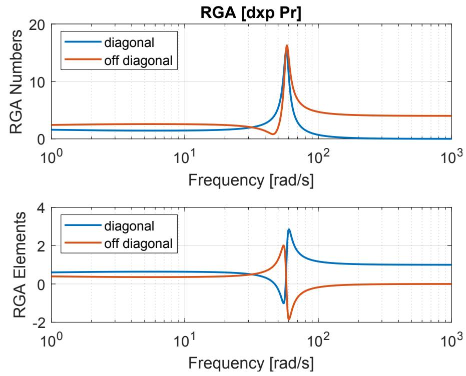

Figure A.119: RGA for x_p=0.928m

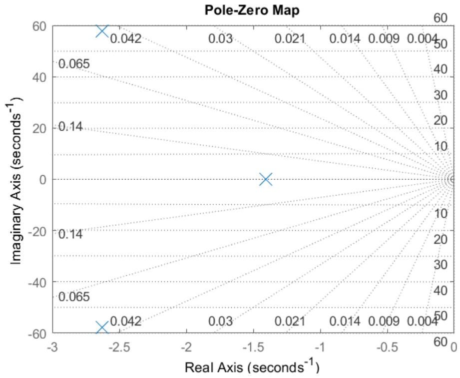

Figure A.120: Eigenvalues: -1.4057, -2.6262 $\pm$ 57.6792i

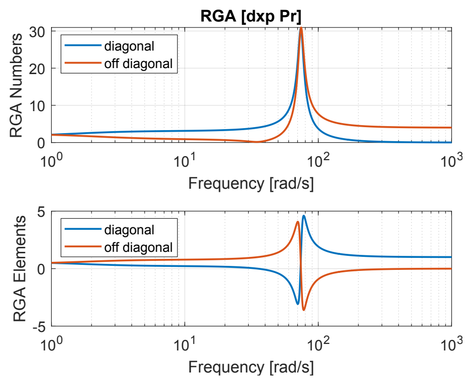

Figure A.121: RGA for x_p=1.67m

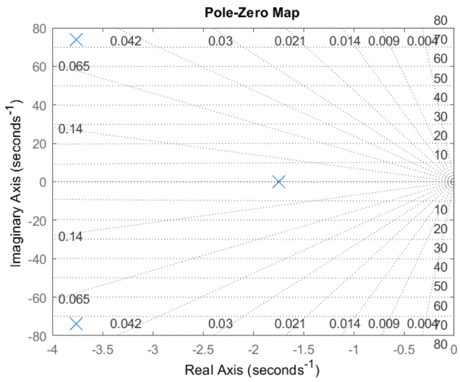

Figure A.122: Eigenvalues: -1.7446, -3.7630 $\pm$ 74.0301i

Parameters	p_p [bar]	p_r [bar]	F_{ext} [kN]	x_{vp} [%]	x_{vr} [%]	$\dot{x}_p[\frac{m}{s}]$	m [kg]
Values	185	19.7	150	-0.303	-0.174	-0.03	12 $\times 10^3$

Table A.33: Parameters used in RGA analysis

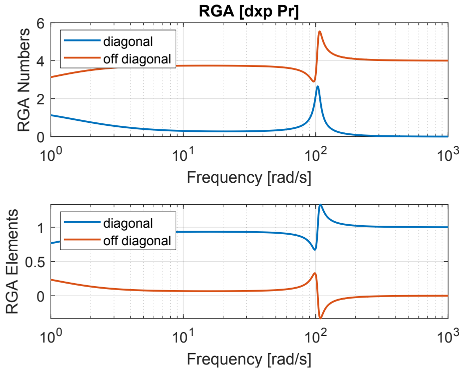

Figure A.123: RGA for x_p=0.185m

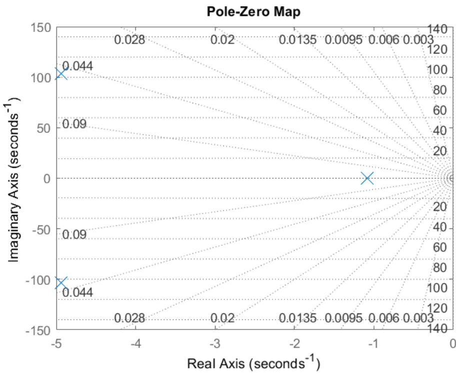

Figure A.124: Eigenvalues: -1.08, -4.94 $\pm$ 103.74i

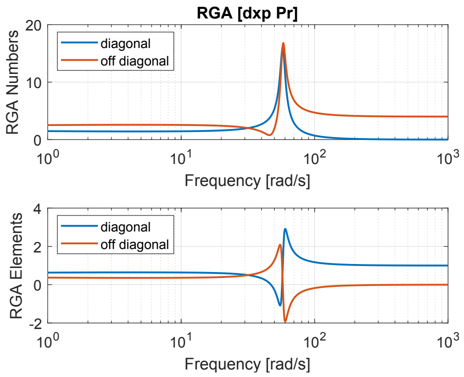

Figure A.125: RGA for x_p=0.928m

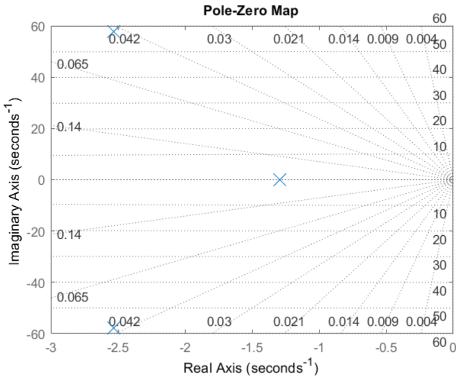

Figure A.126: Eigenvalues: -1.2907, -2.5320 $\pm$ 57.6776i

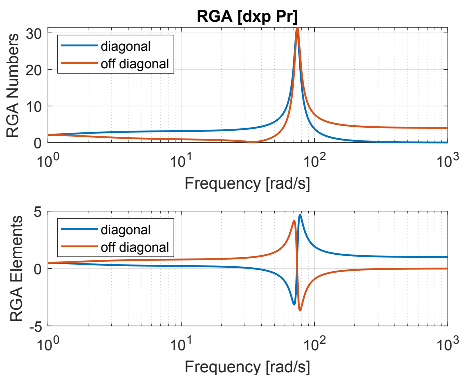

Figure A.127: RGA for x_p=1.67m

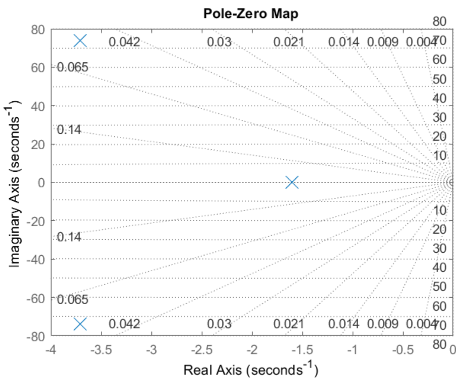

Figure A.128: Eigenvalues: -1.6017, -3.7061 $\pm$ 74.0297i

RGA and Pole/Zero figures for cylinder in Vertical Position. Applying Negative Velocity, Varying External Force Load and Controlling for $\mathbf{p_p}$ State

Parameters	p_p [bar]	p_r [bar]	F_{ext} [kN]	x_{vp} [%]	x_{vr} [%]	$\dot{x}_p[\frac{m}{s}]$	m [kg]
Values	155	24	100	-0.332	-0.176	-0.03	12 $\times 10^3$

Table A.34: Parameters used in RGA analysis

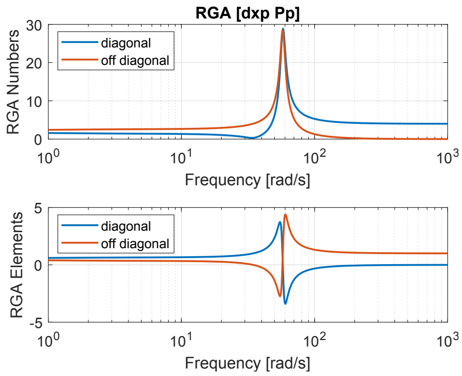

Figure A.129: RGA for x_p=0.928m

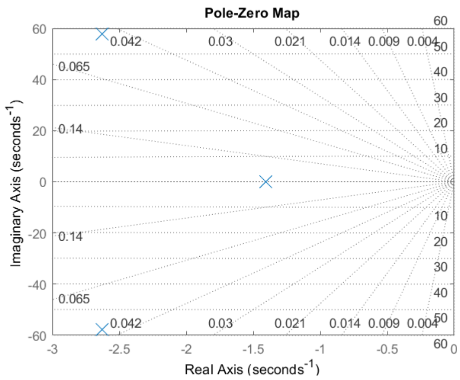

Figure A.130: Eigenvalues: -1.4057, -2.6262 $\pm$ 57.6792i

Parameters	p_p [bar]	p_r [bar]	F_{ext} [kN]	x_{vp} [%]	x_{vr} [%]	$\dot{x}_p[\frac{m}{s}]$	m [kg]
Values	185	19.7	150	-0.303	-0.174	-0.03	12 $\times 10^3$

Table A.35: Parameters used in RGA analysis

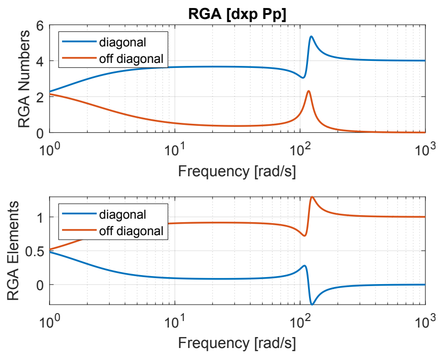

Figure A.131: RGA for x_p=0.928m

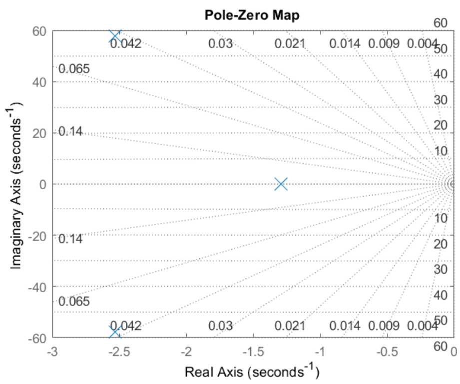

Figure A.132: Eigenvalues: -1.2907, -2.5320 $\pm$ 57.6776i

B Linearisation

Linearization for negative spool position is obtained by the continuity equations with the orifice equations included.

$$\dot{p_p} = \frac{\beta}{V_{p0} + A_p x_p}(k_v x_v p\sqrt{|p_p - p_t|}sgn(p_p - p_t) - \dot{x_p}A_p) \tag{B.1}$$

$$\dot{p_r} = \frac{\beta}{V_{r0} + A_r(L_{stroke} - x_p)}(\dot{x_p}A_r - k_v x_v r\sqrt{|p_s - p_r|}sgn(p_s - p_r)) \tag{B.2}$$

Linerazation for p_r

$$\Delta\dot{p_p} = \left.\frac{\delta\dot{p_p}}{\delta x_p}\right|_0 \Delta x_p + \left.\frac{\delta\dot{p_p}}{\delta x_v p}\right|_0 \Delta x_v p + \left.\frac{\delta\dot{p_p}}{\delta p_p}\right|_0 \Delta p_p + \left.\frac{\delta\dot{p_p}}{\delta p_t}\right|_0 \Delta p_t + \left.\frac{\delta\dot{p_p}}{\delta\dot{x_p}}\right|_0 \Delta\dot{x_p} \tag{B.3}$$

$$\Delta\dot{P_r} = \left.\frac{\delta\dot{p_p}}{\delta x_p}\right|_0 \Delta x_p + \left.\frac{\delta\dot{p_r}}{\delta x_v r}\right|_0 \Delta x_v r + \left.\frac{\delta\dot{p_r}}{\delta p_s}\right|_0 \Delta p_s + \left.\frac{\delta\dot{p_r}}{\delta p_r}\right|_0 \Delta p_r + \left.\frac{\delta\dot{p_r}}{\delta\dot{x_p}}\right|_0 \Delta\dot{x_p} \tag{B.4}$$

The linearization constants are

$$\left.\frac{\delta\dot{p_p}}{\delta x_p}\right|_0 = \frac{-A_p\beta}{(V_{p0} + A_p x_p)^2}(k_v x_v p\sqrt{|p_p - P_t|} - \dot{x_p}A_p) = nk_{x_{pp}} \tag{B.5}$$

$$\left.\frac{\delta\dot{p_p}}{\delta x_v p}\right|_0 = \frac{\beta}{V_{p0} + A_p x_p}(k_v\sqrt{|p_p - p_t|}) = nk_{x_{vp}} \tag{B.6}$$

$$\left.\frac{\delta\dot{p_p}}{\delta p_p}\right|_0 = \frac{\beta}{V_{p0} + A_p x_p}\left(\frac{k_v x_v p}{2\sqrt{|p_p - p_t|}}\right) = nk_{p_p} \tag{B.7}$$

$$\left.\frac{\delta\dot{p_p}}{\delta p_t}\right|_0 = \frac{\beta}{V_{p0} + A_p x_p}\left(\frac{-k_v x_v p}{2\sqrt{|p_p - p_t|}}\right) = nk_{p_t} \tag{B.8}$$

$$\left.\frac{\delta\dot{p_r}}{\delta\dot{x_p}}\right|_0 = \frac{-A_p\beta}{V_{p0} + A_p x_p} = nk_{\dot{x_{pp}}} \tag{B.9}$$

$$\left.\frac{\delta\dot{p_r}}{\delta x_P}\right|_0 = \frac{A_r\beta}{(V_{r0} - A_r x_p)^2}(\dot{x_p}A_r - k_v x_v r\sqrt{|p_s - p_r|}) = nk_{x_{pr}} \tag{B.10}$$

$$\left.\frac{\delta \dot{p_r}}{\delta x_v r}\right|_0 = \frac{\beta}{V_{r0} - A_r x_p}(-k_v\sqrt{|p_s - p_r|}) = nk_{x_{vr}r} \tag{B.11}$$

$$\left.\frac{\delta \dot{p_r}}{\delta p_s}\right|_0 = \frac{\beta}{V_{r0} - A_r x_p}\Big(\frac{-k_v x_v r}{2\sqrt{|p_s - p_r|}}\Big) = nk_{p_s} \tag{B.12}$$

$$\left.\frac{\delta \dot{p_r}}{\delta p_r}\right|_0 = \frac{\beta}{V_{r0} - A_r x_p}\Big(\frac{k_v x_v r}{2\sqrt{|p_s - p_r|}}\Big) = nk_{p_r} \tag{B.13}$$

$$\left.\frac{\delta \dot{p_r}}{\delta \dot{x_p}}\right|_0 = \frac{A_r \beta}{V_{r0} - A_p x_p} = nk_{\dot{x_{pr}}} \tag{B.14}$$

C | Valve Dynamics

In this project both 4/3 proportional valves are MOOG D633 where the dynamic response have been estimated with a second order transfer function as shown in equation C.1. The transfer function and bode plot which is seen in figure C.1 are obtained from report which utilised same manufacturer hydraulic valves [Bendtsen et al., 2019][MOOG, 2019].

$$G_{D633} = \frac{1.24 \times 10^5}{s^2 + 498s + 1.24 \times 10^5} \tag{C.1}$$

The estimated transfer function is plotted against the manufacturer valve dynamics figure C.1. The hydraulic valves have normalised valve input and output of ±10 volts.

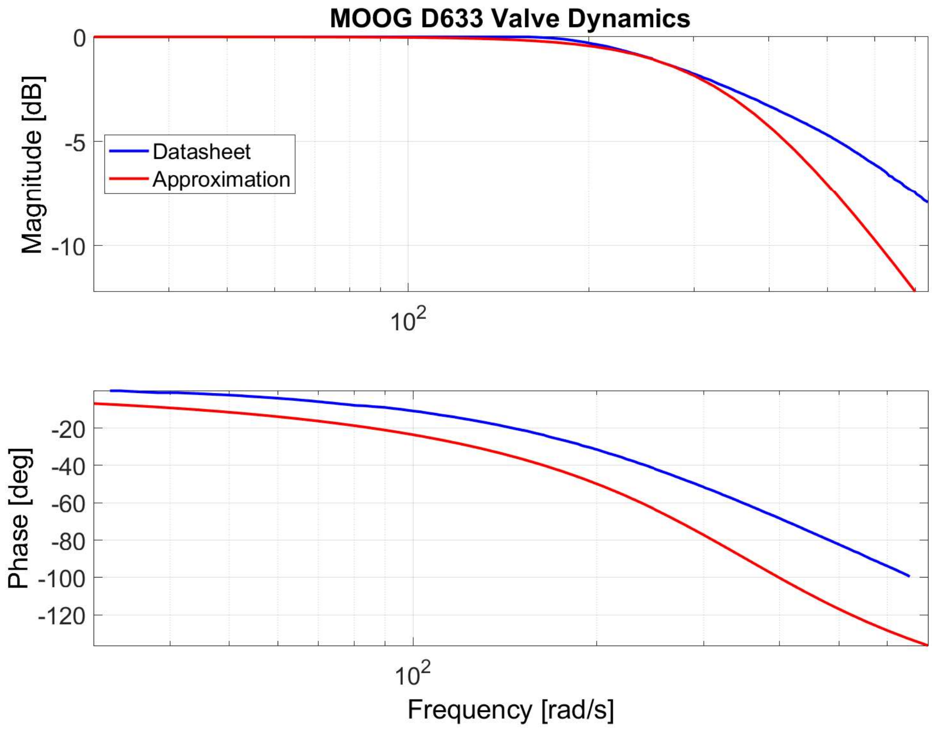

Figure C.1: MOOG D633 valve datasheet comparison with estimated transfer function G_{D633} [Bendtsen et al., 2019]

As it is seen from the figure the approximation in red matches the actual response in blue quite well. There are small deviations that appear after -3dB, and considered to be acceptable. As can be seen from the bode plot the cutoff frequency for the valves is at $350[\frac{rad}{s}]$ which lies more than 2x beyond any cutoff frequency observed from the RGA and SVD plots. From there it is assumed that the valve dynamics can be neglected.